WARSAW UNIVERSITY OF TECHNOLOGY

DISCIPLINE OF SCIENCE - CHEMICAL SCIENCES/

FIELD OF SCIENCE - NATURAL SCIENCES

Ph.D. Thesis

Polina Ivanova M.Sc.

Studies on the Catalytic Activity of Monometallic and Multimetallic Nanozymes and Their Use in the Construction of Biotests

Supervisor

Mariusz Pietrzak, Ph.D., D.Sc.

Second supervisor

Professor Sławomir Sęk, Ph.D., D.Sc.

WARSAW 2023

Promotorzy:

dr hab. inż. Mariusz Pietrzak prof. uczelni (Politechnika Warszawska)

prof. dr hab. Sławomir Sęk (Uniwersytet Warszawski)

Projekt Interdyscyplinarne Studia Doktoranckie "Od chemii do bioinnowacji" TRI-BIO-CHEM jest realizowany w ramach Programu Operacyjnego Wiedza Edukacja Rozwój 2014-2020 współfinansowanego ze środków Europejskiego Funduszu Społecznego

Acknowledgment

First of all, I would like to say thanks to ***Mariusz Pietrzak, PhD. Eng., Associate Professor*** and ***Sławomir Sęk, PhD., Full Professor*** *for the support, scientific supervision, immeasurable help, numerous valuable comments and consultations. Thank you very much for your patience and time devoted to countless discussions during our years of cooperation.*

I would like to thank ***Marcin Drozd, PhD. Eng.*** *for iron oxide nanocubes synthesis, comprehensive help, complex support, valuable advice, and inspiration.*

I would like to thank ***Katarzyna Tokarska, PhD. Eng.*** *for 3D modelling, laser cutting and milling of the cassettes and magnetic separation module parts, and constant psychological support.*

I would like to thank ***Kamil Żukowski, PhD. Eng.*** *for magnetic separation module construction.*

I would like to thank ***Marta Mazurkiewicz-Pawlicka, PhD. Eng.*** *for performing EDXRF analysis.*

I would like to thank ***Sylwia Karoń, MSc. Eng.*** *for preparation of HRP/ABs conjugates.*

I would like to thank ***Kamil Michrowski, MSc. Eng.*** *for helping with implementation and performing of NPs synthesis.*

I would also like to thank all ***members and PhD students of the Department of Medical Biotechnology*** *for a nice working atmosphere, support, and inspiration.*

Additionally, I thank my ***friends*** *and* ***family*** *for their care and support.*

Dedicated to my husband Daniil,

sister Natalia, brother-in-law Artem,

and my parents.

Abstract

The doctoral dissertation titled „Studies on the catalytic activity of monometallic and multimetallic nanozymes and their use in the construction of biotests" describes the synthesis and investigation of the peroxidase-like activity of monometallic and multimetallic nanoparticles (NPs) using various types of substrates. It also focuses on methods of NPs modification, their functionalization with antibodies (ABs), and usage for model antigen detection.

The literature part (Chapter 1) of the dissertation presents information about different monometallic and multimetallic NPs, strategies leading to their synthesis, and their stabilization and post-synthetic surface modification with bioreceptors. This part also contains a discussion on NPs usage in analytical methods for signal generation and premeasurement sample treatment. Since noble metal-based NPs can mimic natural enzyme activity and, therefore, can be responsible for analytical signal generation, a detailed discussion on this matter is also included in the literature part of the thesis. Additionally, various methods for the investigation of NPs enzyme-like activity are described. The newest achievements in magnetic NPs usage in biological sample preconcentration, interferent elimination, and analyte translocation are presented. In addition, peroxidase-like properties of such NPs used for the analytical signal generation are discussed with an emphasis on the comparison of their catalytic properties against noble metal NPs.

Analysis of the literature allowed the formulation of the main aim of the thesis, which concerns the synthesis and application of bimetallic or multimetallic nanozymes for the development of bioassays or biotests for model biomarker detection. To reach that aim, the research leading to the combination of various metals in one type of NPs to obtain paramagnetic and catalytically active NPs with the ability to form conjugates with Abs was proposed and described.

The literature part is followed by the experimental part (Chapter 2), which describes all the chemicals and equipment used. It also provides information about materials used for microfluidic cassette and magnetic separation module manufacturing. All the methods regarding NPs synthesis, surface modification, conjugation with bioreceptors, characterization, catalytic activity examination, NLISA assays development and application, microfluidic cassette and magnetic separation module manufacturing and usage for antigen detection are also described in detail in this chapter.

The obtained results and observations are described in Chapter 3, which particularly concerned the following topics:

- synthesis of stable multifunctional NPs with pronounced peroxidase-like activity and the ability to be conjugated with ABs;
- influence of each step of NPs surface modification on their catalytic activity;
- utility of obtained NPs/ABs conjugates for antigen detection in biological samples;
- selection of antigen detection conditions for immunosorbent assay to increase selectivity and sensitivity and decrease analytical signal background;
- selection of conditions for NPs-based antigen detection in a modified immunosorbent assay provided on flexible polyethylene terephthalate foils and in the microfluidic chip.

The obtained results are discussed in detail, with respective conclusions drawn and noted in this chapter. The most significant achievements of this work are summarized in Chapter 4. It also contains the essential conclusions and key recommendations. The last chapter gives the list of the cited literature, sorted alphabetically.

Keywords: Noble metal NPs, magnetic NPs, antigen detection, nanozyme, horseradish peroxidase mimetics, NLISA.

Streszczenie

Rozprawa doktorska pt. „Badania aktywności katalitycznej nanozymów monometalicznych i multimetalicznych oraz ich wykorzystanie w konstrukcji biotestów" przedstawia syntezę i badanie aktywności katalitycznej typu peroksydazy nanocząstek monometalicznych i multimetalicznych (NPs) z wykorzystaniem różnego rodzaju substratów. Zakres pracy obejmuje również metody modyfikacji nanoczastek, ich funkcjonalizację wybranymi przeciwciałami (ABs) oraz zastosowanie do oznaczania modelowego antygenu, tj. białka C-reaktywnego.

Część literaturowa (Rozdział 1) rozprawy zawiera informacje na temat nanoczastek monometalicznych i multimetalicznych, przedstawia strategie syntezy oraz stabilizacji i post-syntetycznej modyfikacji powierzchni za pomocą bioreceptorów. Ta część przytacza również przykłady wykorzystania nanocząstek w metodach analitycznych w funkcji składników odpowiedzialnych za generowanie sygnału analitycznego oraz użytecznych podczas przygotowania próbek przed wykonaniem oznaczeń. Ze względu na fakt, iż nanocząstki metali szlachetnych mogą naśladować aktywność katalityczną wybranych enzymów, co znajduje zastosowanie w konstrukcji biotestów i biosensorów, szczegółowe omówienie tego zagadnienia zostało również zawarte w te części pracy. Dodatkowo w tej części rozprawy przedstawiono wybrane metody badania aktywności katalitycznej nanozymów oraz przedstawiono najnowsze osiągnięcia w zakresie wykorzystania magnetycznych nanocząstek do wstępnego zatężania próbek biologicznych i oddzielania interferentów/matrycy próbki od analitu. Ponadto omówiono właściwości katalityczne typu peroksydazy nanocząstek magnetycznych w odniesieniu do nanocząstek metali szlachetnych.

Analiza dostępnej literatury pozwoliła sformułować główny cel pracy, który dotyczy syntezy i zastosowania nanozymów bimetalicznych lub multimetalicznych do opracowania biotestów oraz metod analitycznych do wykrywania modelowych biomarkerów. Aby osiągnąć ten cel, zaproponowano i opisano badania prowadzące do połączenia różnych metali w obrębie jednego rodzaju nanocząstek w celu uzyskania nanocząstek paramagnetycznych o wysokiej aktywności katalitycznej, jednocześnie zdolnych do tworzenia koniugatów z ABs.

Po części literaturowej przedstawiono część doświadczalną (Rozdział 2), w której opisano wszystkie zastosowane odczynniki, materiały i wykorzystaną aparaturę. Dostarcza ona również informacji o materiałach użytych do wytworzenia kaset mikroprzepływowych oraz modułu do magnetycznej separacji. Wszystkie metody i procedury dotyczące syntezy nanocząstek, modyfikacji ich powierzchni, koniugacji z bioreceptorami, charakteryzacji, badań

aktywności katalitycznej, opracowania i zastosowania testów NLISA, produkcji kaset mikroprzepływowych i modułu do magnetycznej separacji analitu oraz ich zastosowania do wykrywania antygenów są również szczegółowo opisane w tym rozdziale.

Uzyskane wyniki i obserwacje przedstawiono w Rozdziale 3, który dotyczy następujących zagadnień:

- syntezy stabilnych multifunkcyjnych nanocząstek o wysokiej aktywności typu peroksydazy i zdolności do koniugacji z przeciwciałami;
- wpływu poszczególnych etapów modyfikacji powierzchni nanocząstek na ich aktywność katalityczną;
- użyteczności otrzymanych koniugatów NPs/ABs do wykrywania antygenów w próbkach biologicznych;
- doboru warunków detekcji antygenu do przeprowadzenia testu immunosorpcyjnego, w celu zwiększenia selektywności i czułości oraz zmniejszenia sygnału tła;
- doboru warunków metody oznaczania antygenu z wykorzystaniem nanocząstek w zmodyfikowanym teście immunosorpcyjnym opracowanym z wykorzystaniem elastycznych folii z poli(tereftalanu etylenu) oraz w mikrosystemie przepływowym.

Wszystkie otrzymane wyniki zostały szczegółowo omówione i na ich podstawie wyciągnięto wnioski, które przedstawiono w niniejszym rozdziale. Najważniejsze osiągnięcia tej pracy zostały podsumowane w Rozdziale 4. Zawiera on również najistotniejsze wnioski i podsumowanie rezultatów przeprowadzonych badań. Ostatni rozdział rozprawy zawiera spis cytowanej literatury w porządku alfabetycznym.

Słowa kluczowe: nanocząstki metali szlachetnych, nanocząstki magnetyczne, wykrywanie antygenów, nanozymy, mimetyki peroksydazy chrzanowej, NLISA.

List of abbreviations

4-AAP - 4-aminoantipyrine

ABs - antibodies

ABTS - 2,2′-azino-bis(3-ethylbenzothiazoline-6-sulfonic acid) diammonium salt

BRP - bromopyrogallol red

BSA - bovine serum albumin

BSI - British Standards Institution

CTCs - circulating cancer cells

DAB - 3,3'-diaminobenzidine

DLVO - theory - Derjaguin, Landau, Verwey, and Overbeek theory

DTPA - diethylenetriaminepentaacetic acid

EDC - 1-ethyl-3-(3-dimethylaminopropyl)carbodiimide

EDX - energy dispersive X-ray analysis

ELISA - enzyme-linked immunosorbent assay

EPR - electron paramagnetic resonance

HBPG - hyperbranched polyglycerol

HPPA - 3-(*p*-hydroxyphenyl)propionic acid

HSA - human serum albumin

HRP - horseradish peroxidase

HVA - homovanillic acid

LOD - limit of detection

MES - 2-ethanesulfonic acid

NHS - N-hydroxysuccinimide

NLISA - nanozyme-linked immunosorbent assay

NPs - nanoparticles

NPs/ABs - nanoparticles/antibodies

OPD - *o*-phenylenediamine

PDDA - poly(diallyl dimethylammonium) chloride

PEEK - polyether ether ketone

PEG - poly(ethylene glycol)

PET – poly(ethylene terephthalate)

PMMA - poly(methyl methacrylate)

PG - pyrogallol

PhOH - phenol

PBS - phosphate buffer saline

PBST - phosphate buffer saline with Tween (0.05%)

PTC - plasma thromboplastin component

QD - quantum dots

LOD - limit of detection

TA - terephthalic acid

TAOH - 2-hydroxyterephthalic acid

TEM - transmission electron microscopy

TMB - 3,3,5,5-tetramethylbenzidine

TnI – troponin I

SEM - scanning electron microscopy

USFDA - United States Food and Drug Administration.

EDXRF- energy dispersive X-ray fluorescence

Table of Contents

Introduction

The intensive development of novel methods for disease biomarker detection has been observed over the last decades. It has aimed at searching for new techniques and materials which would allow the development of cheap, simple, sensitive, and selective disease biomarkers detection assays. Taking into account the fact, that a big part of analytical assays uses natural enzymes for signal generation, some efforts have been made to replace natural enzymes with their cheaper and more stable mimetics.

A significant part of disease biomarkers can be detected with immunosorbent assays in the case of which enzymes are used as catalytic labels for ABs. Enzymes are produced by plants, animals, and cell lines, and must be collected and purified before application in bioassays, biotests and biosensors. Processes of enzyme production and purification are complicated and expensive, and require specific equipment. In addition, enzymes need to be stored in appropriate conditions as breaching the temperature and pH limits can lead to enzyme activity decreasing and even full deactivation. NPs that mimic the activity of natural enzymes are a good alternative for them. Such NPs are called nanozymes and are characterized by good temperature and pH stability in comparison to natural enzymes. A variety of synthesis methods allows for obtaining NPs of the desired shape, size and composition. The synthesis method plays a crucial role in nanoparticle physicochemical and biological properties. Nonetheless, post-synthesis surface modification not only allows for changes in NPs characteristics obtained as a result of the initial synthesis step, but also promotes the new ones. Due to unique and promising physicochemical and biological properties, nanomaterials are widely used in analytical methods. Different types of NPs can be used for analytical signal generation and sample premeasurement treatment. For example, noble metal-based NPs are widely used as natural enzyme mimetics. Iron oxide-based NPs can also show enzyme-like activity; however, such activity is displayed on a significantly lower scale than one of the noble metal-based NPs. Iron oxide paramagnetic NPs have interesting properties, making them a worthwhile subject of closer investigation. Paramagnetism allows for the separation, relocation and preconcentration of an analyte before the analytical examination. Besides well-known nanozyme activity, gold NPs can be easily modified and used as a platform for ABs immobilization. ABs immobilization is a major process for preparing labelled ABs used in the immunoadsorption assay. Paramagnetic and NPs with enzyme-like activity can potentially be used for disease biomarkers detection. Each type of NPs listed above has some essential properties used in analytical assays but not all or not at the required level.

Combining multiple metals in one type of NPs allows one to combine their properties and sometimes achieve a new one that is not derived directly from its components. Multifunctional NPs can be obtained by combining iron oxide with chosen noble metal decoration with gold and modification with ABs NPs with paramagnetic properties can help to eliminate interferents influence and concentrate samples, whereas the noble metal part of NPs participates in conjugation with bioreceptors and signal generation process.

NPs-based immunosorbent assay can not only be performed on multi-well plates but also on microfluidic chips. The complex construction of microfluidic chips allows for a combination of premeasurement sample preparation with an analytical signal generation in one. Such a combination decreases the assay cost and analysis time, thus paving the way for using the microfluidic nanoparticle-based assay as a point-of-care for antigen detection.

1. Literature review

1.1. NPs. Short overview

According to International Organization for Standardization, NPs are "nano-object with all three external dimensions in the nanoscale". Nanoscale, in this particular case, was defined as a size range between 1-100 nm (Boverhof *et al.*, 2015). A similar definition for NPs is used by the United States Food and Drug Administration (USFDA). According to USFDA, NPs are defined as "materials that have at least one dimension in the range of approximately 1 to 100 nm and exhibit dimension-dependent phenomena". The deviating definition was proposed by the British Standards Institution (BSI), where NPs are nanoscale objects, e.g. objects with one or more nanoscale dimension. BSI definition is based on the nanoscale definition of the International System of Units, where "nanometer" equals 10^{-9} meters. System of Units, where "nanometer" equals 10^{-9} meters. It must be pointed out that, in this work, NPs are defined as objects ranging from 1 to 100 nm in each dimension. Pokropivny and Skorokhod proposed in 2007 a classification of NP based on NP dimensionality. Based on it, NPs can be divided into 0D, 1D, 2D or 3D nanostructures. The electrons movement along with the dimensions of NPs determine NPs shape. For example, in 0D NPs, electrons cannot move and are entrapped in dimensionless space. In the case of 1D NPs, electrons can move along the x-axis but not further than 100 nm. Similarly, in 2D and 3D NPs, electrons are free to move along the x and y or x, y and z-axes (Pokropivny and Skorokhod, 2007; Tiwari and Kim, 2012). Simultaneously with dimension classification, NPs can be organized with material-based classification. According to material, NPs can belong to carbon-based, inorganic-based, organic-based, composite-based and mixed subgroups (Jeevanandam *et al.*, 2018). Taking into account the topic of this work, going forward the most focus will be placed on the metal and metal oxide NPs.

The first documented synthesis and application of metallic NPs was made in the 14th-13th century BC. Egyptians and Mesopotamians used copper or copper oxide NPs to make red-coloured glass (Schaming and Remita, 2015). Later, in the late Bronze Age, Cu NPs were applied in glass production in Fratessina di Rovigo in Italy (Artioli, Angelini and Polla, 2008). Cu and Cu_2O NPs were found in Celtic red enamels dated 400-500 BC (Brun, Mazerolles and Pernot, 1991). Nevertheless, the most well-known historical example of metallic NPs application is Roman Lycurgus Cups, dated the 4th century AD. The popularity of this particular application of NPs could be related to the fact that Lycurgus Cups were made from dichroic glass, which can have red or green colour depending on the angle at which light passes (Leonhardt, 2007). Detailed examination found that Lycurgus Cups contain Ag/Au alloy NPs

with the addition of Cu NPs. (Freestone *et al.*, 2007) Therefore, Roman glass can be classified as the first historical application of Ag/Au alloy NPs. The first scientific description of colloidal Au NPs synthesis was made by Michael Faraday in 1857. Faraday's Au NPs description compares optical characteristics of bulk and colloidal Au. Later, in 1908, Gustav Mie delivered an investigation of phenomena presented by Faraday and explained metallic NPs specific colour nature (Mie, 1908). Besides optical characteristics, NPs are characterized by tuneable physicochemical and biological properties different from their bulk counterparts.

1.2. Synthesis methods of NPs containing metals

NPs synthesis methods can be divided into chemical, physical, biological and combined ones. Taking into account the way in which NPs are formed synthesis methods can be divided into top-down and bottom-up ones.

1.2.1. Top-down synthesis methods of NPs

Top-down methods are based on the fragmentation of bulk material into 0-3D NPs. Milling, thermal evaporation, laser ablation and sputtering are the main methods of the top-down synthesis approach.

Mechanical milling is the simplest top-down NPs production technique. It can be utilized to alter the structure, size, and shape of NPs. Milling production of NPs includes vibratory milling, rotatory milling, planetary milling, horizontal milling and attrition milling (Abid *et al.*, 2022). NPs synthesis based on milling process is characterized by high capacity and simplicity. However, NPs obtained using such methods usually have a lot of structural flaws (Neikov, 2009). The milling process can be used to produce monometallic and metal alloys along with metal oxide NPs - for example: Ag, CuO, ZnO, and Cu_5FeS_4 (Ostovari Moghaddam *et al.*, 2018; Reverberi *et al.*, 2019; Wei *et al.*, 2020; Otis, Ejgenberg and Mastai, 2021).

Thermal evaporation is another efficient top-down technique for NPs synthesis. It is an endogenic process of chemical bonds breakdown in molecules; such breakdown is caused by heat and does not require solvents (Ijaz *et al.*, 2020). NPs synthesis based on thermal evaporation is affected by evaporation duration, temperature and distance from the metal source (Zahra *et al.*, 2019). Thermal evaporation can be partially applied for materials characterized with low melting point and cannot be used for metal alloy NPs synthesis (Mattox, 2002). Thermal evaporation can facilitate synthesizing Ag, Zn_2GeO_4 and MoS_2 NPs (Guo, Fu and Peng, 2018; Zahra *et al.*, 2019; Khurana, Rathee and Jaggi, 2020).

Sputtering is a non-thermal evaporation process maintained under low pressure (<0.67 Pa) (Oluwatosin Abegunde *et al.*, 2019). During sputtering synthesis, NPs are produced due to the metal substrate surface being bombarded with high-energy ion beam. The size of produced NPs can be determined by temperature, the thickness of the metal substrate layer and synthesis duration (Anu Mary Ealia and Saravanakumar, 2017). Sputtering can be used for the synthesis of Cu, Pt, Pd, CuO and Fe_2O_3 NPs (Mahmoodi, Ghoranneviss and Asgary, 2017; Shameem, Mekala and Kumar, 2017; Verma *et al.*, 2017; Deng, Nguyen and Yonezawa, 2018; Eberhardt *et al.*, 2018).

Laser ablation is a top-down technique that allows synthesizing NPs with different shapes (spherical NPs, nanowires, nanotubes) and structures (core-shell) (Semaltianos, 2016; M. Kim *et al.*, 2017). Laser ablation uses a high-intensity beam of electromagnetic radiation to disconnect molecules from a bulk metal surface. Ablation occurs only when a metal substrate can absorb enough energy to be melted or evaporated. NPs production based on metal substrate irradiation is made in the aqueous or organic solvent solution. A wide range of solvents used in laser ablation allows for obtaining ligand-free noble metal NPs. Ablation efficiency can be affected by produced NPs distribution along the laser beam, and is negatively correlated with the time of the ablation process (Ijaz *et al.*, 2020). The synthesized NPs properties depend on laser settings (wavelength, pulse duration, fluency and repetition rate), solvent chemical components, and metal substrate light absorption efficiency. In addition, efficient ablation requires a lot of energy (Sportelli *et al.*, 2018). Laser ablation is used to produce metal and metal oxide NPs such as Ag, ZnO, TiO_2 and CdO NPs (Guillén *et al.*, 2017; Mostafa *et al.*, 2017; Gavrilenko *et al.*, 2019; Menazea, 2020).

1.2.2. Bottom-up NPs synthesis methods

Bottom-up methods of NPs synthesis are based on the assembly of basic units into the larger structures in the nanoscale. Depending on the nature of processes and components used in bottom-up synthesis, such NPs production methods can be divided into chemical and biological methods. Products of chemical synthesis are usually characterized by precise size, composition and shape. In chemical synthesis, hazardous chemicals can be involved. Some researches propose to use biological synthesis to avoid the usage of hazardous chemicals and make NPs less toxic (Pal, Rai and Pandey, 2019).

1.2.2.1. Chemical NPs synthesis methods

Chemical reducing methods are characterized by simplicity, versatility and precision of NPs size and shape and are usually based on the reduction of soluble metal salts. During the

synthesis process, metal ions are reduced to atoms and form metal NPs. Chemical reduction NPs synthesis depends on the type of reductant and precursor, pH, temperature, mixing condition and synthesis duration (Khan *et al.*, 2016; Nam and Luong, 2019). A $NaBH_4$, sodium citrate, ascorbic acid, hydrazine or hydroxylamine hydrochloride can be used as reducing agents (Furst, Berlo and Hooton, 1965; Slepička *et al.*, 2019; Zhang *et al.*, 2019; Demirkan *et al.*, 2020; Wang *et al.*, 2021). Sodium borohydrate and other reducing agents can be used in both homogenous (aqueous or organic solutions) and heterogenous synthesis of nanoparticles as it was shown in 1994, when thedodecanethiol-water system, was used for Au NPs synthesis (Brust *et al.*, 1994).

Seeding synthesis is connected to the chemical reduction method. It was discovered by G. Frens in 1972. Such a method is based on NPs growing due to metal salt reduction in solutions that already contain seeds of NPs (Frens, 1972). Depending on the precursor and seed type, the mentioned method can be used to synthesize mono- and multimetallic NPs. In this work, seeding synthesis was used to prepare multimetallic NPs. As "seeds", iron oxide NPs were used, and noble metal precursors were utilized to obtain multimetallic NPs.

Precipitation synthesis is another bottom-up NPs synthesis method based on precipitate formation under certain conditions. For example, such a process can occur when precursor concentration reaches saturation point and the nucleation process appears in a solution. The nucleation growth process continues until NPs are formed. To obtain NPs of a specific size, nucleation growth should be slowed down and stopped.

The microemulsion synthesis method allows for controlling NPs size, shape, and composition. Such methods can be used to synthesize monometallic NPs, alloy NPs and metal oxide NPs. Usually, the microemulsion synthesis method allows for obtaining smaller NPs compared to the coprecipitation method (Pawlonka *et al.*, 2014). Microemulsion synthesis system composition includes the aqueous phase, oil phase, surfactant and metal salt precursor. After precipitation, NPs are present only in one phase and can be easily collected (Liu *et al.*, 2004).

Polyol synthesis method is an efficient method for preparing the size-, shape- and composition-precise NPs. This method was first developed by Figlarz and co-workers in 1988 for Co, Ni and Cu NPs synthesis. The polyol method presented by Figlarz et al. is based on mixing precursors with ethylene glycol and sulfuric acid. In the next step, the solution is heated up to the boiling point. Generally, such a method covers the mixing of metal salt precursor with ethylene glycol and heating obtained solution until reaching the refluxing temperature.

Modification of temperature and precursor concentration enables the production of NPs of varying size. (Eid, Wang and Wang, 2017).

1.2.2.2. Biological synthesis of NPs

Increased biocompatibility and avoidance of hazardous compounds are the main benefits of biological metal and metal oxide NPs synthesis. Biological NPs synthesis can be based on biosourced compounds as reducing agents, or living microorganisms to maintain the whole synthesis process. Depending on the microorganism, NPs synthesis can be based on different mechanisms. Nevertheless, usually, such a process starts with the entrapment of metal ions on the surface or inside of the microorganism and then such ions are reduced by enzymes (Li *et al.*, 2011). Depending on the location, microorganisms-synthesized NPs are classified as intracellular or extracellular (Talham, 2002). Two pathways of NPs synthesis with microorganism participation can be determined. First, when microorganisms modify the composition of the surrounded solution and make it saturated, NPs are formed in the same way as they are for chemical precipitation. The second one is based on microorganisms production of polymers, which can play the role of NPs seeds (same as for the chemical seeding method) (Benzerara *et al.*, 2011).

Biological synthesis can be applied to the production of monometallic and multimetallic NPs. For example, Au NPs can be synthesized by bacteria (*Thermomonospora sp., Rhodococcus sp., Lactobacillus*), fungi (*Verticillium sp., Fusarium oxysporum*) and filamentous cyanobacteria (Mukherjee *et al.*, 2001, 2002; Nair and Pradeep, 2002; Ahmad, Senapati, M Islam Khan, *et al.*, 2003; Lengke, Fleet and Southam, 2006). Yeast cells and fungi are used for alloy NPs synthesis (Dasaratrao Sawle *et al.*, 2008; Zheng *et al.*, 2010). Metal oxide NPs, such as Fe_3O_4, TiO_2, and Sb_2O_3, can also be synthesized by microorganisms (Jha, Prasad and Kulkarni, 2009; Zhou *et al.*, 2009). Even though biological synthesis is characterized by high yield and low cost, it requires expensive post-synthesis separation NPs from a batch medium and microorganisms mass and therefore it is not always environmentally friendly.

NPs synthesis with plant extracts is a subgroup of biological synthesis methods. Plants extracts used in biological synthesis usually contain polyphenols, ascorbic and citric acid, flavonoids, and terpenoids which play the role of active synthesis agents. Moreover, plant oils also can be used for NPs synthesis as reducing agents. The main drawback of plant extracts use in NPs synthesis is that such extracts are multi-component and introduce difficulties into NPs post-synthesis purification process. The biggest number of synthesis methods based on plant-sourced active agents were developed for Ag NPs. For example, Ag NPs can be synthesized

with the usage of cashew oil, *Cinnamomum Zylinicum* extract, *Berberis vulgaris extract*, *P. granatum L.* extract, end many others (Kumar *et al.*, 2008; Behravan *et al.*, 2019; Almalah, Alzahrani and Abdelkader, 2019; Shahid-ul-Islam *et al.*, 2019).

1.3. NPs morphology

NPs consisting of more than one metal, can have different morphologies, which affect their properties and performance in various applications.

A core-shell structure, in which the NP has a core made of one material, and a shell made of another material opens up a possibility of matching of materials of different properties, e.g. NPs with a magnetic core and a conductive shell can be a good example. Core-shell approach can also provide increased stability and protection for the core material, and can enhance the catalytic activity of the NPs. Core-shell NPs morphology has multiple subtypes (Scheme 1) (Khatami et al., 2018):

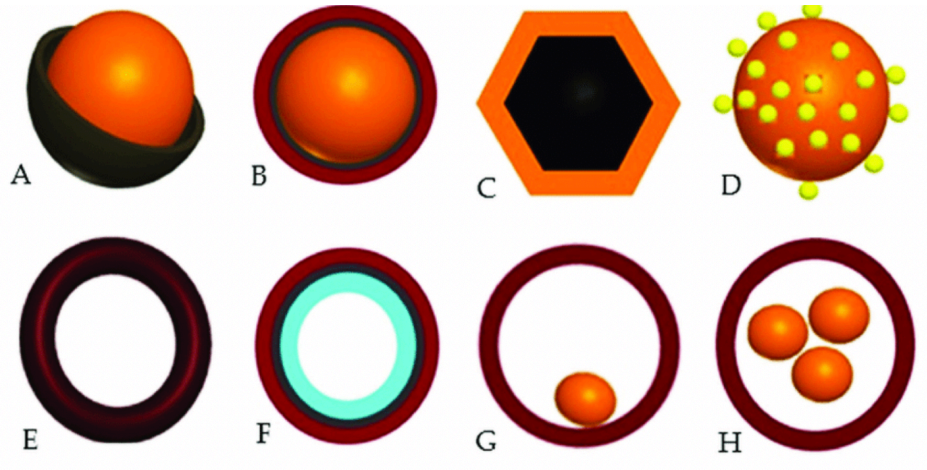

Scheme 1. Core-shell NPs morphology: (A) Core-shell; (B) Core-double-shell or core-multi-shell; (C) Polyhedral core-shell; (D) Core-porous shell; (E) Hollow core-shell or single shell (F) Hollow core-double shell; (G) Moveable core-shell; (H) Multi core-shell (Khatami et al., 2018).

Core-double shell or core-multishell: This structure has a core surrounded by multiple layers of shells. Each shell can have different properties, and the number of shells can be tailored to achieve specific properties or functions (Tahmasbi, Koukabi and Seidi, 2022).

Polyhedral core-shell: This structure has a core with a polyhedral shape, such as a cube or a sphere, surrounded by a shell. This structure can be useful for applications such as catalysis, where the specific shape of the core can influence the catalysts activity (Long *et al.*, 2011).

Core-porous shell: This structure has a solid core that is surrounded by a porous shell. The core provides the material with its strength and stability, while the porous shell enhances its overall surface area and allows for the exchange of fluids and gases. The pores also can be

used to encapsulate other materials, such as drugs or enzymes, or to enhance the surface area of the NP for catalytic reactions (Kim, Ko and Nam, 2016).

Hollow core-shell or single shell NPs: This structure consists of a hollow core surrounded by a single shell. This structure can be useful for applications such as drug delivery, where the hollow core can be used to encapsulate drugs and the shell can control the release of the drugs (Soares *et al.*, 2019).

Hollow core-double shell: This structure has a hollow core surrounded by two layers of shells. This structure can provide additional protection for the hollow core, and the different properties of the two shells can be utilized for specific functions (Guan *et al.*, 2016).

Moveable core-shell NPs: This structure has a core that can move within the shell. The core can be made of a magnetic material, allowing the NP to be directed by an external magnetic field (Liu *et al.*, 2006).

Multi core -hell NPs: This structure is characterized with multiple cores surrounded by a single shell. Each core can be made of a different material, and the different properties of the cores can be utilized for specific functions (Kim *et al.*, 2014).

Irregular shape core-shell: This structure has a core with an irregular shape, surrounded by a shell. The irregular shape of the core can provide unique properties, and the shell can protect the core and control the release of any encapsulated materials (Khatami et al., 2018).

Another bimetallic or multimetallic NPs morphology which must be listed is an alloy, which is made of two or more different types of metal atoms (Scheme 2).

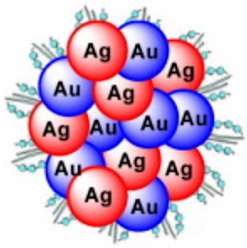

Scheme 2. Au-Ag alloy NPs (Malathi *et al.*, 2014).

In alloys, atoms of the different metals are randomly and homogeneously distributed throughout the NP on the atomic level. The composition of the alloy NPs can be tuned to control their properties, which can be useful for different applications such as catalysis and analytics *(*Malathi *et al., 2014)*.

Janus NPs have two distinct and different functionalities on opposite sides of the NPs. These NPs are made of two different materials or are characterized with different surface chemistry on each side. They can act as a two-faced particles with two different chemical

environments on each of the sides. Janus NPs can be used in a variety of applications such as catalysis, drug delivery, and sensing. (Le *et al.*, 2019).

NPs of mixed morphology can be also created by combining different materials of NPs together. They can be a combination of core-shell, alloy, or Janus structures within one nanoparticle. The combination of different morphologies within one nanoparticle can provide unique properties and functionalities, which can be useful for various applications such as these mentioned above. For example, recently nanoparticles of a mixed morphology with a core-shell structure of a magnetic core and a conductive shell, as well as a Janus structure with different surface chemistry on each side were synthesized and applied for magnetic targeting and controlled release of drugs (Eom *et al.*, 2021).

1.4. Stabilization of colloidal NPs

Insoluble NPs suspended in a liquid can be identified as a colloidal solution. The attraction between NPs in solution leads to aggregation, agglomeration, overgrowing and precipitation, affecting the stability of NPs colloidal solution and catalytic activity of NPs. The terms “aggregation” and “agglomeration” are being mixed up frequently (Nichols *et al.*, 2002). In this work, the definitions accepted by the International Union of Pure and Applied Chemistry (IUPAC) are used. According to IUPAC agglomeration is a reversible clustering process caused by weak physical NPs interactions. When clusters of strongly bonded NPs are formed during the aggregation, it is not possible to reverse this process (Sokolov *et al.*, 2015). The main goal of stabilization is to increase the repulsion and decrease the attraction of NPs. It should be noted that stabilizing agents not only stabilize NPs but, in addition, can change their physicochemical and biological properties (Niu and Li, 2014). Two stabilizing strategies are used to avoid NPs aggregation – electrostatic and steric stabilization (Scheme 3).

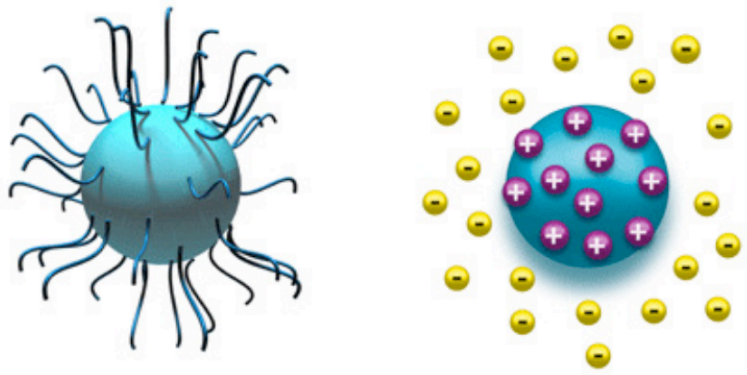

Scheme 3. Steric(left) and electrostatic(right) NPs stabilization (Saidina, Abdullah and Hussin, 2020).

1.4.1. Steric stabilization

Steric stabilization is based on the adsorption of large non-ionic molecules on the NPs surfaces, which prevents NPs aggregation. Polymers and surfactants are used for steric stabilization of NPs. The degree of steric stabilization depends on the size and nature of the stabilizing agent (Kraynov and Müller., 2011). Steric stabilization is based on molecule repulsion by the excluded volume effect. Compared to electrostatic stabilization, steric one can be provided in both water-based and organic solvents. Moreover, steric stabilization can be completed with a wide range of stabilizing agent concentrations in the medium. Depending on steric stabilizing agent concentration, NPs of different properties can be obtained (Mo *et al.*, 2016). Steric stabilizing agents absorbed on NPs surfaces create a physical barrier between catalytically active NPs surface and substrates, affecting NPs catalytic activity (Niu and Li, 2014). For efficient stabilization, the stabilizer should be strongly adsorbed on NPs surfaces to prevent unprompted desorption and NPs stability loss. A stabilizer with more than one absorption centre towards NPs decreases the chances of spontaneous desorption. Chemisorption is often determined as the strong adsorption of stabilizers on NPs surfaces. Metal NPs with an electron-deficient surface have a higher amount of valence orbitals than valence electrons. Therefore, molecules that can easily donate electrons are strongly absorbed on NPs surfaces. The properties of steric stabilizers used in this work for NPs synthesis are described below (Adair, Suvaci and Sindel, 2001; Kraynov and Müller., 2011).

Poly(ethylene glycol) (PEG) is non-toxic, soluble in aqueous and organic solvents steric stabilizing agent widely used for metal-based NPs synthesis (Choukourov *et al.*, 2021). PEG-stabilized NPs are characterized by their biocompatibility and processability. Moreover, it was found that PEG can act as both NPs stabilizing and reducing agents (Luo, Zhang and Wang, 2005). This polymer is commercially available in various forms, starting from relatively short-chained polymers (oligomers) to polymers reaching a molar mass of several hundred thousand Da, and all of them can be used as stabilizers. PEG-based stabilization prevents NPs aggregation and precipitation without drastically influencing NPs catalytic activity (Ma *et al.*, 2008). Moreover, PEG-stabilized NPs were described as reusable multiple times saving their catalytic activity on the same level. But it should be underlined, that their reusability depends on the type of PEG-stabilized nanoparticles, the conditions under which they are used, and the specific catalytic activity examined. (Luo, Zhang and Wang, 2005). Stabilization with PEG decreases protein adsorption on NPs surfaces and prevents loss of NPs activity due to protein corona formation in biological systems (Otsuka, Nagasaki and Kataoka, 2003). PEG-stabilized NPs are characterized by high blood compatibility and non-immunogenicity, which prolongs their

circulation in living organisms and makes them good candidates for efficient drug delivery (Kwon and Kataoka, 1995).

Hyperbranched polyglycerol (HBPG) (Scheme 4) was developed as an alternative to PEG and is used for stabilizing monometallic, multimetallic and metal oxide NPs.

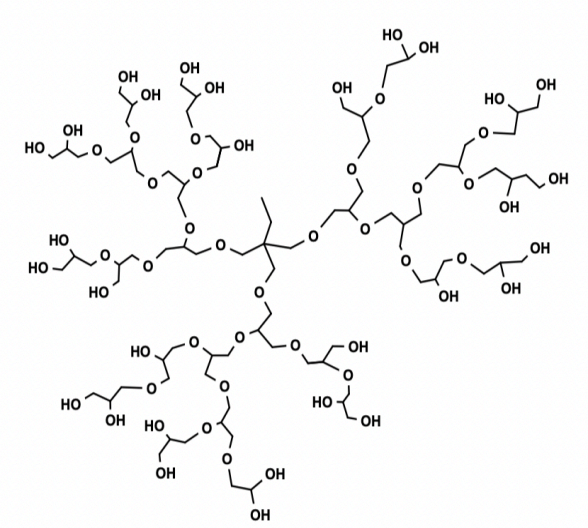

Scheme 4. Exemplary HBPG chemical structure.

Compared to PEG, HBPG is characterized by increased hydrophilicity and more efficiently covers NPs surface with no significant influence on the catalytic activity of NPs (Zamboulis *et al.*, 2019). HBPG shows excellent biocompatibility and can be used for stabilizing NPs for in vivo applications. It was proved that specific types of HBPG-stabilized NPs are blood compatible, show no immunogenic effects and low protein adsorption (Kainthan *et al.*, 2006). Moreover, HBPG-stabilized NPs are characterized by high hydroxyl groups density on the reactive surface (Hu, Zhou and Gao, 2011). NPs stabilized with HBPG show outstanding solubility in water and polar solvents (N,N-dimethylformamide, ethylene glycol, methanol), simultaneously paving the way for further NPs surface modification and biological applications. In addition, HBPG-stabilized NPs, in comparison to NPs stabilized with linear polymers are more stable in high temperatures for an extended period of time (Zhou *et al.*, 2011)

1.4.2. Electrostatic stabilization

Without the addition of the stabilizing agent, colloidal NPs are attracted to each other due to van der Waals forces. The attraction of NPs can be counterbalanced by Coulomb forces that occur between charged NPs. Van der Waals and Coulomb forces are an essential part of Derjaguin, Landau, Verwey, and Overbeek (DLVO) theory that describes the colloidal stability of NPs. In 1948 Derjaguin, Landau, Verwey, and Overbeek proposed an equation that described

the interaction of NPs in solution. According to DLVO theory, NPs stability depends on the relation between the kinetic energy of particle motion (E_k) and total potential energy (V_T). Average kinetic energy is calculated according to the classical equation:

$$E_k = \frac{mV^2}{2} = \frac{3}{2}kT$$

Total potential energy can be determined with the following equation:

$$V_T = V_A + c + V_S.$$

Where V_A is NPs attractive contribution and can be calculated as:

$$V_A = \frac{-A}{12\,\pi D^2}$$

Where A equals to Hamaker constant and D is particle separation. The following equation can be used to determine the repulsive separation V_R.

$$V_R = 2\pi\varepsilon\alpha\xi^2 \exp\,(-kD)$$

Where a is the particle radius, π describes solvent permeability, ε is the dielectric constant of the solvent, ξ is the zeta potential, and k function describes ionic composition.

If ($E_k < V_T$), NPs are not attracted to each other, they do not create aggregates and, as a result, form a stable colloidal solution. When ($E_k > V_T$), NPs are not stable and can create aggregates. Electrostatic NPs stabilization based on repulsive electrostatic force occurs for NPs surrounded by an electric double layer. This layer consists of ions adsorbed on the NPs surface and an oppositely charged layer of dispersion medium that surrounds the NPs (Kraynov and E., 2011). The electric double layer includes surface charge, stern layer, and diffuse layer (Scheme 5).

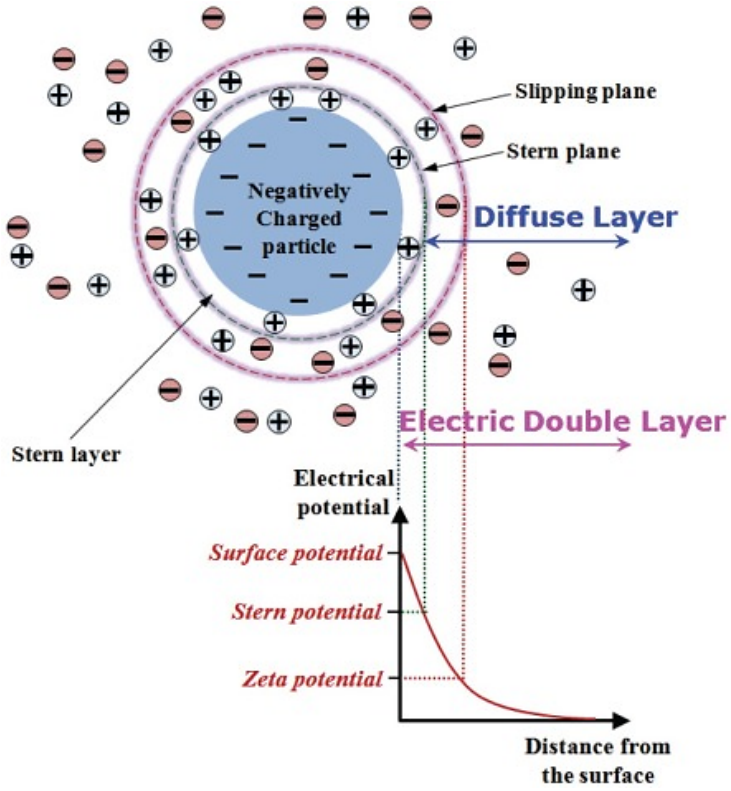

Scheme 5. Electric double layer composition (Park and Seo, 2011).

Surface charge is determined by charged ions adsorbed on the NPs surface. The stern layer is oppositely charged to surface charge and attracted to the NPs surface by electrostatic force. The diffuse layer is a region surrounding the NPs where the concentration of counterions, or ions of opposite charge to the NPs, is higher than that of other free ions in solution. Diffuse layer ions are affected by a charged particle electrostatic force. The electric double layer electrical potential decreases with an increased distance from NPs and shows the maximum value at the stern layer. The electrical potential of the electric double layer boundary is equal to 0. During movements in the solvent, NPs are attached to the layer of the surrounding liquid. The boundary of the attached layer is called the slipping plane or share plane. The zeta potential of the slipping plane electric potential is one of the main parts of the DLVO theory (Doroszkowski, 1999; Pate and Safier, 2016; Abdi *et al.*, 2022). Electrostatic stabilization can be carried out only in aqueous solutions and depends on electrolyte concentration and ionic strength (Hierrezuelo *et al.*, 2010). Citric acid and cysteamine are commonly used as Au NPs electrostatic stabilization agents. Negatively charged citric ions adsorbed on NPs surface prevent aggregation of NPs. Cysteamine-stabilized NPs, in contrast to the citric acid-stabilized ones, are positively charged (Alkilany *et al.*, 2014; Wai and New, 2020). At specific pH, thiol-containing stabilization agents can introduce a positive charge on NPs surface and increase NPs cellular uptake. To achieve a desired charge during stabilization of NPs using citric acid or

thiol-containing stabilizers, it is important to control the pH of the solution appropriately. (Hock *et al.*, 2022). Polymers, e.g. poly(diallyl dimethylammonium) chloride (PDDA) water-soluble cationic polyelectrolyte are used to synthesize Au, Ag, Pt and Pd NPs. PDDA, the same as PEG, can act as a reducing and stabilizing agent. PDDA, poly(sodium acrylate) and linear polyethyleneimine prevent aggregation of NPs due to electrostatic stabilization (Chen *et al.*, 2006; Chen, Wang and Dong, 2007). Some authors mention, that electrostatic stabilization is efficient only during a short period of time (Kraynov and Müller, 2011).

1.5. NPs application

NPs can exhibit a wide range of interesting physiochemical properties that strongly depend on factors such as material, size, shape, and surface modification. These properties can vary widely depending on the specific type of NP, and this variability can enable the use of NPs for various applications (Table 1).

Table 1. Biomedical and industrial application of metallic and metal oxide NPs.

Material	**Application**	**literature**
Au	Cancer diagnostic and therapy	(Q. Zhang *et al.*, 2022)
	Immunolabelling	(Lv *et al.*, 2021)
	Imaging	(Page Faulk and Malcolm Taylor, 1971; Lin *et al.*, 2022)
	Antibacterial agent	(Das and Patra, 2017)
	Gene therapy supporting	(Nour, Bolandi and Imani, 2020)
	Delivery of therapeutic agents	(Ray and Mitra, 2017)
	Enzymes mimetics	(Zhang *et al.*, 2020)
Pt	Antibacterial agent	(Bloch *et al.*, 2021)
	Enzymes mimetics	(Chen *et al.*, 2021)
	Cancer treatment	(Al-Radadi, 2019)
	Cocatalysts in photocatalysis	(Dong *et al.*, 2018)
	Hydrogenation reaction catalysts	(Li *et al.*, 2014)
Pd	Enzymes mimetics	(Dadigala *et al.*, 2022)
	Antibacterial agent	(Seku *et al.*, 2022)
	Cancer imaging and therapy	(Liu *et al.*, 2020)
Rh	Enzymes mimetics	(Miao *et al.*, 2020)
	Antibacterial agent	(Shin *et al.*, 2019)
	Furfuralacetone hydrogenation catalysts	(Bordet *et al.*, 2020)
Ru	Enzymes mimetics	(Ren *et al.*, 2022)
	Fischer-Tropsch synthesis catalysts	(Axet and Philippot, 2020)
	C–H activation catalysts	(Flegeau *et al.*, 2011)
Ag/Au	Enzymes mimetics	(Han *et al.*, 2015)
	Antibacterial agent	
	Cancer therapy	(Shanmugasundaram *et al.*, 2017)
	Computed tomography imaging agent	(Chu *et al.*, 2019)
Ag/Pd	Electrocatalytic reduction of benzyl chloride catalysts	(An *et al.*, 2011)
	Hydrogenation catalysts	(Lu *et al.*, 2014)
	Enzymes mimetics	(Aghahosseini *et al.*, 2021)
Ag/Pt	Enzymes mimetics	(He *et al.*, 2010)
Pt/Au	Photocatalysts for hydrogen production	(Ding *et al.*, 2016)
	Enzymes mimetics	(Zhang *et al.*, 2022)
Pt/Pd	Oxygen-reduction reaction catalysts	(Lim *et al.*, 2009)
Pt/Ru	Enzymes mimetics	(Gupta, Son and Seong, 2021)
TiO_2	Photocatalysis	(Wilkes and Zaworotko, 1992)
	Pollutant elimination	
	Solar cells	
Ce_2O_3	Antibacterial agent	(Abid *et al.*, 2020)
	Enzymes mimetics	(Wang *et al.*, 2019)
	Angiogenesis inhibitor	(Chaudhury *et al.*, 2013)
ZnO	Antibacterial agent	(Hatamie *et al.*, 2015)
	Photocatalytic degradation of organic pollutant	
	UV-blocking agent	
Fe_3O_4	Thermal and immune therapies	(Soetaert *et al.*, 2020)
	Enzymes mimetics	(Wang *et al.*, 2020)
	Drug delivery	(Vangijzegem, Stanicki and Laurent, 2019)
	Proteins, cells, and microorganism magnetic separation	(Xu *et al.*, 2011; Hola *et al.*, 2015; Thomas *et al.*, 2020)
	Imaging	(Israel *et al.*, 2020)z
Al_2O_3	Antibacterial agent	(Baghdadi *et al.*, 2022)
	Drug delivery	(Aramesh *et al.*, 2017)
	Cell imaging	
	Intracellular cargo monitoring	
	Cancer therapy	(Hassanpour *et al.*, 2018)

The optical properties of NPs are utilized for labelling and imaging proteins, cells and microorganisms (Meder *et al.*, 2016). One of the most important NPs characteristics is the high surface-to-volume ratio which is responsible for the high catalytic activity of NPs and the ability to interact with other particles. Due to their high activity, metal-based NPs (NPs) are highly effective industrial catalysts for hydrogenation, C-C coupling reactions, and the production of alternative fuels. (Roucoux, Schulz and Patin, 2002; Navalón and García, 2016). NPs ability to mimic the activity of biological catalysts and catalyze the formation of electrochemically active, coloured, and luminescent products are widely used in analytical methods and therapies (Ren *et al.*, 2022). In medicine, they have been explored as a means of delivering drugs in various treatment methods such as radiotherapy and phototherapy. NPs also have bioactive properties that make them promising agents for cancer therapy. For example, NPs can cause cell apoptosis via cell cycle arrest, biomolecule damage and cell energy metabolism disruption (Miranda, Sampaio and Zucolotto, 2022). Moreover, NPs can bind or penetrate bacteria cell wall and cause bacterial death (Hatamie *et al.*, 2015; Gavrilenko *et al.*, 2019; Shin *et al.*, 2019; Abid *et al.*, 2020; Seku *et al.*, 2022). NPs usage in analytical methods can be divided into sample treatment before measurement and analytical signal generation or enhancement. According to the main topic of this work, the description of NPs application in analytical methods is focused on NPs usage as catalytic labels and as agents for antigen separation and manipulation.

1.5.1. NPs application in samples premeasurement treatment

Biological samples are multi-component and complex. The presence of interferents in samples can affect results of analyses and cause high background noises, which is why it is crucial to follow specific sample preparation steps before measurement. Interferents can also compete with antigens and produce false positive or negative results. To avoid such drawbacks, magnetic NPs can be used. Modified metal oxide NPs which show supermagnetic/paramagnetic activity can be used for the extraction and purification of bio-macromolecules. Such NPs are biocompatible and easy to synthesize and modify. The magnetic NPs separation process can be divided into two steps: interaction with the target molecule and their relocation using a magnetic field. For high specificity and sensitivity of interaction with biomolecules, magnetic NPs are modified with ABs (Asgharnasl *et al.*, 2020). Compared to classical protein separation methods such as chromatography and electrophoresis, magnetic NPs-based separation is characterized by good efficiency, simplicity, low cost, and high operation speed. In addition, magnetic NPs-based separation does not require specific sample preparation (centrifugation of filtration) (Tran and Webster, 2010).

Supermagnetic or paramagnetic NPs can also help in the case of the situation when an analyte is present in a very low concentration in a sample (Eivazzadeh-Keihan *et al.*, 2021). For example, iron oxide magnetic NPs are used to separate circulating tumour cells (CTCs) from whole blood samples before cytometric detection. Examination of CTCs presence in whole blood samples is a double challenge but is very important for the early stages of cancer diagnosis (Lin *et al.*, 2021). First of all, CTCs concentrations, depending on cancer type, can range from 0 to 50 per ml of a blood sample. Compared to CTC, human blood contains between $3\text{-}9\cdot10^9$ blood cells per ml and $3\text{-}10\cdot10^6$ per ml. Therefore, only 0 to 50 CTCs can be present in 10 billion blood cells. Secondly, whole blood is a very complex sample and requires special preparation to be used for CTCs detection. For instance, such samples should be diluted with several buffers and centrifuged before cytometric detection of CTCs. Mentioned sample pre-treatment can destroy some CTCs, thus decreasing their concentration. ABs-modified iron oxide NPs with bind to CTCs and, via the following magnetic field, separate the analyte from the sample and concentrate it. Therefore, iron oxide NPs application successfully solves declared challenges and improves the detection sensitivity (Xu *et al.*, 2011). As mentioned, magnetic NPs can be used in sample preparation before analytical examination and for analytical signal generation. For example, iron oxide NPs show peroxidase-like activity and can play the role of the catalytic label. Peroxidase-like activity of iron oxide NPs is lower than other peroxidase mimetics. To enhance the enzyme-like activity of magnetic NPs they can be decorated with Au or Pt (Kim *et al.*, 2017).

1.5.2. Application of NPs as catalysts

As it was mentioned, NPs have been used as catalysts due to their unique properties. Their small size and large surface area can result in a high number of active sites for catalytic reactions, which lead to increased catalytic activity. Additionally, NPs have a high surface-to-volume ratio which can make them more reactive than larger particles of the same composition. The catalytic properties of metal-based nanocatalysts are highly dependent on various factors, including the size, shape and overall morphology.

NPs can be used as catalysts in heterogeneous reactions, which occur at the interface between the solid catalyst and the reactant present in the gaseous or liquid phase. It must be mentioned that in the case of colloidal solutions of NPs, the heterogeneous mechanism of catalysis is also often indicated. As a result of this mechanism, substrates adsorb on the surface of such catalysts, and then the formation of the desired products is observed. It is also true for nanozymes. (Ni and Wang, 2015; Sápi *et al.*, 2021). Modification of the size and shape of NPs

can also improve catalytic activity. This is because the number of active sites increases, leading to improved accessibility. For example, star-shaped Ag NPs have been found to have more active sites than spherical and pyramid-shaped Ag NPs (Waqas, Zulfiqar and Ahmad, 2018).

NPs can also exhibit a homogeneous mechanism of catalytic activity. Homogeneous catalysis refers to a scenario where the catalyst is present in the same phase as the reactants, specifically in a liquid or gaseous state; for the colloidal solution of NPs it seems obvious that such criterion is met, but as it was mentioned above, the heterogenous mechanism is indicated in such a case. This type of catalysis is observed for NPs is not the most typical in their case and the digestion of the NPs-based catalyst in the reaction medium, which allows for intimate mixing between the reactants and the catalyst, leading to enhanced catalytic activity (Harvey *et al.*, 2019), can be given as an example. Homogeneous catalysis can also therefore based on catalytically active ions released (intentionally or not intentionally) from NPs. For example, digesting of CuO NPs in HCl can result in the release of catalytically active Cu^{2+}. These ions have been reported to act as nanozymes (Sun, Xia and Yuan, 2020). Under specific conditions, Co^{2+} similarly to Cu^{2+} exhibits peroxidase-like activity through a homogenous mechanism (Gao, Xu and Liu, 2020; Xu, Xue and Sai, 2022). The ions released from NPs can act as co-catalysts and enhance the overall catalytic activity of the NPs. In this scenario, NPs act as a source of catalytically active ions and can follow both homogeneous and heterogeneous (because NPs in some cases are still present) catalytic activity mechanism depending on the reaction conditions (Yan, Yuan and Dyson, 2013).

Ions released from NPs can be potentially harmful for living organisms. For example, the release of metal ions from metal NPs can lead to toxicity in living systems, particularly in the case of NPs made of heavy metals, such as silver. These ions can interact with biomolecules, such as proteins and DNA, leading to cellular damage and potentially causing adverse effects on the health of living organisms. (Sorinolu *et al.*, 2022). On the other hand, such mechanism is often responsible for the antimicrobial activity of NPs (Godoy-Gallardo *et al.*, 2021).

1.5.3. Nanozymes as promising alternative for natural enzymes

During the last decade, the application of biotests and biosensors in medicine, food industry, and environmental control sharply increased. A big group of such analytical devices is based on natural enzymes as catalysts due to their efficiency and selectivity. Production, storage, and usage of enzymes usually require special conditions and equipment, which are often associated with high costs. In addition, natural enzymes usually cannot be reused or

recycled. To solve such issues, the efficient alternative for natural enzymes was developed. In 1970 in Breslow's and Overman's pioneering work was given a definition that artificial enzymes are "imitating the catalytic processes that occur in living systems" (Breslow and Overman, 1970). It was discovered that cyclodextrins and their derivatives could mimic catalytic activity of enzymes like hydrolases or cytochromes. Such discovery inspired scientists to test numerous materials as natural enzyme mimetics (Wang *et al.*, 2016). It was proven that some metal, metal oxide, carbon-based NPs, and metalorganic framework-based nanomaterials can mimic the catalytic activity of natural enzymes (Sun *et al.*, 2016; Yang *et al.*, 2017; Fan *et al.*, 2018; Stasyuk *et al.*, 2020; Khade *et al.*, 2021). In 2004 Pasquato, Screamin, and their co-workers termed NPs with enzyme-like activity as "nanozymes" (Manea *et al.*, 2004). It was discovered by Gao et al. in 2007 that Fe_2O_3 NPs can mimic the activity of peroxidase and be used in immunoassays (Gao *et al.*, 2007). Later in 2013, Wei and Wang published work that defined nanozymes as "nanomaterials with enzyme-like characteristics" (Wei and Wang, 2013).

In comparison to natural enzymes, metal and metal oxide-based nanozymes are more stable and save their catalytic activity in a wide range of pH and temperature, do not require special equipment for storage or production, and can be reused multiple times (Wei and Wang, 2013; Nath, Chakraborty and Verpoort, 2016; Chen *et al.*, 2018; Wu *et al.*, 2019). In addition, due to unique physicochemical properties, metal and metal oxide-based nanozymes can be structurally modified and moreover, chemically and biologically functionalized, which increase their application range (Liang and Yan, 2019). Moreover, there is the possibility of combining two or more metals in one type of nanoparticle, which is coming together with a combination of specific properties derived from each metal individual properties and the appearance of new properties (Pietrzak and Ivanova, 2021). It was described that some metal and metal oxide-based nanozymes, like natural enzymes, obey Michaelis–Menten kinetic model toward glucose, H_2O_2, some peroxidase substrates, and starch (Lewandowska, Wójciuk and Karczmarczyk, 2021).

It was proved that some noble metal NPs can mimic the activity of peroxidase, catalase, oxidases, nitrate reductases, and hydrolases (Chen *et al.*, 2020; Lan *et al.*, 2014; Li *et al.*, 2015; Ye *et al.*, 2016; Landry *et al.*, 2017; Huang, Ren and Qu, 2019; Liang and Yan, 2019; Weerathunge *et al.*, 2019; Xi *et al.*, 2020; Logan *et al.*, 2020; Pietrzak and Ivanova, 2021).

1.6. Activity mechanism of peroxidase mimetics

There are different theories explaining peroxidase-like activity mechanisms of nanozymes. According to one of them, activated H_2O_2 adsorbed on NPs surface can donate

electron, experiences decomposition with hydroxyl and oxygen superoxide anions formation. Formed radicals take part in substrate oxidation reactions. In some cases, the peroxidase-like activity of Au, Pt and Pd NPs can follow the so-called "one-step electron transfer mechanism" when negatively charged NPs electrostatically react with positively charged substrates. The reaction between NPs surface and hydrogen peroxide is based on electron transfer, which leads to the formation of two hydroxyl radicals. These radicals participate in the oxidation reaction of the peroxidase substrate (Das *et al.*, 2021).

Another theory proposed that the peroxidase-like activity of nanozymes can be described as an electron transfer process or Fenton-like reaction (Scheme 6) (Adeniyi, Sicwetsha and Mashazi, 2020).

$$Fe^{2+} + H_2O_2 \longrightarrow Fe^{3+} + OH^{\bullet} + OH^{-}$$

$$Fe^{3+} + H_2O_2 \longrightarrow Fe^{2+} + OH_2^{\bullet} + H^{+}$$

Scheme 6. Fenton-like reaction.

Fenton reaction was first presented in 1894 for tartaric acid oxidation by H_2O_2 in the presence of ferrous ions (Fenton, 1894). Horseradish peroxidase (HRP), a haem-containing enzyme, like ferrous ions, can take part in the Fenton reaction under weakly acidic conditions and react with organic compounds (Liu, Huang and Liu, 2022).

According to reaction (Scheme 7), proposed by Wang et al., hydrogen peroxide is adsorbed on Fe_3O_4 NPs surfaces and activated by $Fe^{2+}$and Fe^{3+} derived from NPs.

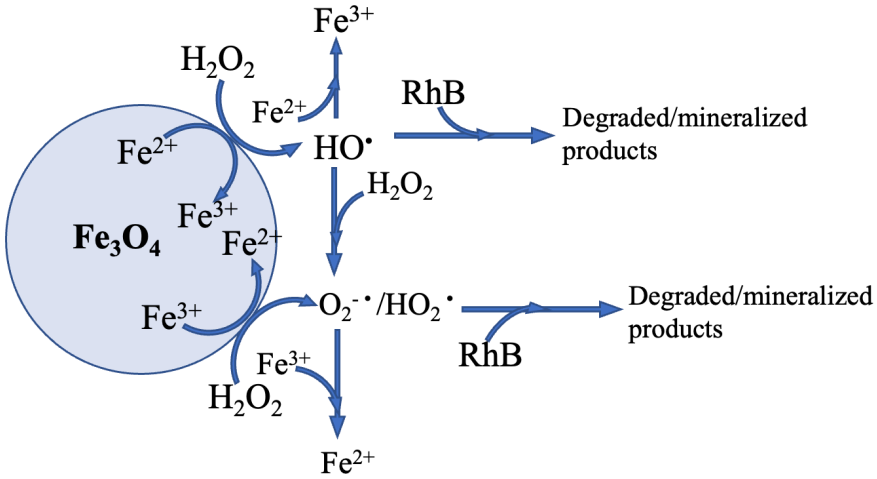

Scheme 7. Mechanism of Fe_3O_4 NPs peroxidase-like activity proposed by Wang et al.

As a result, $^{\cdot}OH$ and $O_2^{\bullet-}/HO_2^{\bullet}$ radicals are produced and participate in the substrate (RhB) degradation and mineralization process (Wang *et al.*, 2010).

In 2011, Voinov et al., based on the spin-trapping electron paramagnetic resonance (EPR) experiments, made another explanation of NPs peroxidase-like activity mechanism (Scheme 8).

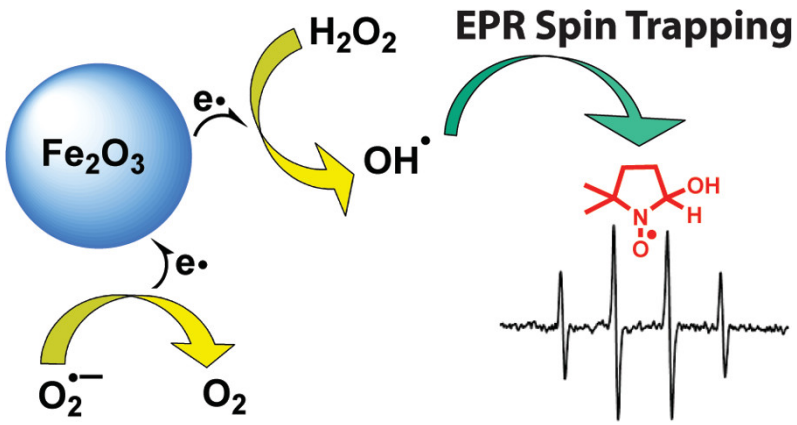

Scheme 8. NPs peroxidase-like activity mechanism provided by ERP spin-trapping (Voinov et al., 2011)

According to experimental results, Fe_2O_3 NPs acted as heterogeneous catalysts in Fenton-like reaction of surface-mediated production of •OH radicals (Scheme 9).

$$Fe^{2+} + H_2O_2 \longrightarrow Fe^{3+} + OH^- + OH\cdot$$

Scheme 9 Fenton-like reaction initiated by Fe_2O_3 NPs.

In addition, it was shown that the catalytic effect derived from Fe_3O_4 NPs surface was stronger than the catalytic effect from dissolved ions (Voinov *et al.*, 2011). The electron transfer-based mechanism was also used as the peroxidase-like activity explanation of other metal and metal oxide NPs. For example, it was proposed that Ir NPs work as electron transfer mediators between H_2O_2 and a substrate. A similar mechanism was described for MnO_2 nanowires. Due to substrate oxidation, one electron is transferred to MnO_2 nanowire and then donated to H_2O_2 (Cui *et al.*, 2017). The identical activity mechanism was described for Co_3O_4, gold@carbon dots, and FePt-Au hybrid NPs (Mu *et al.*, 2012; Zheng *et al.*, 2016).

1.7. Methods for peroxidase-like activity detection

1.7.1. Spectrophotometric methods of peroxidase-like activity detection

In numerous works, NPs are defined as peroxidase mimics if such NPs catalyze reactions with typical enzyme substrates, however, the detailed investigation and description of the activity mechanism are not given. *o*-phenylenediamine, 4-aminoantipyrine/phenol, 3,3',5,5'-tetramethylbenzidine, 2,2′-azino-bis(3-ethylbenzothiazoline-6-sulfonic acid) diammonium salt, 3,3′-diaminobenzidine, pyrogallol, and 3-amino-9-ethylcarbazole are used as substrates which

in presence of natural peroxidase or peroxidase mimics and H_2O_2 lead to the formation of the same product (He *et al.*, 2014; Lin *et al.*, 2018; Zhuge *et al.*, 2019; F. Nie *et al.*, 2020; Mahmudunnabi *et al.*, 2020). Mentioned substrates are oxidized to coloured products formation or initial solution decolourization is observed. Such a process can be evaluated spectrophotometrically. Spectrophotometry is a common, comparatively simple and cheap analytical technique (Germer, Zwinkels and Tsai, 2014).

1.7.1.1. *o*-phenylenediamine (OPD)

OPD aromatic amine is a colourless and nonfluorescent chromogenic horseradish peroxidase substrate. In the presence of H_2O_2 and natural enzyme or HRP mimetics, OPD is oxidized to coloured, fluorescent and electrochemically active product 2,3-diaminophenazine (DAP) (Scheme 10) (Zhao *et al.*, 2016; Yu *et al.*, 2017; Abdel-Lateef, 2022; L. Li *et al.*, 2022).

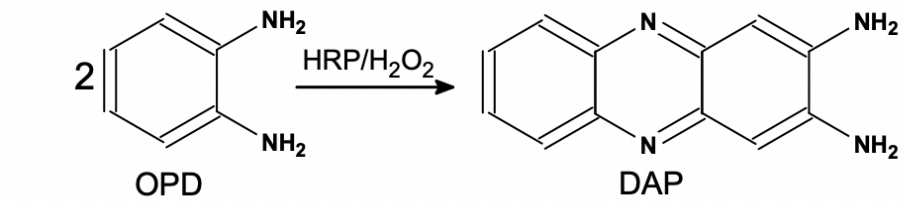

Scheme 10. OPD oxidation and DAP formation in presence of catalysts.

The optimum pH range for DAP formation is 5.0-6.0 The formation of yellow-orange DAP can be detected with spectrophotometry (at 450 nm) and fluorescence spectroscopy (λ_{ex}=412 nm, λ_{em}=568 nm) (Liu *et al.*, 2018). DAP is a stable product under weak acid conditions that plays an important role in kinetic measurements and makes OPD a popular substrate for HRP and HRP-like activity in bioanalytical assays. OPD can be easily oxidized in the presence of H_2O_2, atmospheric oxygen and light before the addition of catalyst. Such spontaneous oxidation can be avoided by optimizing substrate preparation processes (avoidance of light, using deionized and deoxygenated water) (Minic and Zivkovic, 2021).

1.7.1.2. 3,3',5,5'-tetramethylbenzidine

Peroxidases can work as catalysts in aromatic amines and benzidine oxidation reactions. Such a reagent was used in the "Benzidine test" test to detect fecal occult blood. Benzidine test is based on peroxidative properties of red blood cells, which catalyse oxidation of benzidine and formation of blue product (Culliford and Nickolls, 1964). In 1974, Holland et al. synthesized 3,3',5,5'-tetramethylbenzidine (TMB). Compared to benzidine, TMB substrate is characterized by lower carcinogenic properties and TMB-based assays are characterized by

higher sensitivity (Josephy, Eling and Mason, 1982). In addition, chromogenic oxidation of TMB is characterized by low spectral background, which is very important for developing sensing systems with high sensitivity (Huang *et al.*, 2018). TMB oxidation mechanism was investigated using spectroscopy methods and electron spin resonance. The first stage (λ_{max}=285 nm) of TMB oxidation in the presence of HRP and H_2O_2 started with TMB electron donation and formation of TMB cation radical, or charge transfer complex consisting of electron donor diamine (λ_{max}=370 nm) and electron acceptor diamine (λ_{max}=652 nm). TMB cation radical can be in rapid chemical equilibrium with charged transfer complex. The second stage was based on two electrons donation and the formation of diamine (λ_{max}=285 nm) (Scheme 11).

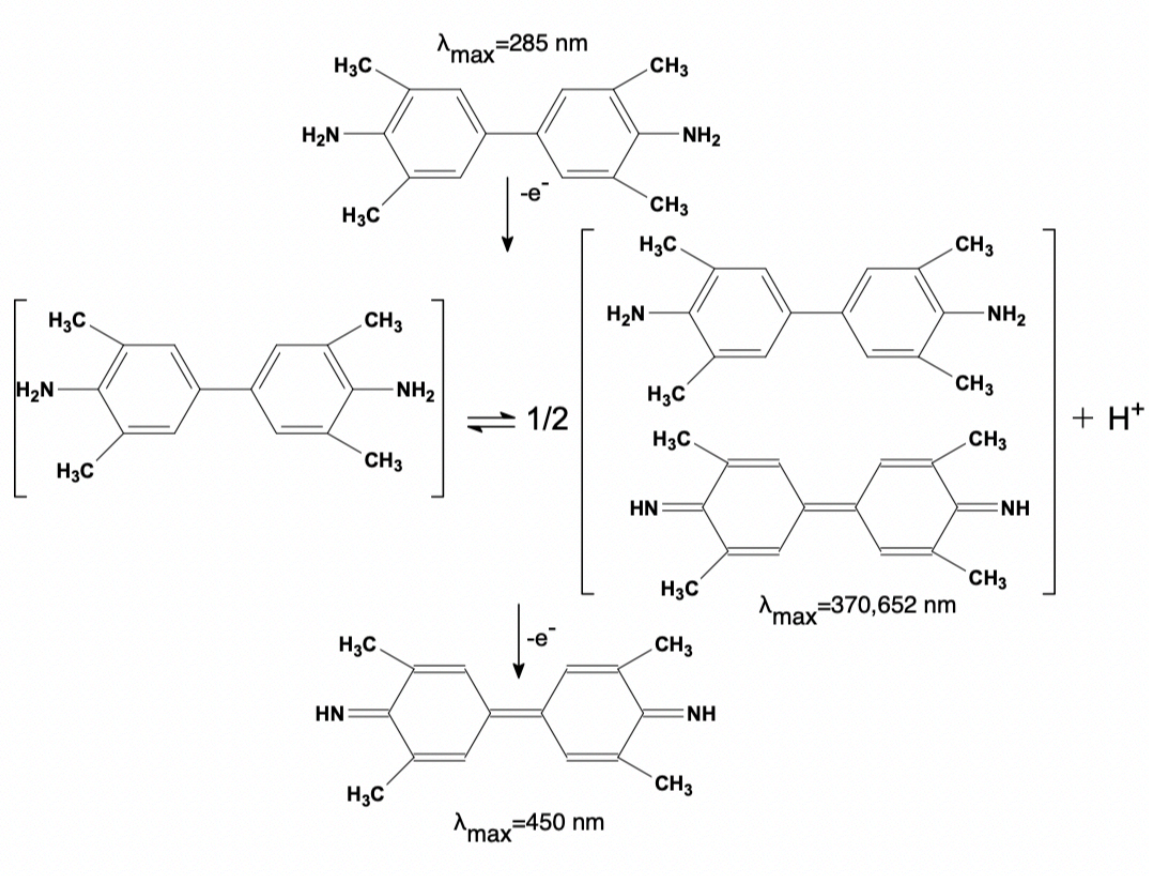

Scheme 11. TMB oxidation reaction in presence of hydrogen peroxide and peroxidase mimetics.

During experiments provided by the Josephy group in 1982, it was discovered that when H_2O_2 was present in a sufficient amount, all TMB molecules were expected to convert into diamine form Also, it was reported that TMB charge transfer complex and diamine have different optical properties and based on that fact, molar absorption constants were determined (ε_{652} = 3.9 x 10^4 M^{-1} cm^{-1} for charge transfer complex and ε_{450} = 5.9 x 10^4 M^{-1} cm^{-1} for diamine

product at pH 5.0 (Josephy, Eling and Mason, 1982). These molar absorption constants were commonly accepted and are used till today without any changes and additional experimental approval.

It was studied that TMB oxidation, carried out in the presence of platinum NPs immobilized in spherical polyelectrolyte brushes that show HRP-like activity, follows the same reaction stages as TMB oxidation with natural enzyme (Gu *et al.*, 2020).

1.7.1.3. ABTS

In 1964, Hünig et al. described reactions of one- and two-electron ABTS chemical oxidation (Hünig, 1964). Later in 1975, ABTS was described as a chromogenic substrate for HRP, and since then, it has become a very popular substrate for immunoenzymatic assays. HRP can catalyze the ABTS one-electron oxidation in the presence of H_2O_2 (Scheme 12).

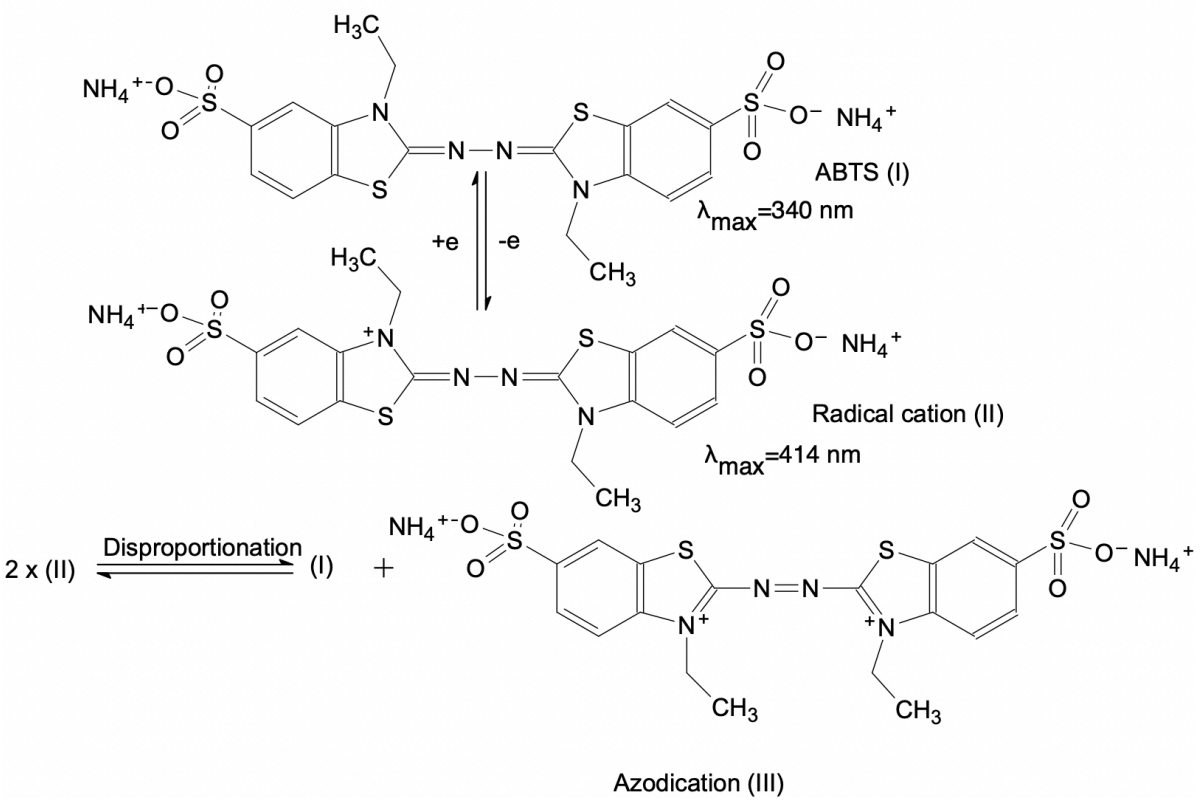

Scheme 12. ABTS oxidation reaction pathway.

As a result of such reaction the metastable radical cation with an absorbance maximum at 414 nm (ε_{414}=3.6×10^4 M^{-1} cm^{-1}) is formed. Formed metastable radical cation slowly disproportionates to ABTS and azodication. Due to the cationic nature of the product, the reaction should be provided in acidic mediums. The speed of disproportionation is comparatively low (more than 10 min), which allows detection of radical cation formation and can be neglected during HRP catalyzed kinetic reactions (Hünig, 1964). The successful usage

of ABTS as HRP substrate inspired the researchers to apply chromogenic reagents to investigate the peroxidase-like activity of nanomaterials. It was described that Fe_2O_3, Au, AuAgPd, Ag, and CeO_2 NPs can catalyze formation of colour ABTS product (Wang *et al.*, 2012; Nie, Shi and Yu, 2016; Kumar, Chandrasekaran and Mukherjee, 2018; Yang *et al.*, 2018; Kong *et al.*, 2021)

1.7.1.4. Phenol/4-aminoantipyrine

4-aminoantipyrine (4-AAP), under acidic conditions, in the presence of oxidising agent, can take part in a condensation reaction with primary, secondary and tertiary aromatic amines (Emerson, 1943). Under alkaline conditions, in the presence of an oxidising agent 4-AAP reacts with phenol (PhOH), primary and secondary amines to form a coloured reaction product (Scheme 13).

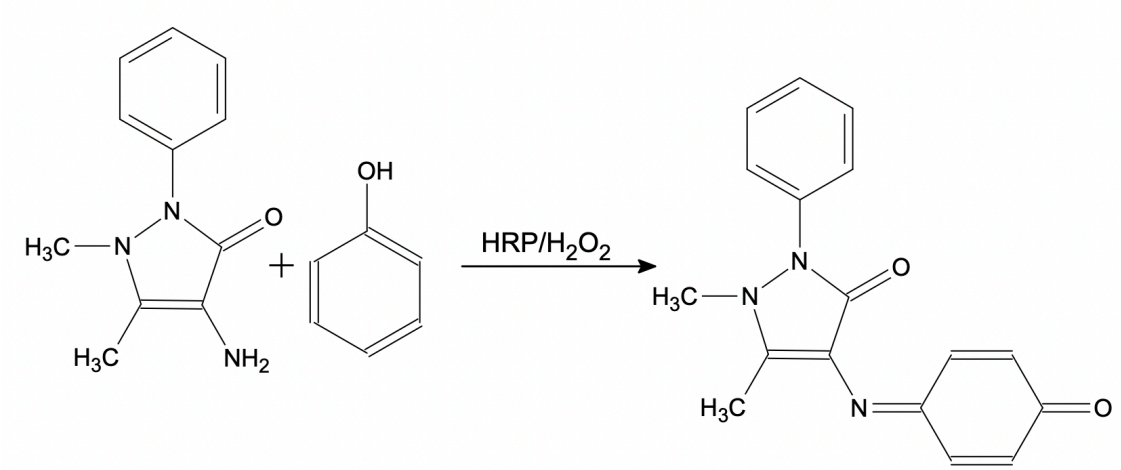

Scheme 13. 4-AAP/PhOH oxidation reaction under alkaline conditions in the presence of oxidising agent.

In 1938, Emerson described the reaction of PhOH with 4-AAP maintained in the presence of cupric ions in ammoniacal solution (Edgar I. Eisenstaedt, Chicago, Ill. and Emerson, 1938). In 1943, Emerson presented a spectrophotometric method of phenol detection based on 4-AAP usage (Emerson, 1943). This method has become very popular among phenol detection methods due to its low cost, simplicity, and speed. In 1953, Powell and Smith presented a method for alkaline phosphatase detection and enzyme activity examination based on the usage of 4-AAP and PhOH (Powell and Smith, 1954). Trinder was inspired by the phosphatase detection method when 4-AAP and PhOH react in the presence of the oxidizing agent, and a coloured product was formed. Trinder assumed that H_2O_2 could play the role of an oxidation agent in the 4-AAP/PhOH reaction.

In 1956, during glucose detection method development, Trinder discovered that 4-AAP/PhOH system could be used for H_2O_2 and HRP detection (Trinder, 1969). Despite the high popularity of the 4-AAP-based method for PhOH detection, the same substrate is not often used in HRP detection. In the presence of H_2O_2, PhOH is oxidized and phenoxyl or 2,5-cyclohexadienone radicals are formed. Later, phenoxide radical reacts with 4-AAP to form 4-AAP radical. Finally, coloured quinone imide (λ_{max}=506 nm) is formed during the coupling reaction of 4-AAP radical with 2,5-cyclohexadienon (Scheme 14) (Fontana *et al.*, 2019)

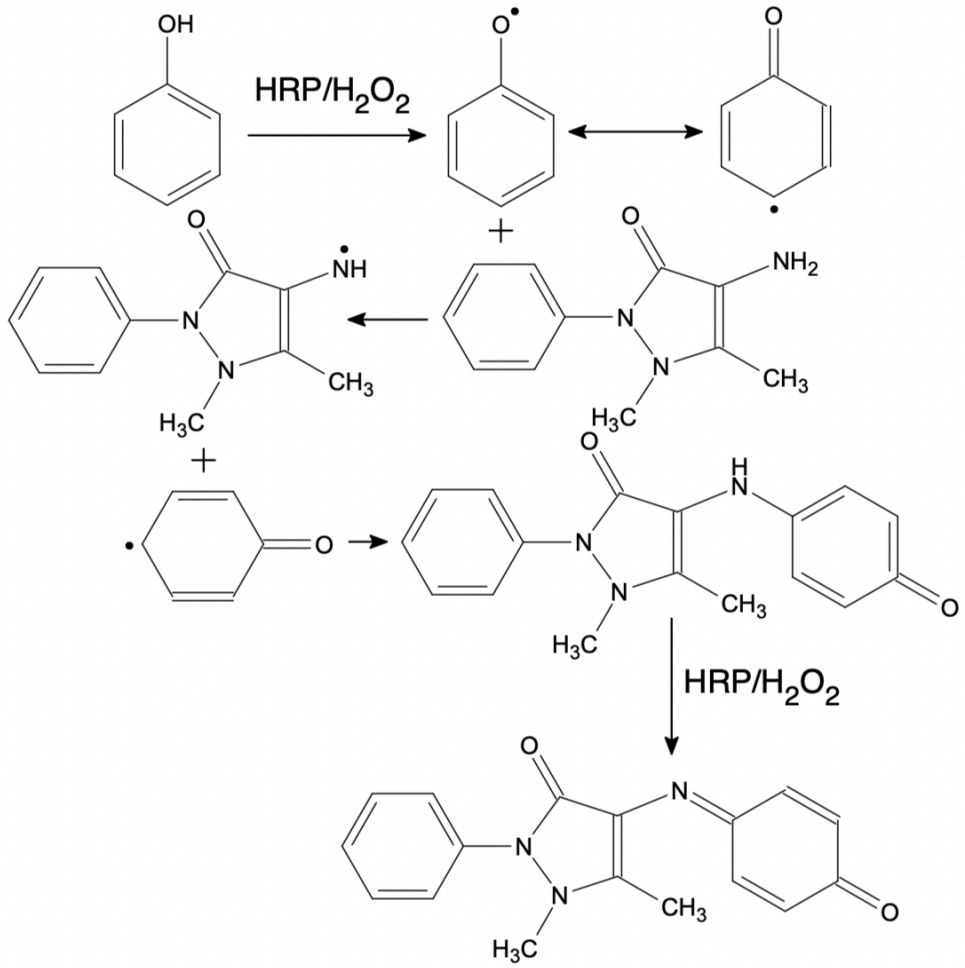

Scheme 14. Quinone formation catalyzed with HRP in presence of H_2O_2.

Since phenolate plays an essential role in quinone imide formation, such reactions should be carried out in a basic environment. 4-AAP/PhOH containing mixture can be used as a substrate for HRP-mimetic. For example, such substrate was used to determine the peroxidase-like activity of glass-beads modified with metal-porphines, single-atom copper anchored on bovine haemoglobin-template gadolinium NPs, and Fe_2O_3 NPs (Mifune *et al.*, 2000; Wu *et al.*, 2020; S. Li *et al.*, 2022).

1.7.1.5. Bromopyrogallol red

2-(2,7-dibromo-4,5,6-trihydroxy-3-oxo-3H-xanthen-9-yl) known as bromopyrogallol red (BRP) was initially used as a chromogenic pH indicator. In 1985, Ansari and Ottaway patented the BRP-based method for Cu^{2+} detection. Later, in 1992, the BRP-based method for vanadium ions detection was presented (Gao, Morison and Kundur, 1992). In 1999, Guo and Shen discovered that BRP could also be used as a peroxidase substrate. The authors used BRP for HRP, H_2O_2 and glucose detection and quantification (Guo, Li and Shen, 1999). Scheme 15 represents BRP decolorisation reaction in presence of hydrogen peroxide and peroxidase mimetics.

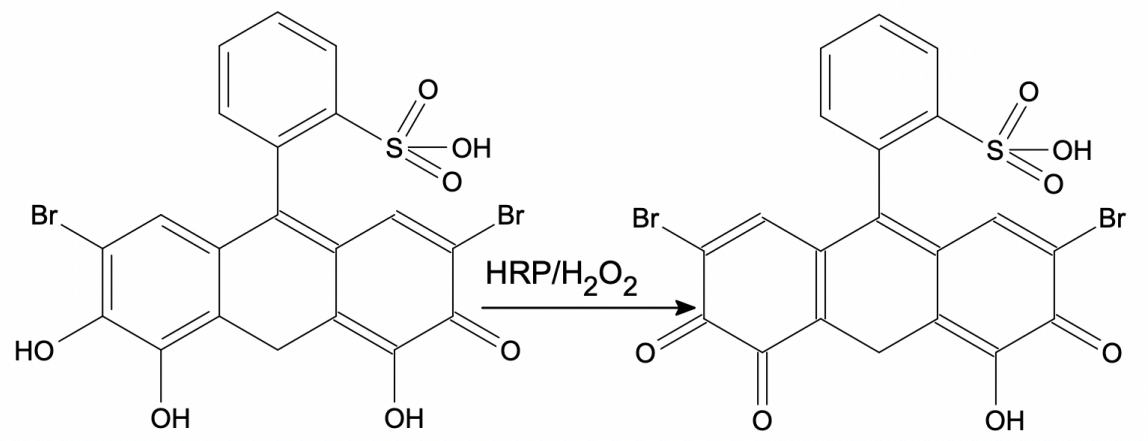

Scheme 15. BRP decolorization reaction in presense of hydrogen peroxide and peroxidase or its mimetics.

Compared to OPD, TMB and ABTS, catechol derivatives can work as HRP or HRP-mimetic substrates in pH >5.0. However, in the presence of oxygen, catechol derivatives are unstable and autoxidize with the formation of superoxide radical anions (Marklund and Marklund, 1974; Llobat-Estelles, Sevillano-Cabeza and Medina-Escriche, 1986; Mochizuki *et al.*, 2002).

1.7.1.6. Pyrogallol

Another catechol derivative which can be used as a peroxidase substrate is the pyrogallol (PG). Historically, such reagent was used for metal cations and oxygen detection. For example, in alkaline solutions, PG forms a yellow compound in presence of niobium oxalate complex (Lee, Price and Land, 1956). The same coloured product, purpurogallin imide (λ_{max}=420 nm) can be formed during the oxidative coupling reaction of PG in the presence of HRP (Scheme 16) (McCarthy and White, 1983).

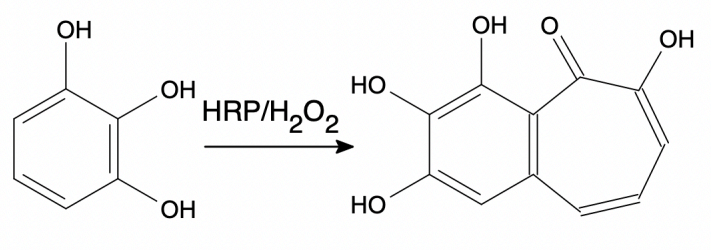

Scheme 16. Conwertion of pyrogallol to purpurogallin in presence of peroxidase or its mimetics.

In the literature, there are several examples of the PG application as a substrate for peroxidase mimetics, such as Au, Pt, graphene-based and prussian blue/nickel hexacyanoferrate core-shell NPs (S. Bin He *et al.*, 2014; Garg, Bisht and Ling, 2015; Drozd *et al.*, 2016; Karpova *et al.*, 2021).

1.7.1.7. 3,3'-diaminobenzidine

Benzidine derivative (DAB) is the primary precursor for polybenzimidazole fibre, characterized by unique thermal and chemical stability (Bocarsly and Niangar, 2009). In the presence of peroxidase and H_2O_2, DAB takes part in the oxidative coupling reaction of polycondensation with the formation of insoluble coloured indamine polymer. Formed indamine polymer participates in oxidative cyclization and formation of phenazine polymer (Scheme 17).

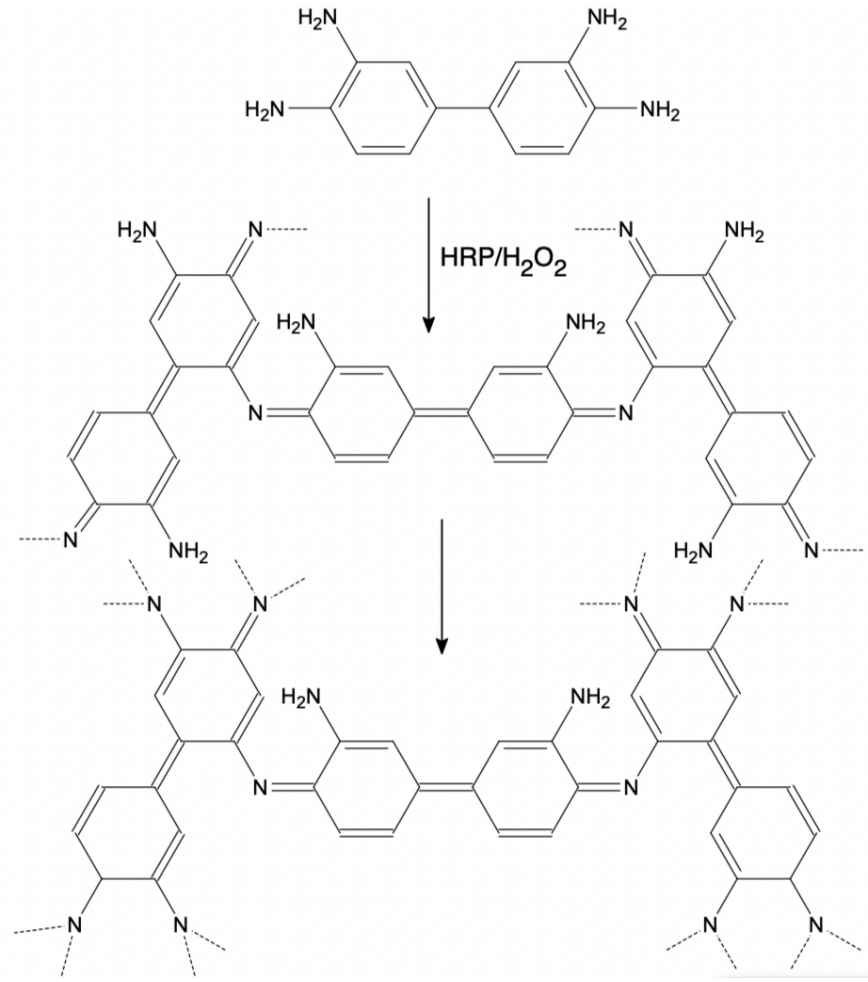

Scheme 17. DAB oxidative polycondensation coupling reaction with formation of insoluble coloured indamine polymer.

Due to DAB ability to form coloured stable precipitate in the presence of peroxidases, DAB is very popular for tissue staining in electron microscopy, immunohistochemistry, blotting and detection of endogenous peroxidases (Krieg and Halbhuber, 2010). Furthermore, due to heat resistance, DAB can be used in immunohistochemistry/in situ hybridisation dual-labelling protein and RNA presence/localization detection methods (Lopez, 2014). In addition, it was reported that DAB was used for the determination of the peroxidase-like activity of such NPs as Ir, Co_3O_4, Fe_3O_4, Au/Pt and platinum/graphene-oxide hybrid ones (Gao *et al.*, 2007; Dong *et al.*, 2014; Lin *et al.*, 2015; Amourizi, Dashtian and Ghaedi, 2020; Panferov *et al.*, 2020).

1.7.2. Fluorescence-based detection of peroxidase activity

Fluorescence spectroscopy is another technique which can be applied for peroxidase and peroxidase-like activity detection. After excitation, intensity fluorescence (the emitted electromagnetic radiation) is measured (Kannan *et al.*, 2022). Fluorescence spectroscopy, due to its direct measurement method, has a lower detection limit and can be up to 1000 times more sensitive than spectrophotometry.

In addition, the emitted electromagnetic radiation can be controlled by changing the intensity of the excitation energy. (Karoui, 2018). The most popular peroxidase substrates used in combination with spectrofluorimetry are described below.

1.7.2.1. Terephthalic acid

Since 1980, conversion of non-fluorescent terephthalic acid (TA) to highly fluorescent hydroxyterephthalic acid (TAOH) (λ_{ex}=300 nm, λ_{em}=425 nm) has been widely used in chemical dosimeters (Matthews, 1980; Brandenburg and Moll, 1984). In 1993, Faust and Allen used TA to determine hydroxyl radicals, and in 1995 Fang and co-workers studied the reaction mechanism of the fluorescent product formation from TA (Scheme 18).

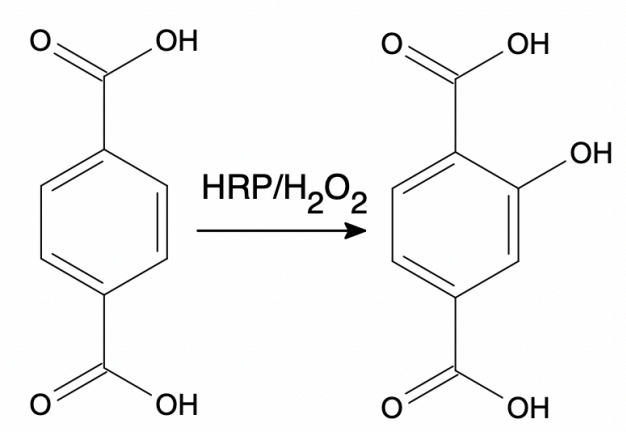

Scheme 18. Conversion of non-fluorescent TA to highly fluorescent hydroxyterephthalic acid in presence of peroxidase or its mimetics.

Fang *et al.* described the reaction of TA hydroxylation dependence on oxygen presence in the sample. It was shown that in the O_2-free reaction system, TAOH formation yield could be up to 84%, and the presence of O_2 decreased TA hydroxylation yield to 35%. Authors explained changes in TAOH formation efficiency by the different positions of hydroxy radical addition to carboxylate groups (Faust and Allen, 1993; Fang, Mark and von Sonntag, 1996).
Natural peroxidases and NPs with peroxidase-like activity can catalyze the reaction of TAOH formation in the presence of hydrogen peroxide. Due to high reaction efficiency and reaction system stability, TA is the most popular fluorogenic substrate for peroxidase-like activity determination of metal and metal oxide NPs (Xiang *et al.*, 2016; Li *et al.*, 2018; Wu, Gao and Du, 2019; Q. Wang *et al.*, 2020; Song *et al.*, 2020).

1.7.2.2. Amplex Red™

Amplex Red™ is the commercial name of 10-acetyl-3,7-dihydroxyphenoxazine developed by biotechnology company Molecular Probes for the detection of hydrogen peroxide released as a result of processes in biological samples (Karakuzu *et al.*, 2019). Peroxidase, in

the presence of hydrogen peroxide, in solutions of pH 7.0-8.0, can catalyse oxidation of Amplex Red™ with the formation of red fluorescence product resorufin (Scheme 19).

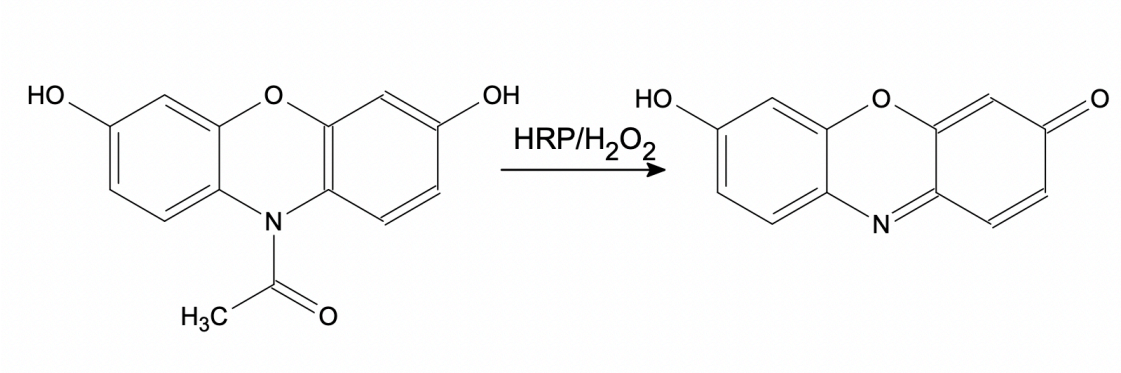

Scheme 19. Oxidation reaction of Amplex Red™ and resorufin formation.

Such process is based on deacetylation of nitrogen atom of Amplex Red™ with further aromatization that leads to resorufin formation. Resorufin formation can be detected with spectrophotometry (λ_{max}=571 nm) and fluorometry (λ_{ex}=571 nm, λ_{em}=585 nm) (Mohanty *et al.*, 1997) . However, due to higher sensitivity, the fluorometric technique allows for the detection of lower concentrations of hydrogen peroxide. In the literature, Au-based NPs of various shape, size and surface modifications are the most commonly used catalysts for Amplex Red™ oxidation (Li *et al.*, 2012; Hsu *et al.*, 2016; Żukowski, Kosman and Juskowiak, 2020; António, Vitorino and Daniel-da-Silva, 2021; Wang *et al.*, 2022).

1.7.2.3. Homovanillic acid

In 1969, Guilbault, Brignac, and Zimmer presented a method for hydrogen peroxide detection based on homovanillic acid (HVA) usage. It was the first mentioning of HVA usage as a fluorescent substrate (Paździoch-Czochra and Wideńska, 2002). Non-fluorescent HVA monomer in the presence of peroxidase and hydrogen peroxide is oxidized to fluorescent HVA dimer (λ_{ex}=315 nm, λ_{em}=425 nm) (Scheme 20) (Guilbault, Brignac and Juneau, 1968).

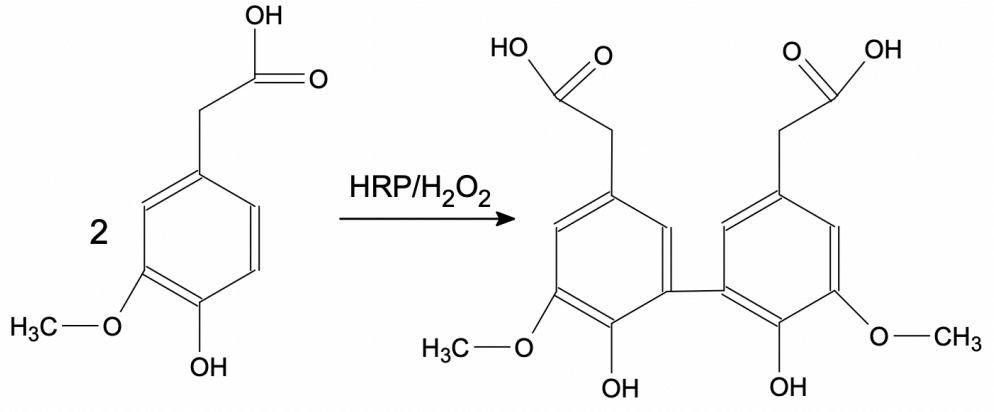

Scheme 20. HVA oxidation in presence of hydrogen peroxide and HRP.

Only few examples of nanoparticle peroxidase-like activity detection based on HVA usage can be found in the literature. HVA-based activity examination was described for Ag NPs, Pt NPs and Pd@Au NPs. (Nangia *et al.*, 2012; Fu *et al.*, 2020; Zaytsev *et al.*, 2020).

1.7.2.4. 3-(p-hydroxyphenyl)propionic acid

In 1980, Zaitsu and Ohkura developed a new sensitive assay for hydrogen peroxide and peroxidase determination based on 3-(*p*-hydroxyphenyl)propionic acid (HPPA) usage. The authors described HPPA dimerization oxidation reaction catalyzed by peroxidase in alkaline solutions (pH 10.0) in the presence of hydrogen peroxide (Scheme 21).

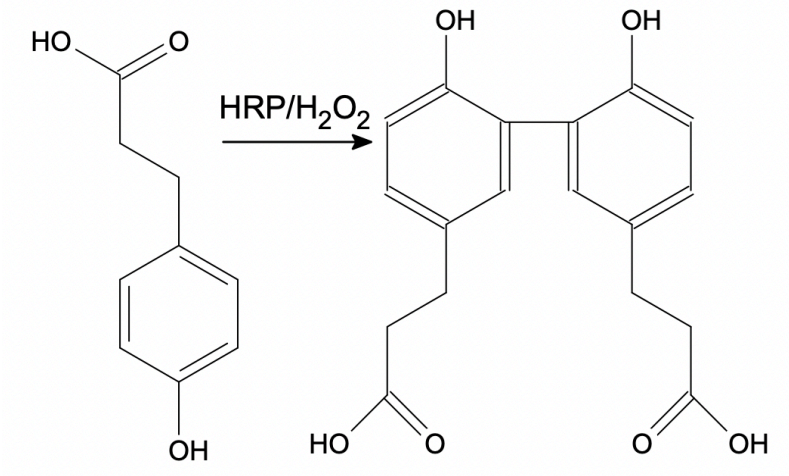

Scheme 21. HPPA oxidation reaction.

It was also discovered that increasing pH (via the addition of NaOH) enhances the fluorescence of HPPA dimer up to five times. HPPA is colourless and not a fluorescent liquid, whereas HPPA dimer can be detected with the fluoroscopic technique λ_{ex}=320 λ_{em}=402 nm) (Zaitsu and Ohkura, 1980).

1.7.3. Chemiluminescence-based detection of peroxidase activity

Compared to spectrophotometric and spectrofluorimetric methods, chemiluminescence-based detection methods are characterized by higher sensitivity due to lower background signal. However, the equipment required for chemiluminescence measurements is less common in comparison to spectrophotometers. The availability and cost of chemiluminescent and spectrophotometric substrates are on approximately the same level (Zhu and Gao, 2019). Chemiluminescence measurements are based on the detection of the luminescence product of the reaction during which electrons in their ground states move to their excited state and back to the ground state. The energy produced in such reaction is emitted as luminescence. Chemiluminescence measurement can be provided in a range from ultraviolet-visible to

infrared wavelengths (Sathe and Dhoble, 2017). Some of the most popular peroxidase chemiluminescence substrates are described in the following parts of this work.

1.7.3.1. Luminol

In 1928, Albrecht discovered that metal ions (Fe^{2+} or Cu^{2+}) or blood presence increase the luminescence of phthalic acid hydrazide with an amino group in the aromatic ring in an alkaline solution of H_2O_2 (Albrecht, 1928). This hydrazide was subsequently named luminol. Later, in 1936, Gleu and Pfannstiel studied this reaction and found that hematin (oxidized heme) present in blood enhanced luminol oxidation (Gleu and Pfannstiel, 1936). Based on the mentioned phenomena, Specht described a method that became a classical forensic method for blood detection (Specht, 1937). In addition, it was discovered that luminol could be used for sensitive and selective peroxidase detection. This peroxidase detection method is based on phenomenon of enzymatic enhancement of luminol luminesce (Thorpe and Kricka, 1986). Luminol dissolved in a basic solution is converted to resonance stabilized dianion. Peroxidase catalyzes oxidation of dianion by H_2O_2 with dicarboxylate ion production. Dicarboxylate ion is in the excited electronic state that can be detected due to photon emission. Photon emission leads to energy loss, resulting in dicarboxylate ion returning to its ground electronic state (Scheme 22).

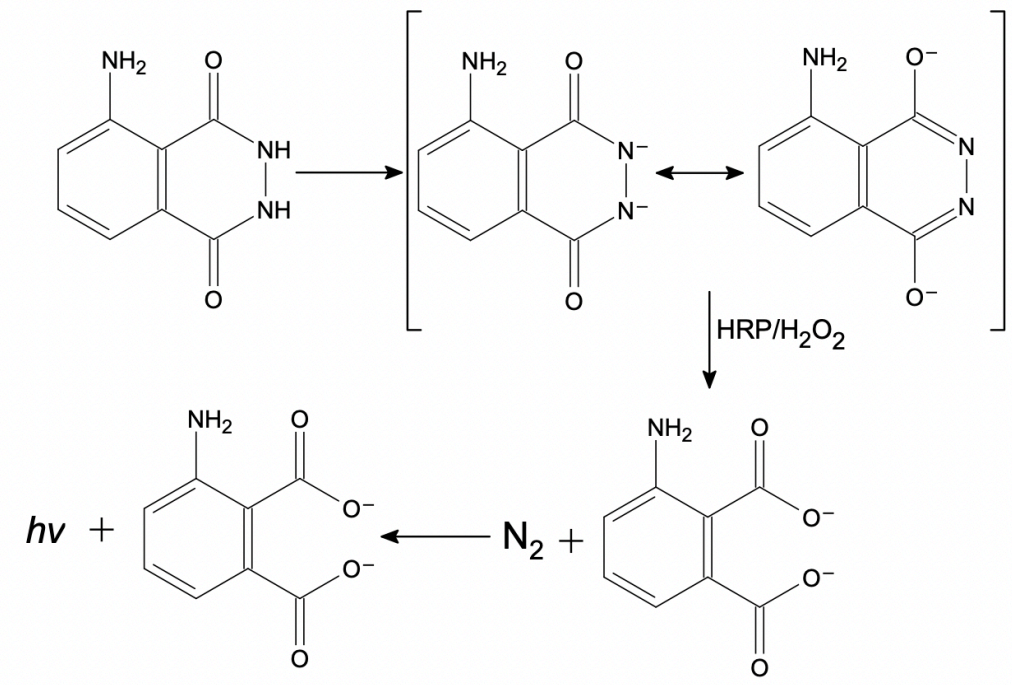

Scheme 22. Luminol oxidation reaction.

Such process can be catalyzed not only with natural peroxidase but also with NPs exhibiting peroxidase-like activity. Luminol was used to detect the peroxidase-like activity of CuO,

Fe_3O_4@Au, $CoFe_2O_4$ and others NPs (Abhijith, Ragavan and Thakur, 2013; Zhang *et al.*, 2013; Nasir *et al.*, 2017; Jiang *et al.*, 2018).

1.8. Peroxidase mimetics application

Compounds and particles of peroxidase activity are used in a variety of applications, including diagnostic tests, organic synthesis, and treatment of diseases such as cancer. In diagnostic tests, peroxidase mimetics are used to detect the presence of specific molecules in samples, such as in the detection of antibodies or antigens in blood tests. In organic synthesis, peroxidase mimetics are used as catalysts in the formation of chemical bonds, allowing for the synthesis of complex molecules in a more efficient and cost-effective manner. In the treatment of cancer, peroxidase mimetics are being studied as active agents in potential therapies for the targeted destruction of cancer cells (Ali Reza Hormozi Jangi, Mohammad Reza Hormozi Jangi, 2020; Thangudu and Su, 2021).

Horseradish peroxidase (HRP) is widely used as a catalyst in the process of analytical signal generation in the case of biosensors and biotests. HRP is particularly useful in immunoassays and electrochemical and optical biosensors. HRP as catalyst, was used in biotests and biosensors to determine hydrogen peroxide, glutathione, glucose, choline, acetylcholine, and ethanol (Avci Duman, 2021). The first case of peroxidase-like activity of NPs was declared in 2007 for iron oxide NPs (Gao *et al.*, 2007). Since 2007, peroxidase mimetics started to be used as promising substitutes for natural peroxidase in food and environmental quality screening and biomedical applications. However, peroxidase mimetics have some limitations, such as low specificity and decreased biocompatibility which should be taken into consideration during the development of NPs based measurements (Alvarado-Ramírez *et al.*, 2021).

1.8.1. Enzyme or nanozyme - linked immunosorbent assays

HRP is one of the catalytic labels used in enzyme-linked immunosorbent assay (ELISA). In 1971, ELISA was independently developed in Sweden by Engvall and Perlman and in the Netherlands by Schuurs and Van Weemen. Research groups found ELISA a promising, not hazardous alternative for radioimmunoassay (Engvall and Perlmann, 1971; Van Weemen and Schuurs, 1971). ELISA is a widely used technique in diagnostic and research applications for detecting and quantifying specific proteins, ABs, and antigens in various samples. (Alhajj and Farhana, 2022).

There are many different types of ELISAs, including direct ELISA, sandwich ELISA, competitive ELISA, and indirect ELISA (Scheme 23).

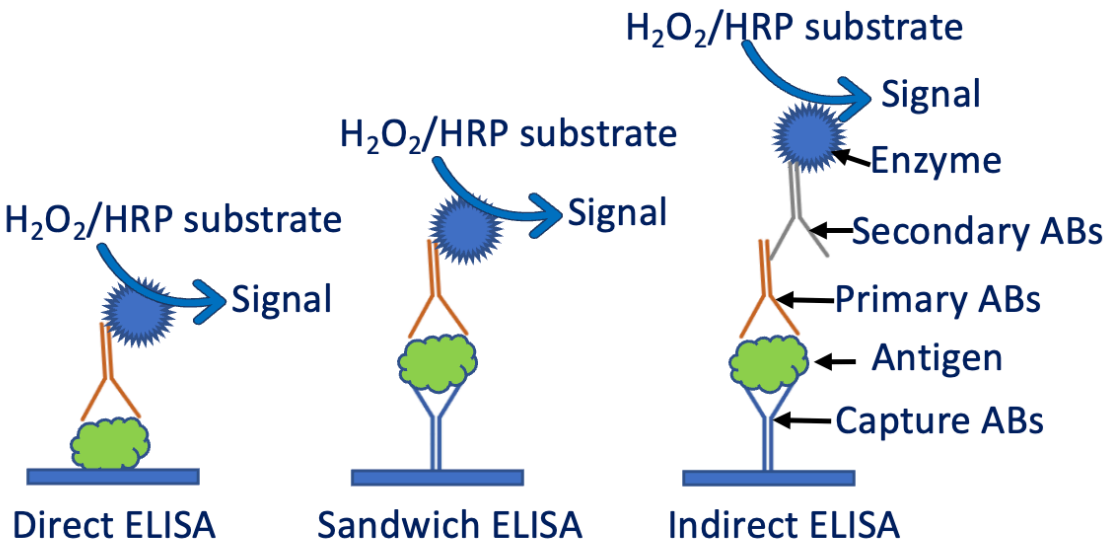

Scheme 23. Chosen types of ELISA.

Direct ELISA is based on the principle of antigen-ABs interaction, where a specific antigen from sample is immobilized on a solid surface, usually a plate, and then incubated with antigen specific ABs conjugated with enzyme. If the target protein is present in the sample, it will be recognized by ABs-enzyme conjugate, forming an antigen-ABs enzyme conjugate complex. The presence of the complex can then be detected using a primary ABs, which is conjugated with an enzyme.

The sandwich ELISA, also known as a capture ELISA, is a two-step assay that utilizes two specific ABs to capture and detect a specific analyte in a sample. The first step involves immobilization of the antigen of interest on a solid surface, such as a microtiter plate. This is typically done by coating the plate with a capture ABs that specifically binds to the antigen. The sample containing the antigen is then added to the plate and allowed to incubate, during which time the antigen binds to the capture ABs on the plate. The second step involves the detection of the antigen-primary AB complex. This is typically done by adding primary ABs conjugated to an enzyme, such as HRP or alkaline phosphatase, which binds to the antigen. After washing away any unbound primary ABs, a substrate for the enzyme is added, which generates a signal that can be quantified. The intensity of the signal is directly proportional to the amount of antigen in the sample. One of the key advantages of the sandwich ELISA is its high sensitivity and specificity. Because the assay uses two specific ABs that bind to different epitopes on the antigen, it is capable of detecting very low levels of the antigen in a sample (Alhajj and Farhana, 2022).

During first step of indirect ELISA, a sample containing the antigen is added to a plate that has been coated with a specific AB. In the second step, the antigen binds to the capture

ABs on the plate, forming an antigen-capture AB complex. During third step, primary ABs specific for the antigen are added to a sample, and allowed to bind to the target antigen. In the fourth step, labelled secondary ABs, which are specific for the host species of the primary ABs, are added. These secondary ABs bind to the primary ABs, allowing the detection of the target antigen by the labelled secondary ABs. (Engvall and Perlmann, 1971; Minic and Zivkovic, 2021).

Competitive ELISA is based on the principle of competition between the antigen in the sample and a known amount of labelled antigen (or hapten) for a limited number of binding sites on a specific AB. In the competitive ELISA, a known amount of labelled antigen (or hapten) is first added to a plate that has been coated with a specific AB. Then, a sample containing the antigen of interest is added to the plate. The antigen in the sample competes with the labelled antigen for binding to the ABs on the plate. The more antigen present in the sample, the less labelled antigen will bind to the ABs, resulting in a lower analytical signal.

NLISA is a variation of the traditional ELISA assay that uses NPs instead of enzymes. In a NLISA assay, the conjugate of a primary or secondary AB is replaced with a nanozyme conjugate, which catalyzes a reaction that generates a measurable signal. One of the advantages of using nanozymes in NLISA assays is the increased sensitivity, as the large surface area of NPs leads to the presence of a higher number of active sites, resulting in a stronger analytical signal. Another advantage of nanozyme-based assays is their potential for multiplexing, where multiple analytes can be simultaneously detected in a single sample. This can be achieved by using different nanozymes with different enzymatic activities, or by using NPs with different surface properties that can be selectively recognized by different ABs. It has been determined that NLISA can be many times cheaper and still has the same level of simplicity. Moreover, some NLISAs do not require a washing step, which decreases test executing time and makes such tests suitable for point-of-care and high-throughput diagnostic (Hansen *et al.*, 2017).

To summarize, NLISA offers a promising alternative to traditional ELISAs, providing improved sensitivity, specificity, and stability. However, further research is needed to fully understand the potential of nanozymes in diagnostic and research applications, and to develop standardized protocols for their use.

1.9. Strategies of NPs conjugation to ABs

To be used in NLISA, or other types of affinity biotests or biosensors based on ABs, NPs should be successfully conjugated with ABs. The best strategy should combine direct immobilization of ABs on NPs surfaces and minimal influence on NPs catalytic activity. The

orientation of ABs after immobilization is very critical for ABs antigen recognition ability. ABs should be immobilized on the NPs surface within the Fc region, while the Fab region should be free and directed forward interaction with antigen (Welch *et al.*, 2017). Any type of NPs surface modification influences their catalytic activity (derived from heterogeneous mechanism) and stability, which should also be considered when choosing a strategy for NPs ABs conjugation. Generally, there are physical and chemical bioconjugation strategies.

1.9.1. Physical strategy

The physical conjugation strategy includes non-covalent-based interactions. The non-covalent conjugation of NPs is based on ionic and hydrophobic/hydrophilic interactions of ABs with NPs surface. Ionic interaction occurs between positively charged groups (lysine, arginine, histidine and N-terminal) present in ABs and negatively charged NPs surfaces. Hydrophobic/ hydrophilic interactions are based on hydrophobic regions of antibodies interaction with hydrophobic regions of the nanoparticles surface, or the hydrophilic antibodies regions interaction with hydrophilic regions of the nanoparticles surface.

The non-covalent physical type of conjugation is characterized by the spontaneous adsorption of ABs on the surface of NPs. The most important is the fact that non-covalent binding does not require any additional modification of NPs surface, which can have negative effect on NPs catalytic activity. Non-covalent conjugation has several minor drawbacks. Compared to covalent conjugation, non-covalent one needs an increased concentration of ABs to obtain the same level of conjugation efficiency (Jazayeri *et al.*, 2016).

Non-covalent conjugation is characterized by strong dependency on pH and ionic strength, random orientation of ABs on NPs surface. ABs non-covalently conjugated with NPs can be easily replaced with other molecules present in biological samples (Kumar, Aaron and Sokolov, 2008). Non-covalent binding based on ionic interaction was used to conjugate anti-epidermal growth factor ABs with Au NPs (Sokolov *et al.*, 2003). Such conjugates were used for biosensing in vivo and in vitro detection of cancer cells (El-Sayed, Huang and El-Sayed, 2005). A combination of ionic and hydrophobic interaction was used to conjugate Au NPs with human IgG to create an electrochemical immunosensor (Chen *et al.*, 2007). Such type of conjugation is characterized by oriented immobilization of ABs on NPs surfaces and was used for the production of various ABs/metal-based NPs conjugates used in disease diagnostic (Yu, Park and Jon, 2012). One of the examples is NPs-based LFA. NPs-based LFA utilizes NPs as the detection agent. In these assays, a sample is applied to a test strip, and as it flows along the strip, it interacts with specific capture molecules that are immobilized on the strip. If the target

analyte is present in the sample, it will bind to the capture molecules, forming a complex. This complex then interacts with the metal NPs, which are usually conjugated to ABs, resulting in a visible signal indicating the presence of the target analyte. NPs-based LFA are used for rapid and simple detection of specific analytes such as proteins, antibodies, nucleic acids and small molecules (Sadeghi *et al.*, 2021).

1.9.2. Chemical strategy

The chemical strategy of ABs immobilization on NPs surfaces is based on the usage of linkers or adapters molecules. For such immobilization surface of NPs should be modified properly. Chemical strategies allow for obtaining strong binding between ABs and NPs surface; however, such methods can have a negative influence on NPs catalytic activity and biological reactivity of ABs.

1.9.2.1. Amine bond-based conjugation

Primary amine and the carboxyl group are present in the ABs structure. Amine groups are derived from lysine, and carboxylic groups are derived from aspartic and glutamic amino acids. Due to their polar nature, amine and carboxyl groups are present on the surface of ABs and can participate in covalent bond formation. During the condensation reaction of carboxylic groups with primary amines (one of them should be present in ABs structure and another on NPs surface) strong amide bond is formed (Scheme 24).

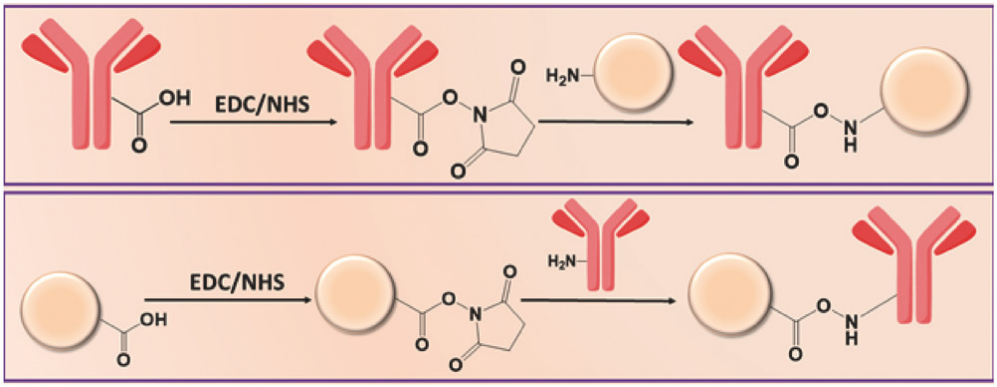

Scheme 24. Amide bond formation between ABs and NPs (Sivaram et al., 2018).

Carbodiimide chemistry, involved in mentioned amide bond formation, is based on activators such as 1-ethyl-3-carbodiimide hydrochloride (EDC), often in combination with succinimidyl esters. Carbodiimides are widely used for the covalent conjugation of ABs with NPs. In the literature, amide bond-based conjugation was used primarily for Au NPs (Mahmoudi *et al.*, 2021; Okyem *et al.*, 2021). Such coupling method was also used to develop Au NPs-based immunosensor for monosodium L-glutamate detection and modification of iron

oxide NPs used in vaccine production (Motamedi-sedeh *et al.*, 2022; Sharma *et al.*, 2022). However, carbodiimide chemistry has a limitation issue – ABs self-crosslinking based on ubiquitous carboxylic groups and primary amines in ABs structure) This drawback can be eliminated via selection of proper experimental conditions and specific order of conjugation steps (Sivaram *et al.*, 2018).

1.9.2.2. Maleimide chemistry

Maleimide chemistry allows directing the immobilization of ABs on NP surface (Scheme 25).

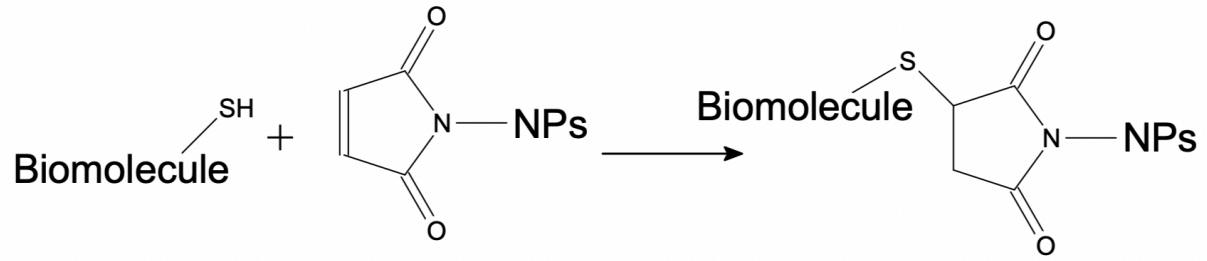

Scheme 25. Maleimide-based chemistry of ABs/NPs conjugation reaction.

Maleimide chemistry is based on thiol reaction with maleimide or iodoacetyl groups (Trilling, Beekwilder and Zuilhof, 2013). Thiols groups, also called sulfhydryl groups, can be naturally present in cysteine residues of ABs. Additionally, thiol groups can also be chemically introduced to the structure of ABs by modifying cysteine residues or by adding new cysteine residues through genetic engineering or chemical modification methods. (Yi *et al.*, 2018). For example, lysine primary amine groups can be converted to thiol using Traut's reagent (2-iminothiolane), *N*-succinimidyl or *S*-acetyl thioacetate(Gauvreau *et al.*, 2004). However, the introduction of multiple thiol groups into the ABs structure decreases NPs/ABs conjugation site-selectivity (Yu, Park and Jon, 2012). Activation of thiol groups via reduction reaction can be done by tris(2-carboxyethyl)phosphine or 2-mercaptoethylamine. Cysteine is internally localized in ABs tertiary structure. Covalent binding within cysteine sites can change ABs conformation and, as a result, negatively influence ABs biological activity (Karyakin *et al.*, 2000).

1.9.2.3. Click Chemistry

Kolb research group presented the "click chemistry" term for the first time in 2001 (Kolb, Finn and Sharpless, 2001). Click chemistry is a group of reactions characterized by simplicity, high reaction speed, versatility, product stereospecificity and excellent product yield. Due to mentioned properties, click chemistry is a promising tool for efficient production of NPs/ABs conjugates (Yi *et al.*, 2018). Cycloaddition, nucleophilic ring-opening and carbon

multiple bond addition are main click chemistry reactions. Lin with co-authors, also added a carbonyl reactions of non-aldol type to mentioned click chemistry reactions list (Lin, O'Reilly Beringhs and Lu, 2021). Such addition was made based on the list of significant click chemistry reactions published in the work of Christopher Hein *et al.* (Hein, Liu and Wang, 2008). Nevertheless, according to the low thermodynamic driving force, prolonged reaction time (approximately 30 min) and presence of a side reaction products, carbonyl chemistry of the non-aldol type cannot be defined as a click chemistry reaction (Kolb, Finn and Sharpless, 2001). Cycloaddition is the most popular click chemistry strategy for ABs immobilization on NPs surfaces (Marques *et al.*, 2020). Azide-alkaline 1,3-dipolar cycloaddition addition catalyzed with Cu cations meets click chemistry requirements and can be provided under room temperature in aqueous solutions in a wide range of pH (pH 4.0-12.0). Moreover, Cu-catalyzed cycloaddition takes part in the highly specific formation of 1,4-disubstituted regioisomers (Scheme 26).

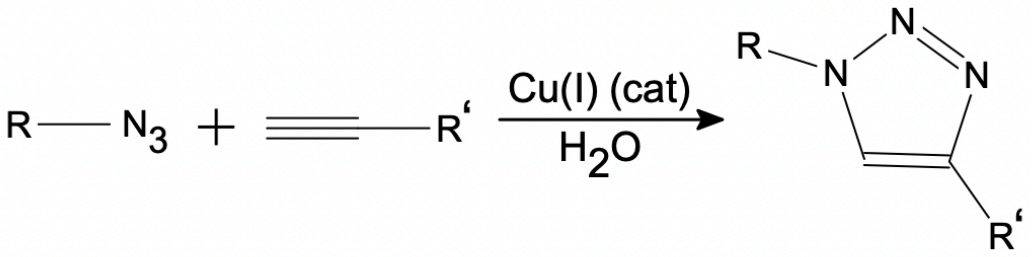

Scheme 26. Cu- catalyzed cycloaddition reaction.

Reaction product separation can be done with simple filtration or extraction without recrystallization or application of chromatography (Kolb, Finn and Sharpless, 2001). Despite its good efficiency, Cu-catalyzed cycloaddition has a limitation of usage in biological systems due to the high cytotoxicity of copper (Sletten and Bertozzi, 2009). The literature describes the usage of cycloaddition for ABs immobilization on NPs surfaces used for targeted drug delivery in anticancer therapy (Shi, Lu and Shoichet, 2009).

1.9.2.4. Adapter molecules

Adapter molecule complexes with strong binding properties can be used for ABs immobilization on NPs surfaces. For this purpose, streptavidin/biotin or avidin/biotin complexes can be used. Streptavidin is a tetramer protein (66 kDa) (Kurdekar *et al.*, 2018). Each streptavidin subunit can bind one molecule of biotin with extremely strong affinity. Avidin, the same as streptavidin, is a tetramer protein (66-69 kDA). The dissociation constant of streptavidin/biotin complex is around 10^{-14} mol/l and avidin/biotin is 10^{-15} mol/l (Green, 1963; Green, 1975). Biotin is a small (244 Da) hapten biocompatible molecule. Biotin can be

conjugated with ABs using NHS. Due to its small size, biotin can be conjugated with ABs without significantly influencing ABs biological activity. Such process is called ABs biotinylation. Due to the randomness of biotinylation, streptavidin/biotin-based conjugation is inferior to the efficiency of chemical covalent conjugations. Streptavidin/biotin is the strongest known non-covalent interaction, but Mir Hadi Jazayeri, with co-authors, mistakenly classified such interaction as covalent (Turková, 1999; Jazayeri *et al.*, 2016). Streptavidin/biotin complex was used for immunobiosensor construction or immobilization of ABs on Au NP surface (You, Lim and Gunasekaran, 2020). In contrast to non-directed conjugation via avidin/biotin or streptavidin/biotin, protein A and G allow direct immobilization of ABs on the NPs surface. Protein A and G bind specifically to Fc region of ABs. Compared to random conjugation of biotinylated ABs with NPs, NPs/ABs conjugates formed with protein A or G show fivefold higher antigen detection efficiency (Welch *et al.*, 2017).

2. Experimental methods

2.1. List of chemical reagents and materials

- The chemicals listed below were obtained from Sigma-Aldrich (Poland):
  - 4-aminoantipyrine (4-AAP), 98%
  - boric acid, 99%
  - dialysis membrane tubing (MWCO 12-14 kDa)
  - gold(III) chloride trihydrate, 99%
  - hydrazine monohydrate, 98%
  - hydroxylamine hydrochloride, 98%
  - iron(II) sulfate heptahydrate, 99%
  - *o*-phenyldiamine (OPD), 99%
  - phenol, 99%
  - sodium borohydride, 98%
  - sodium tetrachloropalladate(II), 98%
- The chemicals listed below were obtained from Merck:
  - 2-ethanesulfonic acid (MES), 99%
  - anti-CRP polyclonal antibody produced in rabbit
  - anti-Rabbit IgG (whole molecule) antibody produced in goat
  - casein from bovine milk
  - chloroplatinic acid solution (8 wt.% in H_2O)
  - diethylenetriaminepentaacetic acid (DTPA), 98%
  - ethanolamine, 98%
  - goat IgG
  - osmium(III) chloride, 99%
  - polydiallyldimethylammonium chloride (PDDA) (20 wt.% in H_2O)
  - potassium phosphate dibasic, 99%
  - sodium hydrogen carbonate, 99%
  - sodium periodate, 99%
  - sodium phosphate dibasic dihydrate, 99%
  - Tween-20
- The chemicals listed below were obtained from Acros Organics
  - N-hydroxysulfosuccinimide (sulfo-NHS), 99%

- potassium chloride, 99%
- sodium chloride, 99%
- 3,3,5,5-tetramethylbenzidine (TMB), 99%

- The chemicals listed below were purchased from POCh, Avantor:
  - acetic acid, 99%
  - phosphoric acid, 85%
  - dimethyl sulfoxide,
  - hydrogen peroxide, 30%
  - sodium hydroxide, 99%
- The chemicals listed below were obtained from Chempur:
  - hydrochloric acid, 35-37%
  - ethanol, 96%
  - glycine, 99%
- The chemicals listed below were obtained from 3M:
  - hydrophilic polyester (PES) foil (9962)
  - polyethylene terephthalate (PET)
  - PS foil covered on both sides with a layer of acrylic glue (9965)

- 1-ethyl-3-(3-dimethylaminopropyl)carbodiimide hydrochloride (EDC) (98%) and Slyde-a-Lyser mini dialysis devices were obtained from Thermo Fisher Scientific.
- Anti-CRP monoclonal antibody produced in rabbit obtained from Medix Biochemica.
- Bovine serum albumin (BSA) (98%) was obtained from Glentham.
- Human C-reactive protein (CRP) was obtained from Prospec.
- Pump tubing LMT-55 Standard id=0.95 mm, wd=0.84 mm, od 2.63 mm type ENFT-10 was obtained from Tygon.
- Poly(methyl methacrylate) (PMMA) sheets were obtained from Evonic.
- Poly(ether ether ketone) (PEEK) sheets were obtained from Ensinger.
- Polyoxymethylene copolymer sheets were obtained from Angst+Pfister.
- Ruthenium(III) chloride (99%) hydrate was obtained from Alfa-Aesar (Poland).
- Thiolated carboxylic-PEG (average molecular weight =3kDa) (90%) was obtained from Rapp Polymere GmbH.
- HBPG (MW∼3.2 kDa) was synthesized by the research group of prof. Paweł Parzuchowski from the Department of Chemistry and Technology of Polymers, Faculty of Chemistry, Warsaw

University of Technology using ring-opening polymerization according to the method developed by (Parzuchowski et al. 2020).

2.2. List of apparatus and equipment

- Spectrophotometric multi-well plate reader with gradient filter Sunrise Magellan (Tecan, Austria);
    - 96-well polystyrene plates with U-shaped bottoms (Greiner);
    - The Nunc MaxiSorp™ high protein-binding capacity flat bottom plates (Thermofisher);
- Spectrophotometric multi-well plate reader Multiskan GO (Thermo Scientific, USA)
- Spectrophotometer V-300 (ABL&E-JASCO, Poland);
    - quartz cuvettes with an optical path length of 1 cm (Hellma Analytics)
- Transmission electron microscope (TEM) Libra 120 (Zeiss, Germany);
- Scanning electron microscope (SEM) coupled with energy dispersive X-ray spectrometer (XEDS) (Bruker, Germany);
    - a set of microscopic formvar coated grids (Agar Scientific);
- Energy Dispersive X-ray Fluorescence (EDXRF) spectrophotometer with a Rh tube and silicon drift (resolution 145 eV) (PANalytical Co, England)
- Particle size and zeta potential analyser Zetasizer Nano ZS (Malvern, England);
    - disposable plastic cuvettes with an optical path length of 1 cm (SARSTEDT AG & Co, Germany)
- pH meter with a combined glass electrode (Elemetron, Poland);
- Ultrasonic bath Sonic-5 (Polsonic, Poland);
- Magnetic stirrer RET basic (IKA®, Poland);
- Shaker KS 130 basic (IKA®, Poland)
- Vortex V-1 plus (Biosun, Lithuania);
- Neodymium magnet N42 (EuroMagnesy, Poland);
- Electromagnets LS-P30/22 (Langshuo.Co., China);
- CO_2 laser ULTRA x6000 (Universal laser systems, USA);
- Milling machine Datron Neo Series 2+ (Datron, Germany).

2.3. Buffers solutions composition

Unless otherwise specified in the detailed description, the tests were carried out with buffer solutions prepared according to the protocols listed below. They were prepared by dissolving

salts or concentrated acids in deionized water and adjusting the pH with HCl or NaOH solutions. The applied deionized water was characterized by a conductivity of <0.055 uS/cm, while the total amount of microorganisms was lower than 1 cfu/ml and the total organic carbon amount was lower than 1.0 ppb. The pH control was ensured using a pH meter equipped with a combination glass electrode. The following buffer solutions were used in the research described in Chapter 3:

- acetate buffer (0.1 M) (pH 4.0)
- universal buffer (acetate-borate-phosphorate (40-40-40 mM) pH 6.5-10.5
- buffer PBS (10 mM Na_2HPO_4, 250 mM NaCl, 1.8 mM KH_2PO_4, 2.7 mM KCl) (pH 7.4)
- PBST buffer (pH 7.4) (PBS buffer and 0.05% v/v Tween-20)
- carbonate buffer (CB) (0.1 M) prepared from $NaHCO_3$ (pH 9.6)
- MES buffer (50 mM) (pH 6.0).

2.4. Synthesis of monometallic and bimetallic NPs

Mono- and bimetallic NPs were synthesized using wet chemical synthesis. Solutions of noble metal precursors (10 mM) were prepared using deionized water. To obtain monometallic NPs, 625 ul of a precursor solution was mixed with 5 ml of an aqueous solution of HBPG (1 mg/ml) and 625 ul of the reducing agent. For the preparation of bimetallic NPs, the solution of Au precursor was mixed in a ratio of 1:2 with Ru, Pt, Os, or Pd precursor to obtain 625 ul. The following steps of mixing with stabilizing and then reducing agent solutions were the same as for monometallic NPs. As a reducing agent, sodium borohydride, hydrazine or hydroxylamine hydrochloride of 30 mM, 40 mM, or 50 mM (aqueous solutions) were used. All synthesis steps were done under mixing conditions and obtained NPs were stored in a dark place.

2.5. NPs characterization methods

DLS was used for measurements of hydrodynamic diameters and ζ -potential of NP. TEM working at 120 kV acceleration voltage together with microscopic formvar coated grids were used for size and shape examination of NPs. SEM coupled with EDX was used for elementary analysis and mapping of NPs. The elemental composition of NPs and dialysate solutions was determined using X-ray fluorescence with a spectrometer equipped with a Rh tube and a silicon drift detector, having a resolution of 145 eV.

2.6. Peroxidase-like activity examination

2.6.1. OPD-based method

OPD was used as a substrate for the evaluation of the peroxidase-like activity of mono- and bimetallic NPs. NPs solutions were diluted 100 times in deionized water before combining them with the substrate solution. 5.8 ml of 20 mM OPD solution was mixed with 1.8 ml of 5.0 M H_2O_2 stock solution. OPD and H_2O_2 stock solutions were prepared with deionized water and mixed with 5.8 ml of 0.1 M acetate buffer to adjust them to pH 4.5. 50 ul of NPs solutions or deionized water were mixed with 200 ul of the substrate solution in a 96-well plate immediately before measurement. Absorbance evolution was measured at 450 nm in 10 sec intervals.

2.6.2. TMB-based method

Different modifications of TMB-based tests were used for determination of peroxidase-like activity of NPs in solution (1st version) and for NPs immobilized on the surface of 96-well plate (2nd version), on foil-based bioreactors (3rd version) and in microfluidic chips. TMB substrate solution consisted of 2.9 ml of acetate buffer of pH 4.0, 900 ul of H_2O_2 (5.0 M), and 200 ul of TMB (20 mM) stock solution. TMB stock solution was prepared with dimethyl sulfoxide, and H_2O_2 stock solution was prepared with deionized water. TMB substrate solution was prepared using the same protocol for all TMB-based tests. Test modifications were done on the test performance steps. Description of TMB test used in microfluidic chips described as a part of microfluidic chip usage protocol.

2.6.2.1. TMB-based method 1st version

1 ul of examined NPs solution was placed on the bottom of the single well of 96-well plate. For blank, 1ul of deionized water was added. The chromogenic reaction was initiated by the addition of 100 ul of substrate solution immediately before measurement. Absorbance evolution was measured at 652 nm in 10 cycles with 10 sec intervals each.

2.6.2.2. TMB-based method 2nd version (immunoassay)

In the case of NLISA assay, 200 ul of TMB substrate was placed in chosen wells of 96-well plate what initiated chromogenic reaction. Absorbance evaluation was done in the same way as represented in TMB-based method 1st version.

2.6.2.3. TMB-based method 3rd version (immunoassay)

In the case of NPs immobilized on the surface of foil-based bioreactors, 30 ul of TMB substrate was placed in bioreactors and incubated for 10 min in increased humidity conditions at room temperature. After incubation, solutions from bioreactors were collected and moved to

chosen wells of multiwell plate which has been filed with 170 ul of acetate buffer. End-point absorbance of solutions was measured at 652 nm.

2.6.3. Influence of pH on peroxidase-like activity of nanozymes (phenol/4-AAP method)

For the investigation of pH influence on peroxidase-like activity of NPs, a solution of 800 ul of 500 mM phenol, 400 ul of 50 mM 4-AAP, and 200 ul of hydrogen peroxide stock solution was used. H_2O_2 stock solution was prepared in the same way as for the OPD substrate. Then the prepared solution was adjusted to the chosen pH (6.5-10.5) using universal buffer. 200 ul of a substrate solution mixed with 50 ul of 100 times diluted NPs or deionized water (blank). The evolution of absorbance in time was measured at 510 nm.

2.7. Examination of stability of quinonimine

1 ml of HRP solution (500 ug/ml) prepared in 0.04 M universal buffer was placed into the dialysis membrane. Dialysis membrane containing HRP solution was placed in a glass vial filled with 20 ml of PhOH/4-AAP modified substrate. Substrate composition modification, in comparison to standard PhOH/4-AAP substrate, was based on changing hydrogen peroxide concentration. Modified PhOH/4-AAP substrate solution contained 4 ul of 9.8 M H_2O_2. Glass vial was placed on the shaker and incubated for 45 min at room temperature under continues mixing condition (600 rpm). After incubation coloured, HRP catalyzed PhOH/4AAP product – quinonimine was diluted five times with 0.1M universal buffer pH 7.5. Spectra of quinonimine were detected in the range 350-750 nm immediately after and in 15 and 30 min using a quartz cuvette.

2.8. Examination of pH influence on optical properties of quinonimine

Quinonimine solution obtained in the same way as described in quinone stability test was diluted five times with 0.1 M universal buffer pH 6.5-10.5. Absorbance of obtained solutions was measured at 510 nm in three runs.

2.9. Detection of metal ions release

Two techniques were used to detect the release of metal ions from NPs. X-ray fluorescence spectrometric analysis was applied to detect the presence of ions in dialysates, and vis spectrophotometry was used to study the catalytic activity of dialysates based on the catalytic activity of released ions in the reaction with the substrates (PhOH/4-AAP).

Samples (400 ul) of diluted (10 times) NPs were enclosed in the dialysis membrane and put into a glass vial filled with 3600 ul of the universal buffer (of various pH). Vials were placed on a shaker and incubated for 24 h at 550 RPM under mixing conditions. After 24 h, the

membranes with the solutions of NPs were removed from the vials, rinsed with deionized water, placed into new vials filled with 3600 ul of a buffer, and incubated under mixing conditions for another 24 h. Described procedure was repeated for 8 successive days. The solutions from the vials were collected for further detection of ions. 50 ul of solutions collected from the vials or 50 ul of deionized water (blank) were mixed with 200 ul of PhOH/4-AAP substrate solution in wells of 96-well plate, and evolution of absorbance in time was measured at 507 nm. Such measurement was executed on the day of the sample collection.

2.10. Production of NPs/ABs conjugates

Synthesis of NPs/ABs conjugates consisted of four individual steps. During the first step magnetic nanocubes were synthesized. During the second step, magnetic nanocubes were decorated with Pt or Ru. The third step was focused on Au deposition on obtained NPs surface.

2.10.1. NPs/ABs conjugates synthesis (I) – synthesis of PDDA-stabilized iron(II,III) oxide NPs

For the synthesis of magnetic nanocubes, a method of controlled oxidation of Fe(II) precursor was used according to a modified protocol described by Goon et.al. (Goon *et al.*, 2009). The mixture of 1.05 g of $FeSO_4 \cdot 7\ H_2O$, 120 ml of H_2O, and 15 ml of 2 M KNO_3 aqueous solution in the three-neck round-bottom flask was deoxygenized by argon purging and then heated to 90°C in an oil bath. Heating and all stages of the synthesis were carried out in argon atmosphere under intensive (2000 rpm) mechanical stirring. After 15 min of mixing at 90°C, 15 ml of 1M NaOH was rapidly injected. After the next 10 minutes of vigorous stirring, 15 ml of aqueous PDDA solution (20 mg/ml) was injected into the flask and stirring was continued for next 2 hrs. After cooling, the nanocubes suspension was poured into a beaker and washed by at least 7 times of alternating magnetic decantation and ultrasound-assisted redispersion in deionized water (~500 ml per single cycle). For further use, the NPs sample was diluted with deionized water to achieve $OD_{380nm}=1.5$.

2.10.2. NPs/ABs conjugates synthesis (II) – Pt and Ru decoration of iron(II, III) oxide nanocubes NPs

Decoration of Fe_3O_4 nanocubes with two types of catalytically active metals - Pt and Ru - was carried out analogously: in both cases by rapid reduction of the precursor followed by adsorption-driven metal nucleation on the PDDA-coated iron(II,III) oxide. Chloroplatinic acid solution (10 mM) was prepared in deionized water and adjusted to pH 7.0 with NaOH solution (1.0 M). $RuCl_3$ solution (10 mM) was prepared in deionized water. 150 ul of Ru or Pt precursors solutions and 150 ul of 50 mM $NaBH_4$ solutions were added per 10 ml of iron oxide NPs (OD_{380}

$_{nm}$=1.5). Mixture was incubated under magnetic stirring conditions (700 rpm) at room temperature for 7 hrs. After incubation NPs solutions were separated in magnetic field and resuspended in deionized water using ultrasonic bath. Separation and resuspension were repeated 5 times.

2.10.3. NPs/ABs conjugates synthesis (III) – Au deposition on Fe_3O_4/Ru and Fe_3O_4/Pt

4 ml of each type of noble metal-decorated nanocubes were magnetically collected and resuspended in 40 ml of NaOH solution (10mM). Then 200 ul of 30 mM hydroxylamine hydrochloride was added to each NCs type under continuous stirring and the mixtures were incubated for a further 5 min. Later, 80 ul of $HAuCl_4$ solution (100 mM) was added and the mixtures were incubated for 1 hr. As obtained, Au-decorated NPs were magnetically separated from an excess of reagents and resuspended in deionized water after brief sonication. The separation process was repeated 4 times until no traces of precursors or residues of NPs not bound to the Fe_3O_4 surface were observed in the supernatant (which was evidenced by stable Vis spectra for subsequent supernatants). As obtained NPs were stored in deionized water for further studies.

2.10.4. NPs/ABs conjugates synthesis (IV) - bioconjugation with anti-CRP Abs

At the first step, PEG-based bifunctional ligand was introduced as NPs capping agent and linker. The conjugation protocol was the same regardless of the type of active metal used. 40 ml of NPs aqueous suspension were separated in a magnetic field and resuspended in 4 ml of deionized water followed by brief sonication. 1 mg/ml aqueous solution of thiolated, carboxy-terminated PEG was injected into NPs under continuous stirring in the volume chosen to reach a final modifier concentration of 200 uM. Then, the mixture was incubated for 16 hrs. PEG-functionalized, -COOH-terminated NPs were washed through fivefold magnetic decantation and finally suspended in 50 mM MES buffer, pH 6.0. Next, per 1 ml of NPs solution were added 200 mM sulfo-NHS (240 ul) and 200 mM EDC (24 ul) solutions. Both EDC and sulfo-NHS solutions were prepared in MES buffer just before use. After 30 min incubation under magnetic stirring, NPs were magnetically separated and suspended in an aliquot of fresh MES to remove excess of reagents. Before conjugation, 30 ul of rabbit polyclonal anti-human CRP ABs (5 mg/ml) was dialyzed using Slyde-a-Lyzer mini dialysis, MWCO 10 kDa against 15 ml of MES buffer. Antibody was added to the activated NPs to obtain 50 ug of antibody per 1 ml of NPs and incubated for 1 hr under mixing conditions at 4^{o}C. Then blocking buffer (10% BSA in PBS buffer with 0.05% Tween20 (v/v)) was added to obtain final concentration of BSA equalled to 1%. The mixture was incubated overnight under mixing conditions at 4^{o}C. NPs/ABs

conjugates were magnetically collected and resuspended in PBST buffer with 0.05% of sodium azide and stored at 4ºC.

2.11. Modification of multiwell plate surface with ABs

Wells of clear flat bottom MaxiSorp™ plate were washed *2* times with carbonate buffer (CB). 50 ul of solutions containing 10 ug/ml of ABs prepared in CB, and ABs-free CB were placed into chosen wells. The plate was incubated at 4ºC for 16 hrs. Incubated solutions were removed from the plate and wells were washed 3 times with 100 ul of PBST. 50 ul of blocking buffer was placed into chosen wells and incubated under mixing conditions at room temperature for 30 min. Protein composition of the blocking buffer varied for different experiments, being a reason why more details will be provided in Chapter 3. After incubation, the blocking solution was removed and wells were washed with PBST. This MaxiSorp™ plate modification protocol was taken as a standard plate modification protocol and used without changes for all experiments where modified MaxiSorp™ plates were utilized.

2.12. Determination of antibody presence on NPs surface using MaxiSorb™ plate

Previously sonicated in an ultrasonic bath at 4ºC NPs/ABs mixtures were diluted 40 times in a dilution buffer to obtain 250 ul of sample. Next, NPs/ABs conjugates were separated from solutions in a magnetic field and resuspended in 250 ul of dilution buffer using ultrasonic bath filed with 4ºC water. The protein composition of dilution buffer varied for different experiments, being a reason why more details will be provided in Chapter 3. 30 ul of NPs/ABs prepared samples were placed in modified MaxiSorb™ plate and incubated for 30 min at room temperature under continuous mixing conditions (500 rpm). MaxiSorb™ plate was modified with ABs following the modification protocol described above. Incubated mixtures were removed and wells were washed three times with 100 ul of PBST. TMB substrate solution preparation and further steps were matched to the 2nd version of TMB-based test protocol.

2.13. Examination of NPs-ABs conjugate antigen detection ability (Analyte detection)

Human CRP solution was prepared with dilution buffer and used to dilute NPs/ABs conjugates 40 times. Protein composition of dilution buffer varied for different experiments, being a reason why more details will be provided in Chapter 3. The concentration of antigen varied for different experiment being a reason why more details will be provided in the "experimental part". Next, NPs/ABs were separated from the solution in a magnetic field,

resuspended in blocking buffer and sonicated. 30ul of prepared mixtures were placed on chosen modified PES bioreactors and incubated under mixing condition (500 rpm) for 30 min at room temperature. Incubated mixtures were removed, and wells were washed three times with 100 ul of PBST. TMB substrate solution preparation and further steps matched the 2nd version of TMB-based test protocol.

2.14. Modification of hydrophilic PES foil surface

First, on hydrophilic PES 3M foil (9962) it was placed a mask made with PES foil covered on both sides with a layer of acrylic glue (9965). 9965 foil was used to create walls of bioreactors and physical border for the solution. CO_2 gas laser with a wavelength of the generated beam of 9.3 um was used to cut desirable shapes and elements in both types of foils. Surfaces of bioreactors were washed with 30 ul of ethanol before immobilization of ABs. ABs were diluted in acetic 50 mM buffer of pH 5.0 to obtain concentration of 10 ug/ml. 30 ul of ABs solutions were placed in bioreactors and incubated for 16 hrs at 4°C in increased humidity environment. After incubation solutions were replaced with a solution containing 3% of casein in PBST and incubated for 30 min at room temperature under increased humidity conditions. Next, the solution was removed, and bioreactors were rinsed three times with PBST and dried in airflow.

2.15. Determination of ABs presence on NPs surface using PES bioreactors

NPs/ABs mixtures that were previously sonicated in ultrasonic bath at 4°C were diluted 20 times in solution containing 1% of casein in PBST obtaining 50 ul of sample. Next, NPs/ABs conjugates were separated from solutions in a magnetic field and resuspended in 250 ul of dilution buffer using ultrasonic bath filed with 4°C water. 30 ul of NPs/ABs prepared samples were placed in modified bioreactors and incubated for 30 min at room temperature in increased humidity environment. Bioreactors were modified with ABs following the modification protocol described above. Incubated mixtures were removed, and bioreactors were washed three times with 100 ul of PBST and dried in airflow. TMB substrate solution preparation and further steps were matched to the 3rd version of TMB-based test protocol.

2.16. Examination of NPs/ABs conjugates antigen detection ability using PES bioreactors

Human CRP solution was prepared with buffer containing 1% of casein in PBST and mixed with NPs/ABs conjugates to obtain 20 times dilution of NPs/ABs conjugates in a final sample volume. The concentration of antigen varied for different experiment that is why more

details about it will be provided in the Chapter 3. Next, NPs/ABs were separated from the solution in a magnetic field, resuspended in solution containinig 1% of casein in PBST and sonicated in ultrasonic bath at 4^0C. 30ul of prepared mixtures were placed on chosen modified PES bioreactors and incubated at room temperature for 30 min in increased humidity environment. Incubated mixtures were removed and PES bioreactors were washed three times with 100 ul of PBST and dried in airflow. TMB substrate solution preparation and further steps were according to 3rd version of TMB-based test protocol.

2.17. Antibody conjugation with HRP enzyme

0.2 mg of HRP was dissolved in 50 ul of deionized water. To obtained HRP solution 10 ul of freshly prepared solution of sodium periodate (0.1 M) was added, and the solution was stirred (600 rpm) for 20 minutes at room temperature, protected from light. The modified enzyme was dialyzed against acetate buffer (1 mM) pH 4.4, overnight at 4°C using Slide-A-Lyzer mini dialysis unit. 0.4 mg anti-human CRP polyclonal ABs was dissolved in 50 ul of 10 mM carbonate buffer, pH 9.5, and dialyzed against this buffer overnight at 4°C. After the dialysis, the total volume of the enzyme solution was adjusted to 50 ul by adding 1 mM sodium acetate buffer, pH 4.4. The final pH of the enzyme solution was adjusted to 9.0-9.5 by adding 1 ul of 0.2 M carbonate buffer, pH 9.5. Dialyzed antibody was immediately added to the enzyme. The mixture was stirred (600 rpm) for 1 hour at room temperature. 5 ul of freshly prepared sodium borohydride solution (4 mg/ml) was added to the mixture and the obtained solution was stirred (600 rpm) for 2 hrs at 4°C. Overnight dialysis against phosphate-buffered saline was then carried out. The final volume of the conjugate solution was adjusted to 140 ul by adding PBS buffer. The conjugate was stored in aliquots at -20°C.

2.18. Multifunctional microfluidic system fabrication

2.18.1. Microfluidic chip fabrication

Multilayer microfluidic chips were consisted of two main parts: a PMMA overlay and a microfluidic PES film-based cassette part. Microfluidic cassette part was made with hydrophilic PES 3M foil (9962) and PES foil (9965) covered on both sides with a layer of acrylic glue. Such materials were chosen because the PES film microfabrication is cheap, available in many variants, very effective and can be adapted to roll-to-roll fabrication technique. In addition, manufacturer provided protocols for in vitro cytotoxicity, skin effects and subcutaneous irritation tests, as well as eye irritation tests. Medical certificates allow easier implementation, application and commercialization of the PES-based Point-of-Care s. CO_2 gas laser with a generated radiation wavelength of 9.3 um was used to cut all microfluidic patterns

in both types of foils. Cassette was assembled precisely layer by layer using dedicated holder (Image 1).

Image 1. Holder with the assembled microfluidic cassette.

4-point fixation of the cassette on the holder ensured accuracy of cassette assembling. Holder was also used for precise attachment of the microfluidic cassette part to the PMMA overlay. Holder was milled using Datron Neo Series 2+ machine from PEEK. Microfluidic cassettes consisted of 6 layers. On the layers 2 and 5 ABs were immobilized using standard protocol of ABs immobilization on PET foils. To ensure proper adhesion of the layer to each other, they were treated with the roller press. Overlay was milled using Datron Neo Series 2+ machine from PMMA.

2.18.2. Magnetic separation module production

Magnetic separation module consisted of portable holder for three microfluidic chips compatible with multiwell plate spectrophotometer and stationary part with three electromagnets. Each electromagnet had magnetic field strength of 0.3 T and 12 V DC operation voltage. Portable holder, same as stationary part, was milled from polyoxymethylene copolymer using Datron Neo Series 2+ machine.

2.18.3. Usage of magnetic separation module together with microfluidic chips

Microfluidic chips had three inlets and two outlets compatible with peristaltic pump tubing (Image 2) with inner diameter 0.95 mm and wall diameter 0.84 mm.

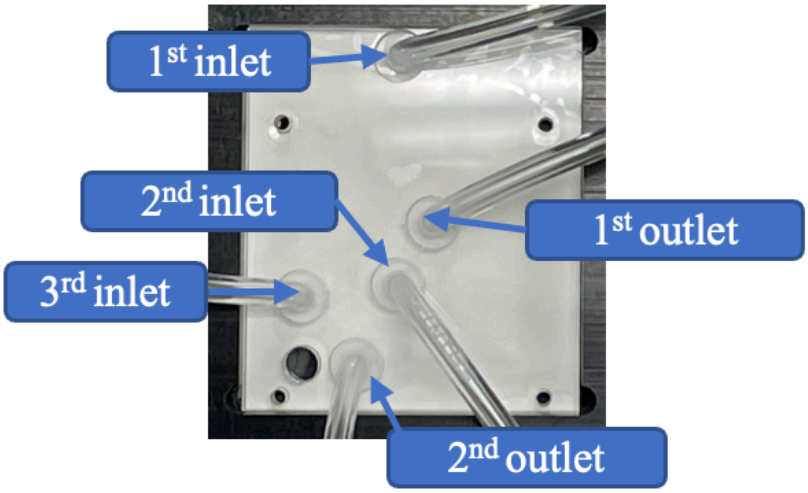

Image 2 Microfluidic cassette chip with mounted peristaltic pump tubings.

The 1st inlet was used to introduce 100 ul of sample containing NPs into magnetic separation chamber. Sample was prepared in the same way as described for tests performed on foils. Solution flow was performed using peristaltic pump with the flow rate of 40 ul/min, and magnetic field was generated by electromagnets and maintained until all solution was collected from 1st outlet. Paramagnetic NPs were entrapped in the magnetic field and stayed entrapped in the magnetic separation chamber, meanwhile solution was removed from microfluidic chip. 20 ul of dilution buffer was introduced to 1st inlet under flow rate of 40 ul/min. Electromagnets were turned off during this step to release the entrapped NPs. The solution containing NPs was collected from the 1st outlet and introduced to the 2nd inlet. The 2nd inlet and the 2nd outlet were connected to the microbioreactor with immobilized ABs. The solution was introduced to microbioreactor for 15 sec with a flow rate of 40 ul/min. Consequently, the flow was stopped, and the solution was incubated during 15 min. After incubation, the solution was removed from microbioreactor under the flow rate of 40 ul/min. To remove not immobilized NPs, 40 ul of dilution buffer was introduced to microbioreactor under the 40 ul/min flow rate. During the next step, 20 ul of TMB substrate was introduced to microbioreactor under the flow rate of 40 ul/min for 14 sec and incubated for 30 min. All solutions from microbioreactor were collected and introduced to detection chamber through the 3rd inlet under the 60 ul/min flow. Next, all microfluidic tubings were disconnected from microfluidic chip, chip holder was placed in the multiwell plate spectrophotometer, and point absorption was measured at 625 nm. Protocol presented above was used for all microfluidic chips-based experiments without modifications. Pt containing NPs/ABs conjugates was diluted 20

times with tested samples or dilution buffer. Sample content varied for different experiments, being a reason why more details about it will be provided in Chapter 3.

3. Results and discussion

3.1. Influence of reducing agent type and concentration on NPs stability

According to the dissertation topic, the main goal was to synthesize stable and catalytically active NPs which could be used in biotests for antigen detection. It was planned to use NPs with enzyme-like activity as natural enzyme alternatives in ELISA-like assays. Such NPs-based assays are called NLISA (nanozyme-linked immunosorbent assays) and are based on NPs/ABs conjugates. To be used in such tests, NPs should possess high catalytic activity and ability to be conjugated with ABs. Conjugation of ABs with Au NPs has been well studied and described in literature (Karyakin *et al.*, 2000; Lv *et al.*, 2021). During previous experiments (realized in the framework of research for master thesis) it was discovered that Au NPs showed lower peroxidase-like activity in comparison to other noble metal-based NPs (Ivanova *et al.*, 2021). Therefore, it was decided to combine Au with Ru, Pt, Os or Pd to obtain NPs with desirable properties. Due to the fact that multimetallic NPs provided for application in NLISA were used in multiple experiments, they were expected to be stable and catalytically active for at least one month. To obtain NPs with the characteristics listed above, the influence of composition was tested together with the influence of reducing agents (sodium borohydride, hydrazine and hydroxylamine hydrochloride) and their concentrations. Bimetallic NPs were synthesized using HBPG as the stabilizing agent due to the high catalytic activity and stability of HBPG-stabilized NPs (Zhou *et al.*, 2011, Zamboulis *et al.*, 2019).

Table 2 contains information regarding the hydrodynamic size (diameter measured using DLS technique of obtained NPs in relation to reducing agent type and its concentration).

Table 2. The hydrodynamic diameter of NPs synthesized with different type and concentrations of the reducing agent. Size measurement was performed with DLS technique using undiluted NPs samples. Each value represents hydrodynamic diameter average value from 6 measurements with standard deviation.

			NPs								
			Au	**Ru**	**Ru/Au**	**Pt**	**Pt/Au**	**Os**	**Os/Au**	**Pd**	**Pd/Au**
Reducing agent	**Hydroxylamine hydrochloride**	**30 mM**	70.20 (±9.05)	83.56 (±3.29)	91.41 (±5.61)	4.94 (±0.60)	not stable NPs	82.93 (±0.80)	not stable NPs	not stable NPs	not stable NPs
		40 mM	58.73 (±5.13)	86.33 (±3.23)	94.16 (±6.46)	72.43 (±12.40)	not stable NPs	57.25 (±7.70)	not stable NPs	not stable NPs	not stable NPs
		50 mM	not stable NPs	70.93 (±6.95)	65.18 (±17.27)	48.27 (±13.70)	not stable NPs	94.32 (±13.80)	not stable NPs	not stable NPs	not stable NPs
	Hydrazine	**30 mM**	not stable NPs	81.72 (±10.30)	not stable NPs	not stable NPs	not stable NPs	not stable NPs	not stable NPs	not stable NPs	not stable NPs
		40 mM	not stable NPs	78.18 (±11.20)	not stable NPs	not stable NPs	not stable NPs	not stable NPs	not stable NPs	not stable NPs	not stable NPs
		50 mM	not stable NPs	105.60 (±9.30)	not stable NPs	not stable NPs	not stable NPs	not stable NPs	not stable NPs	not stable NPs	not stable NPs
	Sodium borohydride	**30 mM**	33.93 (±0.60)	57.20 (±4.30)	not stable NPs	5.62 (±0.20)	35.78 (±25.50)	142.90 (±9.90)	4.30 (±0.70)	not stable NPs	not stable NPs
		40 mM	39.95 (±1.00)	9.50 (±0.7)	not stable NPs	5.74 (±0.40)	5.56 (±0.50)	not stable NPs	not stable NPs	not stable NPs	not stable NPs
		50 mM	6.01 (±0.20)	21.57 (±8.4)	48.1 (±5.0)	30.40 (±1.00)	4.92 (±1.00)	4.31 (±0.75)	434.78 (±31.40)	7.23 (±1.50)	273.37 (±33.09)
			Hydrodynamic diameter [nm]								

Size measurement was done after one month from NPs synthesis. All unstable NPs samples were eliminated from DLS measurements. Regarding the size, the biggest Au NPs were obtained using the solution of hydroxylamine hydrochloride (30 mM) as a reducing agent (70.20 nm), and the smallest Au NPs were obtained using sodium borohydride (50 mM). Au NPs synthesized using solutions of hydrazine (30 - 50 mM) and solution of hydroxylamine hydrochloride in concentration of 50 mM were unstable. Stable monometallic Pt NPs were synthesized using all tested concentrations of hydroxylamine hydrochloride and sodium borohydride. In the case of bimetallic Pt-containing NPs, it was possible to obtain stable NPs

only by using sodium borohydride. Synthesis of Ru monometallic NPs was possible using all reducing agents in all tested concentrations (30 - 50 mM). The smallest Ru NPs (9.50 nm) were obtained using solution of sodium borohydride (40 mM). Stable osmium monometallic NPs were obtained using solutions of hydroxylamine hydrochloride (30 – 50 mM) and solutions of sodium borohydride (30 and 50 mM). Os-containing bimetallic NPs were successfully synthesized only using 30 or 50 mM of sodium borohydride. It was possible to obtain Pd monometallic (7.23 nm) and bimetallic (273.37 nm) NPs using a solution of sodium borohydride (50 mM). All other attempts to synthesize Pd NPs were unsuccessful under applied conditions. DLS results proved the concept that both, the type of the reducing agent and its concentration influence NPs size and stability. After analysis of NPs size, all NPs characterized with hydrodynamic diameter higher than 100 nm were eliminated from the further tests.

3.2. NPs peroxidase-like activity examination

OPD-based method was used to check the usability of synthesized NPs as peroxidase mimetics. In the presence of hydrogen peroxide and natural HRP or nanozyme colourless OPD converts to yellow-orange product at slightly acidic conditions (Yu *et al.*, 2017).

The catalytic activity of enzymes is typically expressed by an increase in product or a decrease of substrate concentration in time and as suggested by The International System of Units, it is given in kats (Kudeyarov *et al.*, 2017). In this work, the catalytic activity was expressed as the increase in the concentration of the product in time, expressed by the evolution of the absorbance of the examined sample. According to Table 3 Au NPs prepared using sodium borohydride showed the highest catalytic activity in comparison to Au NPs synthesized with other types of reducing agents.

Table 3. Evaluation of absorbance increase for samples containing mono- and bimetallic NPs synthesized with different type and concentration of reducing agent against OPD (pH 4.5, at 450 nm). Each value represents an increase of absorbance average value from 5 measurements.

			NPs						
			Au	**Ru**	**Ru/Au**	**Pt**	**Pt/Au**	**Os**	**Os/Au**
Reducing agent	**Hydroxylamine hydrochloride**	**30 mM**	0.07 (±0.01)	0.11 (±0.02)	0.05 (±0.01)	0.02 (±0.00)	not stable NPs	0.08 (±0.01)	not stable NPs
		40 mM	0.03 (±0.01)	0.11 (±0.04)	0.03 (±0.03)	0.05 (±0.01)	not stable NPs	0.12 (±0.00)	not stable NPs
		50 mM	not stable NPs	0.07 (±0.03)	0.05 (±0.02)	0.06 (±0.01)	not stable NPs	0.13 (±0.03)	not stable NPs
	Hydrazine	**30 mM**	not stable NPs	3.87 (±0.18)	not stable NPs	not stable NPs	not stable NPs	not stable NPs	not stable NPs
		40 mM	not stable NPs	6.37 (±0.16)	not stable NPs	not stable NPs	not stable NPs	not stable NPs	not stable NPs
		50 mM	not stable NPs	7.18 (±037)	not stable NPs	not stable NPs	not stable NPs	not stable NPs	not stable NPs
	Sodium borohydride	**30 mM**	0.36 (±0.01)	24.59 (±0.69)	not stable NPs	28.95 (±0.73)	2.46 (±0.04)	>100 nm	not stable NPs
		40 mM	0.52 (±0.01)	44.77 (±1.79)	not stable NPs	24.67 (±1.94)	2.39 (±0.11)	not stable NPs	not stable NPs
		50 mM	0.56 (±0.01)	24.23 (±0.37)	12.16 (±0.78)	34.54 (±1.13)	2.52 (±0.61)	35.46 (±1.38)	>100 nm
			Absorbance increase [hr^{-1}]						

Au NPs, as it was expected, showed lower peroxidase-like activity in comparison to other monometallic and bimetallic NPs synthesized with the same type of reducing agent. The lowest HRP-like activity of Au NPs was detected for NPs prepared with 40 mM hydrazine (0.01 hr^{-1}). The highest catalytic activity among all obtained Ru NPs was detected for NPs synthesized with solution of 40 mM sodium borohydride (44.77 hr^{-1}). The second best with almost the same catalytic activity were Ru NPs synthesized with 30 and 50 mM solution of sodium borohydride (24.59 and 24.23 hr^{-1} respectively). The lowest activity among monometallic Ru-based nanozymes was demonstrated by NPs group synthesized with hydroxylamine hydrochloride. Bimetallic Ru-containing NPs showed decreased peroxidase-

like activity in comparison to monometallic Ru-containing NPs synthesized with the same reducing agent, whilst it was significantly higher in comparison to Au NPs synthesized with the same type of reducing agent. Monometallic Pt NPs synthesized with hydroxylamine hydrochloride were characterized by a decreased catalytic activity (0.02-0.06 hr^{-1}) in comparison to NPs synthesized with sodium borohydride (24.67-34.54 hr^{-1}). Stable bimetallic Pt-containing NPs were synthesized only with sodium borohydride. All three types of bimetallic Pt-containing NPs showed comparatively the same level of HRP-like activity (2.46, 2.39 and 2.52 hr^{-1} respectively). Mentioned bimetallic NPs were characterized by the lowest catalytic activity in contrast to another type of bimetallic NPs. Monometallic Os NPs synthesized using the solution of 50 mM sodium borohydride showed comparatively high 35.46 hr^{-1} peroxidase-like activity in comparison to other types of NPs. Despite the promising catalytic characteristics of monometallic Os NPs, stable bimetallic Os-containing NPs were not obtained with all used concentrations and types of reducing agents.

For Ru NPs, the highest catalytic activity was found to be related to the smallest size of such NPs. However, this relationship was not observed in other types of NPs. Such phenomena can be explained by the fact that catalytic activity of NPs not only related to size, but also other parameters that influence the catalytic activity of NPs.

3.3. Examination of quinonimine stability

To prove that nanozymes can be active in a wide pH range, NPs were also tested in near neutral and weakly alkaline solutions of universal buffer with PhOH/4AAP based method. Before examining the influence of pH on NPs activity, the stability of quinonimine (HRP-catalyzed PhOH/4AAP product) and the influence of pH on its optical properties were tested. The optical properties of some HRP-catalyzed reaction products strongly depend on the pH (Bovaird, Ngo and Lenhoff, 1982). Consequently, it was very important to investigate the influence of pH on optical properties of quinonimine before the mentioned substrate mixture was used for examination of enzyme-like activity in a wide range of pH. First, product stability in time was examined during the 30 min and for this aim, the registration of quinonimine spectra (spectra were registered at t=0, 15 and 30 min) was carried out. PhOH/4AAP substrate solution was isolated from HRP with dialysis membrane to stop the catalytic reaction after enzyme containing solution closed in the dialysis membrane was removed from examined sample. According to Figure 1, which represents quinonimine spectrum measured immediately after separation and in 15 and 30 min after sample separation from the enzyme, formed quinonimine did not decompose and remained stable during 30 min. According to these experimental results,

the validity of using the quinonimine in detection of pH influence on optical properties of such chromogenic product was proven.

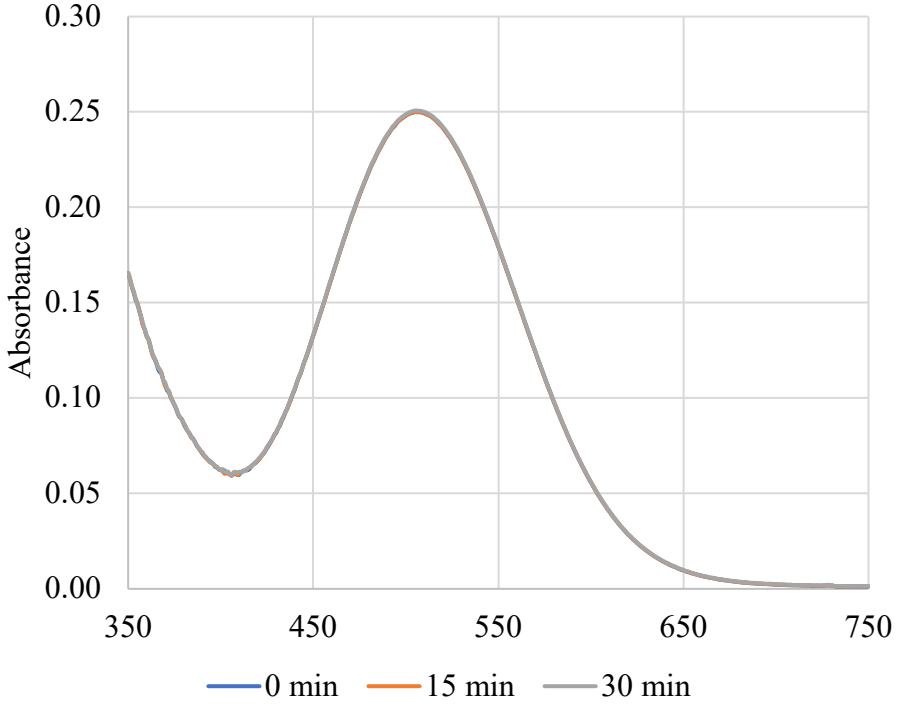

Figure 1. The UV-vis spectra of quinonimine registered at t=0, 15 and 30 min in the range of 350-750 nm.

To detect the influence of pH on optical properties of quinonimine, pH of a solution of such chromogenic product was adjusted to pH from 6.5 to 10.5 with solutions of universal buffer (0.1 M). Figure 2 represents absorbance values obtained for quinonimine at such pH range at 507 nm.

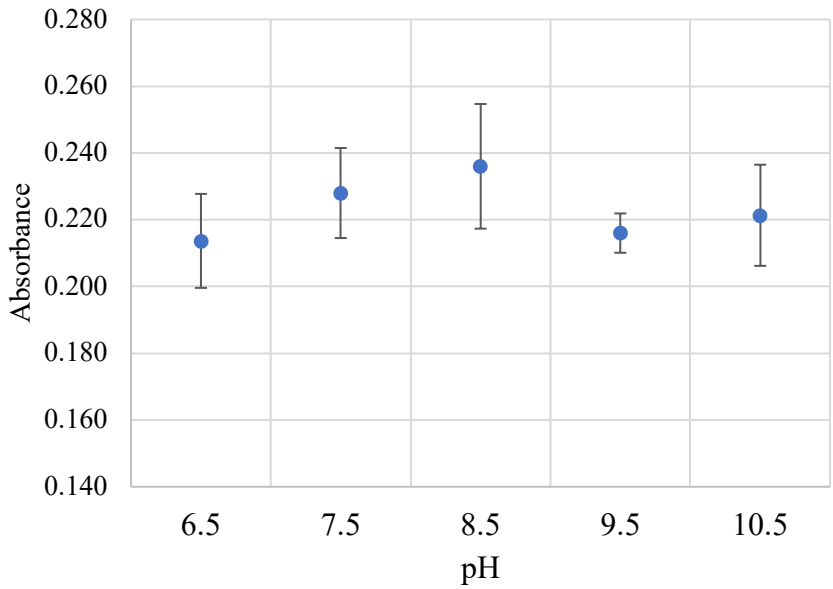

Figure 2. Absorbance of quinonimine solutions at pH 6.5-10.5 measured at 507 nm. Each point represents absorbance average value from 5 measurements with error bars representing standard deviation.

According to Figure 2, pH did not evidently influence absorbance measured at the 507 nm for a solution of quinonimine in the examined range of pH from 6.5 to 10.5. Absorbance detected at the specific wavelength depends on molar extinction coefficient, analyte concentration and light path length. In the previously discussed experiments, concentrations of analyte were the same due to the fact that the same volumes of one primary solution were used for preparation of samples characterized with different pH. Light path lengths were also the same because the same volumes of samples were distributed to the wells of the same 96-wells plate. As it is shown on Figure 2, absorbance of samples was in the range from 0.21 to 0.24. All observations listed above demonstrated that the molar extinction coefficient for quinonimine is virtually the same at pH range from 6.5 to 10.5, with no differences being statistically significant.

3.4. Influence of pH on peroxidase-like activity of nanozymes

Results described above allowed to use PhOH/4AAP substrate mixture for investigation of pH influence on the activity of nanozymes; it became possible, as obtained results proved that the molar extinction coefficient for quinonimine at pH range 6.5 - 10.5 is practically no different. The molar extinction coefficient presented in the literature was determined not in the whole range of pH that was needed for the experiments carried out within the scope of this work. Furthermore, in the literature, for molar extinction determination, different experimental conditions were applied (Yasmineh, Caspers and Theologides, 1992; Bedekar, A. and Jenkins,

Jerry and Sundaram, 2005; Nikolaos, 2007). This fact not only made impossible to directly use the information from the literature but also required an approach to be developed for the specific experiments conducted in this work.

Monometallic and bimetallic Pt- and Ru-containing NPs, along with Au NPs synthesized using sodium borohydride, were selected for investigating the influence of pH on NPs peroxidase-like activity in further experiments due to their stability and promising catalytic activity as tested with OPD-based methods.

Table 4. Evaluation of absorbance increase for samples containing mono- and bimetallic NPs tested with PhOH/4AAP- based method at 507 nm in a different pH. i, ii and iii stand for sodium borohydride concentration of 30, 40 and 50 mM, respectively. Each value represents an average value of absorbance increase from 5 measurements, with error bars representing a standard deviation.

		pH 6.5	**pH 7.5**	**pH 8.5**	**pH 9.5**	**pH 10.5**	
NPs	**Au i**	0.08 (±0.01)	0.17 (±0.03)	0.14 (±0.02)	0.12 (±0.05)	0.08 (±0.01)	**Absorbance increase [hr^{-1}]**
	Au ii	0.29 (±0.02)	0.27 (±0.01)	0.13 (±0.11)	0.10 (±0.06)	0.13 (±0.02)	
	Au iii	0.22 (±0.07)	0.33 (±0.09)	0.30 (±0.01)	0.25 (±0.04)	0.18 (±0.01)	
	Pt i	4.33 (±0.18)	2.68 (±0.07)	1.39 (±0.02)	0.97 (±0.08)	0.72 (±0.10)	
	Pt ii	4.37 (±0.35)	2.88 (±0.15)	2.18 (±0.07)	1.23 (±0.09)	0.93 (±0.02)	
	Pt iii	4.45 (±0.38)	2.46 (±0.08)	1.04 (±0.11)	0.59 (±0.21)	0.43 (±0.03)	
	Pt/Au i	0.20 (±0.04)	0.23 (±0.01)	0.25 (±0.09)	0.31 (±0.04)	0.30 (±0.01)	
	Pt/Au ii	0.17 (±0.06)	0.20 (±0.06)	0.22 (±0.04)	0.31 (±0.08)	0.28 (±0.07)	
	Pt/Au iii	0.73 (±0.09)	0.83 (±0.09)	0.81 (±0.01)	0.81 (±0.06)	0.77 (±0.09)	
	Ru i	11.86 (±0.01	10.95 (±1.09)	11.73 (±0.21)	12.38 (±0.51)	24.46 (±0.31)	
	Ru ii	10.12 (±0.98)	13.07 (±1.74)	14.61 (±0.20)	15.04 (±0.09)	23.28 (±0.82)	
	Ru iii	3.53 (±0.40)	4.13 (±0.24)	4.08 (±0.11)	2.38 (±0.05)	2.03 (±0.57)	
	Ru/Au iii	1.20 (±0.66)	1.10 (±0.03)	0.92 (±0.01)	0.61 (±0.05)	0.45 (±0.07)	

According to Table 4, all types of Au NPs in the applied pH range showed lower catalytic activity in comparison to Pt and Ru monometallic and bimetallic NPs. Furthermore, for Au NPs activity there were no significant changes in a function of pH observed. Within the pH range between 6.5-10.5, monometallic Ru i and Ru ii NPs synthesized with 30 and 40 mM

solution of sodium borohydride, respectively, demonstrated increased catalytic activity in comparison to other types of NPs. Moreover, the peroxidase-like activity of mentioned NPs increased with the increase of the pH. The highest activity of Ru iii NPs was detected at pH 7.5 (4.13 hr^{-1}) and 8.5 (4.08 hr^{-1}). The nanozyme activity of bimetallic ruthenium NPs decreased when increasing the pH. The highest peroxidase-like activity for bimetallic Ru/Au iii NPs was detected at pH 6.5 (1.20 hr^{-1}). Combination of Ru with Au in NPs gave nanozymes decreased peroxidase-like activity in comparison to monometallic ruthenium NPs; however, bimetallic Ru/Au NPs had higher catalytic activity in comparison to Au NPs. The catalytic activity of monometallic Pt NPs decreased with the increase of pH. The highest catalytic activity of such NPs was detected at pH 6.5 and was comparatively same for all three types of monometallic platinum NPs (4.33, 4.37 and 4.45 hr^{-1}). Bimetallic Pt/Au i and Pt/Au ii NPs were characterized with the lowest activity in comparison to Pt/Au iii and Ru/Au iii. Pt/Au iii NPs exhibited the highest catalytic activity among bimetallic platinum NPs (0.73 - 0.77 hr^{-1}) without significant dependence on pH value.

3.5. Investigation of catalytic activity mechanism of Ru-containing NPs

According to OPD- and PhOH/4AAP-based tests results, Ru-containing NPs showed the highest peroxidase-like activity in comparison to other examined NPs. Furthermore, the increased catalytic activity of such NPs in higher pH brought the suspicion that activity of the solution of Ru NPs could be the result of homogeneous and heterogeneous catalytic activity mechanism. A combination of these two mechanisms could result in the increased catalytic activity of the Ru-containing NPs. High catalytic activity is an important characteristic of the nanozymes used in NLISA. The homogeneous mechanism can be based on the activity of ions released from NPs, while heterogeneous mechanism results from the active sites located on the surface of NPs (Rodrigues, da Silva and Camargo, 2019). To prove the existence of homogeneous catalytic activity mechanism of Ru NPs ions, which could be released, PhOH/4AAP-based tests were utilized. NPs solutions were entrapped in a dialysis membrane (and dialyzed against appropriate buffer solutions) to separate NPs from contacting solutions which, according to the assumption, should contain released ions. Dialysates were collected every day for 4 days, their activity was confirmed and released ions were detected (Table 5).

Table 5. Absorbance increase for NPs dialysate solutions incubated at different pH. i, ii and iii stand for sodium borohydride concentration of 30, 40 and 50 mM, respectively. Analytical signals were measured at 507 nm with PhOH/4AAP-based test Each value represents an average value of absorbance increase from 5 measurements with standard deviation.

NPs/pH	Absorbance increase [hr^{-1}]		
	2nd	3rd	4th
Ru i / 6.5	0.41 (±0.07)	0.43 (±0.03)	0.44 (±0.02)
Ru i / 7.5	0.53 (±0.04)	0.51 (±0.02)	0.53 (±0.03)
Ru i / 8.5	0.53 (±0.04)	0.51 (±0.02)	0.50 (±0.10)
Ru i / 9.5	0.55 (±0.01)	0.55 (±0.04)	0.59 (±0.04)
Ru i / 10.5	0.70 (±0.02)	0.72 (±0.03)	0.71 (±0.06)
Ru ii / 6.5	0.20 (±0.03)	0.18 (±0.05)	0.18 (±0.03)
Ru ii / 7.5	0.18 (±0.04)	0.18 (±0.05)	0.17 (±0.04)
Ru ii / 8.5	0.20 (±0.04)	0.20 (±0.02)	0.20 (±0.08)
Ru ii / 9.5	0.34 (±0.03)	0.37 (±0.06)	0.38 (±0.05)
Ru ii / 10.5	0.13 (±0.04)	0.12 (±0.02)	0.13 (±0.02)
Ru iii / 6.5	0.09 (±0.02)	0.07 (±0.01)	0.09 (±0.02)
Ru iii / 7.5	0.12 (±0.04)	0.09 (±0.03)	0.11 (±0.04)
Ru iii / 8.5	0.16 (±0.02)	0.14 (±0.00)	0.14 (±0.03)
Ru iii / 9.5	0.19 (±0.03)	0.20 (±0.03)	0.19 (±0.04)
Ru iii / 10.5	0.11 (±0.01)	0.11 (±0.01)	0.12 (±0.02)
Ru/Au iii / 6.5	0.04 (±0.00)	0.05 (±0.02)	0.05 (±0.01)
Ru/Au iii / 7.5	0.08 (±0.01)	0.07 (±0.03)	0.06 (±0.03)
Ru/Au iii / 8.5	0.09 (±0.00)	0.10 (±0.02)	0.09 (±0.01)
Ru/Au iii / 9.5	0.03 (±0.02)	0.02 (±0.01)	0.03 (±0.02)
Ru/Au iii / 10.5	0.10 (±0.02)	0.06 (±0.01)	0.08 (±0.01)

Results for experiments derived from dialysates collected on the first day are not present due to their possible contamination with NPs stacked in membranes wrinkles and knots; these results were eliminated completely and not compared with the rest of the data. DLS measurement was used to prove the NPs absence in dialysates collected on 2nd, 3rd and 4th day. Dialysates collected from consecutive three days were similar in terms of catalytic activity, which confirmed continuous ion release from examined NPs. Such phenomenon could be

explained with possible partial oxidation and dissolution of Ru-containing NPs. The catalytic activity detected for dialysates samples derived from Ru i NPs increased together with the increasing pH, peaking 0.72 hr^{-1} at pH 10.5. Ru ii and Ru iii dialysates samples demonstrated the highest catalytic activity at pH 9.5 (0.34-0.38 and 0.19-0.20 hr^{-1}, respectively). It was discovered that dialysates of bimetallic NPs were characterized with lower catalytic activity in comparison to monometallic ones. Such phenomenon has a simple explanation – monometallic NPs contained higher amount of Ru (Lawrence, Bullock and Holder, 2017; Verma and Mohapatra, 2021). Due to the fact that Ru chemistry is quite complex and diverse, at different pH various Ru ions could be formed, and their complexes show different catalytic activity, which influenced results shown above (Arends, Kodama and Sheldon, 2004). However, the speciation of ruthenium was significantly beyond the conducted research plan, and it was not investigated further. The results of peroxidase-like activity of Au- and Pt-containing NPs dialysates are not presented due to lack of ions released under applied experimental conditions, which was also reported in the literature (Bradley, Arking and Beers, 1960).

Table 6. Concentrations of Ru-based ions in 3rd day dialysates as a function of pH, examined with EDXRF technique. i, ii and iii stand for sodium borohydride concentration of 30, 40 and 50 mM, respectively.

	Ru concentration [ppm]			
pH	**Ru i**	**Ru ii**	**Ru iii**	**Ru/Au iii**
6.5	43.70	36.70	31.90	26.90
7.5	23.90	34.90	22.30	44.70
8.5	41.50	38.10	31.70	38.00
9.5	34.50	31.70	30.90	37.20
10.5	37.10	38.70	45.30	38.20

Presence of Ru ions in dialysates collected on the 3rd day was additionally verified using the EDXRF technique (Table 6). This technique allowed to detect only elements presence without their speciation. According to the presented results, pH can influence the release of Ru ions, just as it was expected. According to Table 6, the highest amount of Ru ions that was released from NPs was detected for Ru iii dialysates at pH 10.5 (45.30 ppm). The smallest concentration of ruthenium was found in Ru i and Ru iii dialysate at pH 7.5 (23.90 and 22.30 ppm, respectively). Concentration of ruthenium detected in examined samples did not overlap with peroxidase-like activity of such dialysates. This phenomenon can be explained by the presence of ruthenium forms characterized with different solubility and catalytic activity.

3.6. Concept of multimetallic multi-functional NPs

Based on the results shown in Chapters 3.1, 3.2 and 3.4 above, combinations of Pt or Ru with Au was chosen to be used in further experiments as the ones being the most catalytically active and stable. Platinum NPs were typical heterogeneous catalyst, in which the active sites were mainly represented by surface-zero Pt atoms and bounded Pt^{2+} ions typically generated during reduction. In addition, platinum has a low tendency to spontaneous formation of its oxidized forms. On the other hand, ruthenium complexes, as well as its metallic or oxide forms, exhibit strong peroxidase-like activity. Moreover, catalytic activity mechanism of Ru-based nanomaterials can be based on electron transfer acceleration process. Ru-catalyzed dissociation of hydrogen peroxide occurs in a wider pH range in comparison to nanocatalysts with a typical activity mode dependent on an $^{\bullet}OH$ radical generation (Cao *et al.*, 2017).

According to the results shown in Chapter 3.5, Ru-containing NPs are classified as catalysts with a mixed mechanism, combining both homogeneous and heterogeneous activity, and their catalytic activity is partially independent of the availability of the active surface. The presence of gold in the structure is crucial from the point of view of NPs functionalization; this metal itself is a relatively weak mimetic of HRP, but it is an incomparable platform for the needs of bioconjugation due to the stability of the thiol-Au bond, superior to other, more catalytically active noble metals. Therefore, hybrid NPs were used in the immunoassay development, combining the advantages of magnetic cores of Fe_3O_4, the activity of Pt and Ru coatings and the chemisorption capability of Au towards thiols.

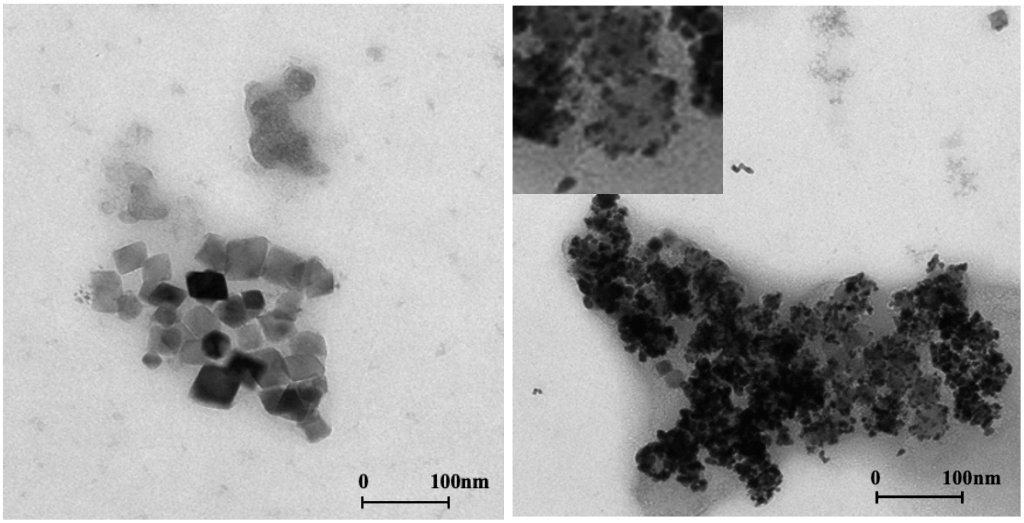

Image 3. ***Left*** *– TEM image of Ru-containing NPs.* ***Right*** *– TEM image of Pt-containing NPs.*

Image 3 shows TEM images of multimetallic NPs (Fe_3O_4/Ru/Au and Fe_3O_4/Pt/Au) synthesized as a part of this work. Their morphologies were coherent with the morphology of

platinum-decorated oxide NPs obtained earlier for iron(II, III) by M.S. Kim in 2017, in which characteristic flower-like morphology was observed, attributed to the large lattice mismatch between core and shell material forcing a growth according to Volmer-Weber mode (M. S. Kim *et al.*, 2017). To ensure a strong response of the particles to magnetic field and a convenient interface for nucleation and growth of metallic components, a modified method of synthesizing of cubic magnetite cores using the controlled oxidation of iron(II) precursor described by Goon et al. was used (Goon et al., 2009). The synthesis and stabilization with the strongly cationic PDDA as capping agent was carried out entirely in the aqueous environment, and was found to be an effective synthetic approach, perfectly limiting the aggregation of NPs, which facilitated the control of their size and magnetic properties. Obtained non-spherical Fe_3O_4 nanocores (nanocubes) were characterized as good and efficient platforms for noble metal decoration process. Irregular shapes of the cubic iron oxide nanoseeds with corners and edges could serve as high-energy heterogeneous nucleation sites *(Palchoudhury* et al.*, 2010)*.

The ζ -potentials of PDDA-capped nanocubes at pH 7.0 and ~ 12.0, was measured to be +52.0 mV and +41.3 mV, respectively, which confirms that this capping agent brought a stable charge under the conditions of the synthesis and decoration process, minimizing the risk of aggregation and facilitating the growth of the metal islands.

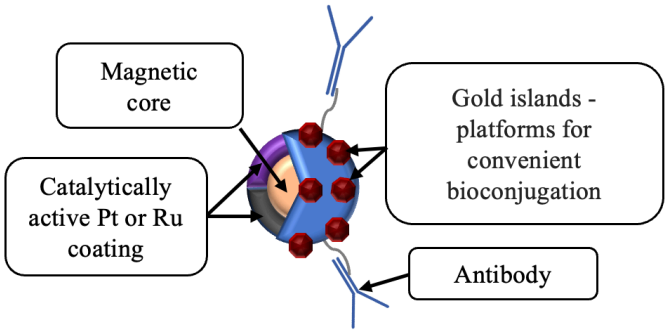

Scheme 27. NPs/ABs conjugate structure (scheme does not represent true size and shape of NPs).

Scheme 27 displays schematic representation of noble metal-decorated magnetic NPs. The NPs do not necessarily have to be characterized with an alloy structure in order to demonstrate certain functions. More importantly, the morphology of the NPs is to be such that the catalytically active parts have access to the substrate, and the parts involved in conjugation have contact with the ABs. Such NPs can be used as multifunctional components of the NLISA immunoassay (Scheme 28).

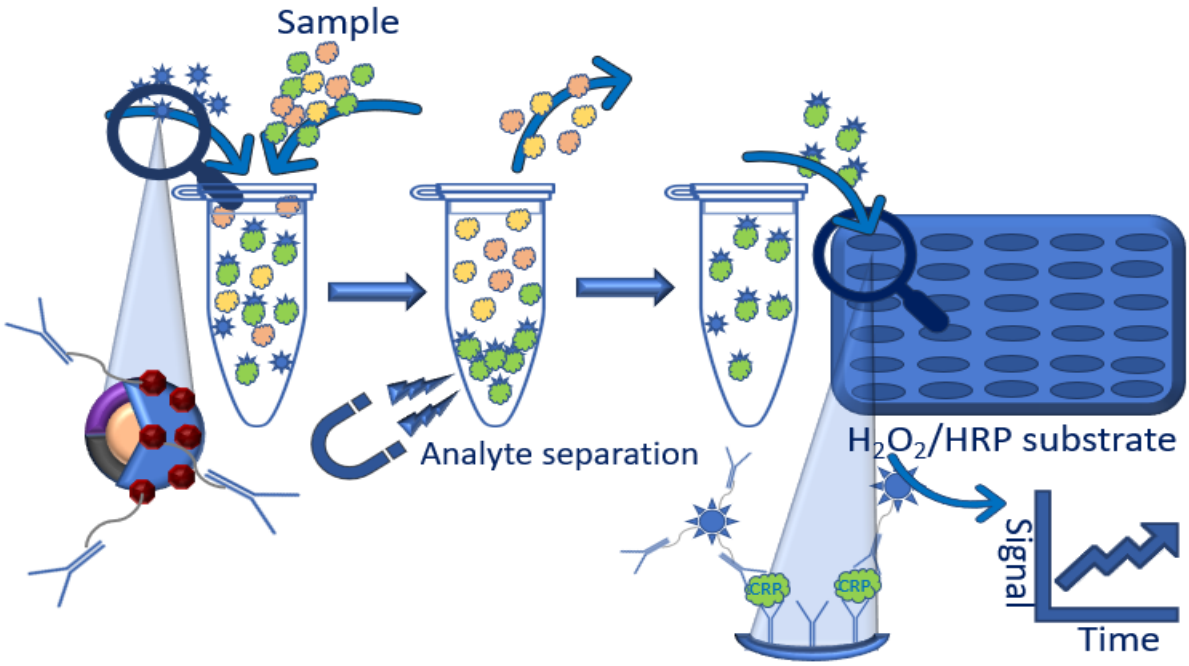

Scheme 28. NLISA test based on usage of multifunctional NPs.

NPs/ABs conjugates were designed to act as both a nanosorbent concentrating antigen by magnetic separation, and as inorganic catalysts (nanozymes) for the analytical signal generation due to the intrinsic peroxidase-like activity. The combination of desirable features of a nanosorbent and an easily functionalized nanozyme required an appropriate design of the synthetic pathway. Iron oxide nanocubes were synthesized using a modified controlled oxidation method and coated in situ with PDDA to give the surface a strongly cationic character, and facilitate the nucleation of noble metal residues in the seed-growth method. Due to the fact that the Pt and Au precursors exist in the form of complex anions - $AuCl_4^-$ and $PtCl_6^{2-}$, respectively - it was suspected that mentioned precursors interact with polycationic capping ligands located on iron oxide nanocubes according to a mechanism similar to one described for the interaction of PEI with hexachloroplatinate (Huang and Liu, 2017).

Synthesized iron(II, III) oxide nanocubes were characterised with size of approximately 36.71 ± 1.80 nm and exhibited superparamagnetic properties allowing for their effective separation in a magnetic field generated using neodymium magnet. Such property can be used for translocation and separation of previously bound analytes, opening the possibilities of sample preconcentration and minimizing the impact of interferents. In turn, Ru or Pt coating provides peroxidase-like activity and takes part in analytical signal generation. Ru or Pt coating was achieved by adding Ru or Pt precursors to a solution of iron oxide nanocubes and reducing it using sodium borohydride. Numerous visible gold nanoislands with a fairly homogeneous

distribution on NPs surface, obtained under mild reducing conditions, were responsible for conjugation with ABs.

Pt and Au were able to grow on the magnetite surface in form of islands and grains, which was confirmed by the analysis of TEM images (Zhang, Shaikhutdinov and Freund, 2015). On the other hand, few reports indicate a moderately homogeneous dispersion of Ru NPs over Fe_3O_4 in form of a semi-continuous interface obtained in the processes of chemical co-precipitation and post-synthetic galvanic decoration, which is in line with results obtained for seed-growth, reductive Ru deposition (Ai *et al.*, 2022; Kumar *et al.*, 2022). Furthermore, fairly homogeneous deposition of Ru-residues was observed without the formation of distinct regions of atomic separation in the form of visible islands. It was expected that the Pt and Ru NPs would cause the growth of Au interphases to start as separate, monometallic Au islands on the Pt/Ru facets, followed by gradual Au atom diffusion. (Prati *et al.*, 2011; Wu *et al.*, 2015). However, due to the small proportion of Au residuals to the total surface of NPs, no influence of their inhomogeneous distribution on the morphology of the entire nanostructures was observed.

3.7. Examination of influence of surface modification steps on multifunctional multimetallic NPs activity

Literature analysis indicates that any type of surface NPs modification influences the stability and catalytic activity of NPs (Gao *et al.*, 2007). Obtained iron oxide NPs were tested with TMB-based test to examine their peroxidase-like activity (Figure 3).

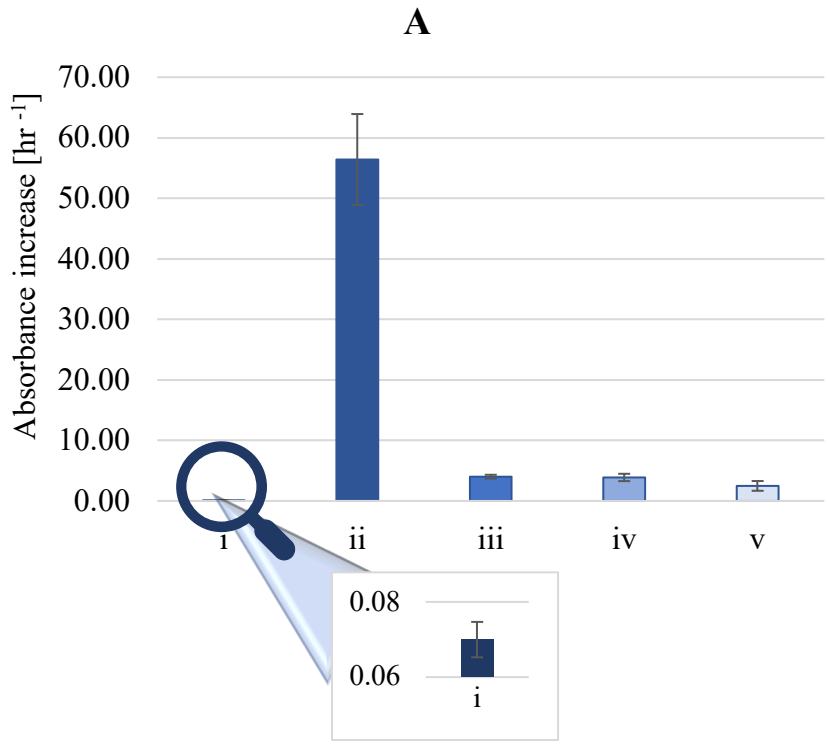

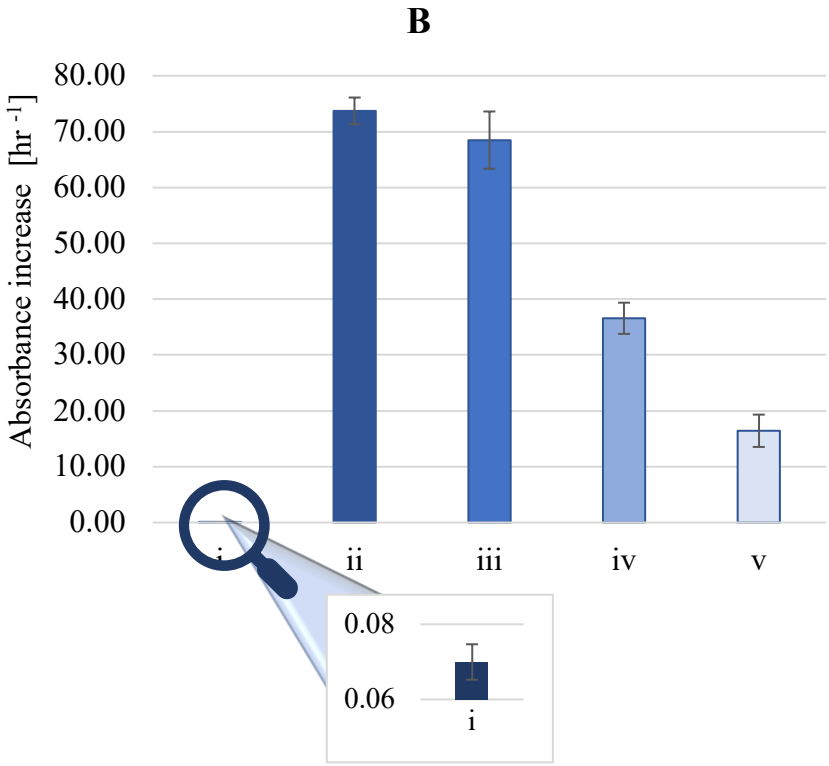

*Figure 3. Absorbance increase for samples obtained for the different stages of RuNPs/ABs (**A**) and PtNPs/ABs (**B**) conjugates synthesis. **i** - analytical signal derived from stabilized iron(II,III) oxide NPs; **ii** - analytical signal derived from samples collected after decoration with Ru (**A ii**) or Pt (**B ii**); **iii** - analytical signal derived from samples collected after Au decoration on Fe_3O_4/Ru (**A iii**) and Fe_3O_4/Pt (**B iii**) and NPs stabilization with thiolated* carboxylic-*PEG; **iv** - analytical signal derived from samples collected after surface activation with sulfo-NHS and EDC; v- analytical signal derived from samples collected after ABs conjugation with NPs.*

TMB substrate was chosen for peroxidase-like activity determination, due to the fact that such substrate is one of the most popular HRP substrates used in ELISA assays, and produced multifunctional NPs were planned to be applied in NLISA assay (Huang *et al.*, 2018). Weak (0.07 hr^{-1}) peroxidase-like activity was detected for iron oxide NPs which is in line with existing examples from the literature (Gao *et al.*, 2007, 2007; Nie, Shi and Yu, 2016). Iron oxide cores were modified with Pt or Ru to increase the catalytic activity. The addition of Pt sharply increased peroxidase-like activity of paramagnetic core from 0.07 hr^{-1} to 73.71 hr^{-1}. Modification with Ru amplified peroxidase-like activity of NPs up to 56.41 hr^{-1}. During the next step, NPs surface was decorated with gold nanoislands NPs and stabilized with thiolated carboxylic-PEG in order to create active sites for conjugation with ABs. Decoration with gold nanoislands together with stabilization slightly decreased catalytic activity for Pt-containing NPs (68.47 hr^{-1}). In the case of Ru-containing NPs, peroxidase-like activity was dramatically

decreased down to 4.01 hr^{-1}. The changes in the catalytic activity of NPs were not only caused by the introduction of metals characterized by lower catalytic activity but also by the addition of a stabilizer that can block catalytically active sites on the NPs surface. In the case of Ru-containing NPs, the stabilizer may have also entrapped released ions and/or taken part in the creation of less catalytically active forms of Ru.

During the next step, PEG carboxylic groups were activated with EDC and sulfo-NHS. Carboxylic groups reacted with EDC and sulfo-NHS, which led to the formation of unstable o-acylisourea ester which was then converted to semi-stable NHS-ester. Excessive or not reacted EDC and sulfo-NHS could interact with NPs surface during the modification process. As any other interaction with NPs surface, such modification changed the activity of NPs. In the case of Ru-containing NPs, catalytic activity was slightly decreased (3.88 hr^{-1}) in comparison to activity detected during the previous modification step. EDC/sulfo-NHS surface modification of Pt-containing NPs sharply reduced their activity approximately two-fold (36.57 hr^{-1}). After the activation of NPs surface ABs were added. As an experimental model, polyclonal anti-CRP ABs were chosen for NPs surface modification. Stable amide bond was formed between NPs and ABs. ABs immobilization on NPs surface also influenced NPs catalytic activity. In the case of Pt NPs/ABs, conjugate activity was decreased approximately two-fold (16.42 hr^{-1}). RuNPs/ABs conjugate peroxidase-like activity was only decreased down to 2.48 hr^{-1}. Presented results proved the theory that modification of NPs surface can decrease a catalytic activity of nanozymes. Nevertheless, the final peroxidase-like activity of modified NPs/ABs conjugates was significantly higher than the primary activity of iron oxide cores.

3.8. Characterization of multifunctional multimetallic NPs

3.8.1. Vis-NIR spectrophotometry

Vis-NIR spectrophotometry was used to control PDDA-stabilized iron(II,III) oxide NPs decoration with Pt or Ru and consequent decoration with Au. NPs samples were collected after, NPs modification with Ru/Pt and Au and absorption spectra of sample solutions were measured and examined. After each step, NPs solution were separated in a magnetic field (generated with neodymium magnet) until no nonmagnetic NPs were found in supernatant. Magnetic separation was repeated 5 times, and already after 4^{th} separation no nonmagnetic NPs were detected. Detection of nonmagnetic NPs was done with Vis-NIR spectrophotometry.

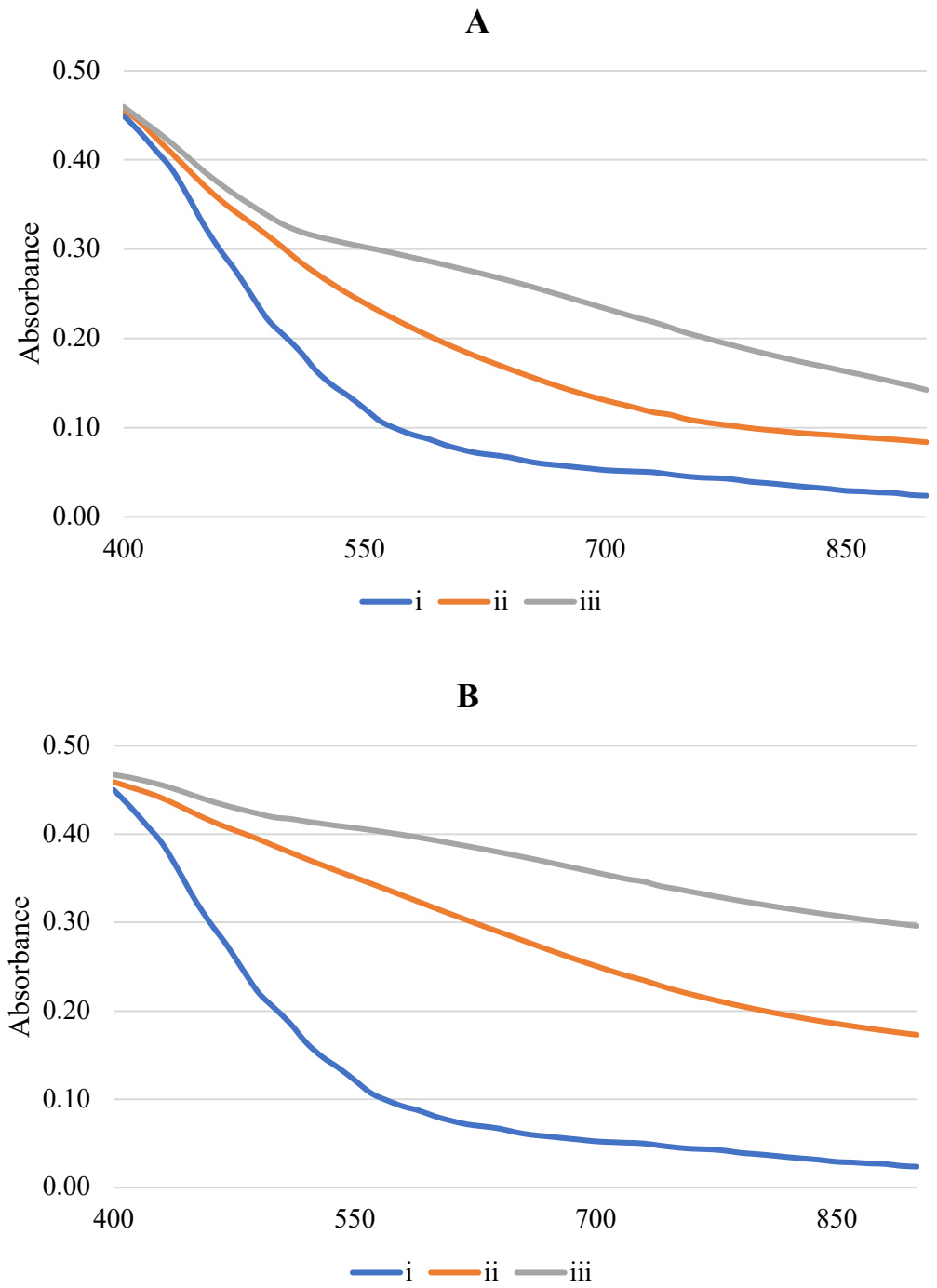

*Figure 4. Vis-NIR spectra of NPs samples obtained on the different stages of RuNPs/ABs (**A**) and PtNPs/ABs (**B**) conjugates synthesis. **i** - spectra of stabilized iron(II,III) oxide NPs; **ii** - spectra measured after decoration with Ru (**A ii**) and Pt (**B ii**); **iii** - spectra measured after Au decoration on Fe_3O_4/Ru (**A iii**) and Fe_3O_4/Pt (**B iii**). All spectra were measured in the range of 400-900 nm.*

Figure 4 shows absorption spectra measured in the range of 400 - 900 nm after each metal addition. Change of absorbance spectrum detected after addition of Pt and Ru pointed to the fact that modification was successful. In addition, such result correlated with catalytic activity increase described in previously presented Chapter 3.7. Subsequent absorbance

spectrum change was detected after NPs modification with gold. Confirmation of NPs modification with gold was made with vis-NIR spectrophotometry and also correlated with previously presented results of peroxidase-like activity decrease detected for the same sample. In the whole tested range absorbance significantly increased. Absorbance increased especially for wavelength longer than 500 nm and at about 600 nm one could observe a formation of a kind of characteristic band.

3.8.2. Elementary analysis

EDX spectroscopy, EDX mapping and EDXRF techniques were used for NPs elementary composition analysis. For NPs synthesis, iron oxide nanoseeds, gold precursor and platinum or ruthenium precursors were used; therefore, final composition of NPs should cover Fe, Pt or Ru and Au. NPs samples were magnetically separated and resuspended in ethanol before the analyses.

A

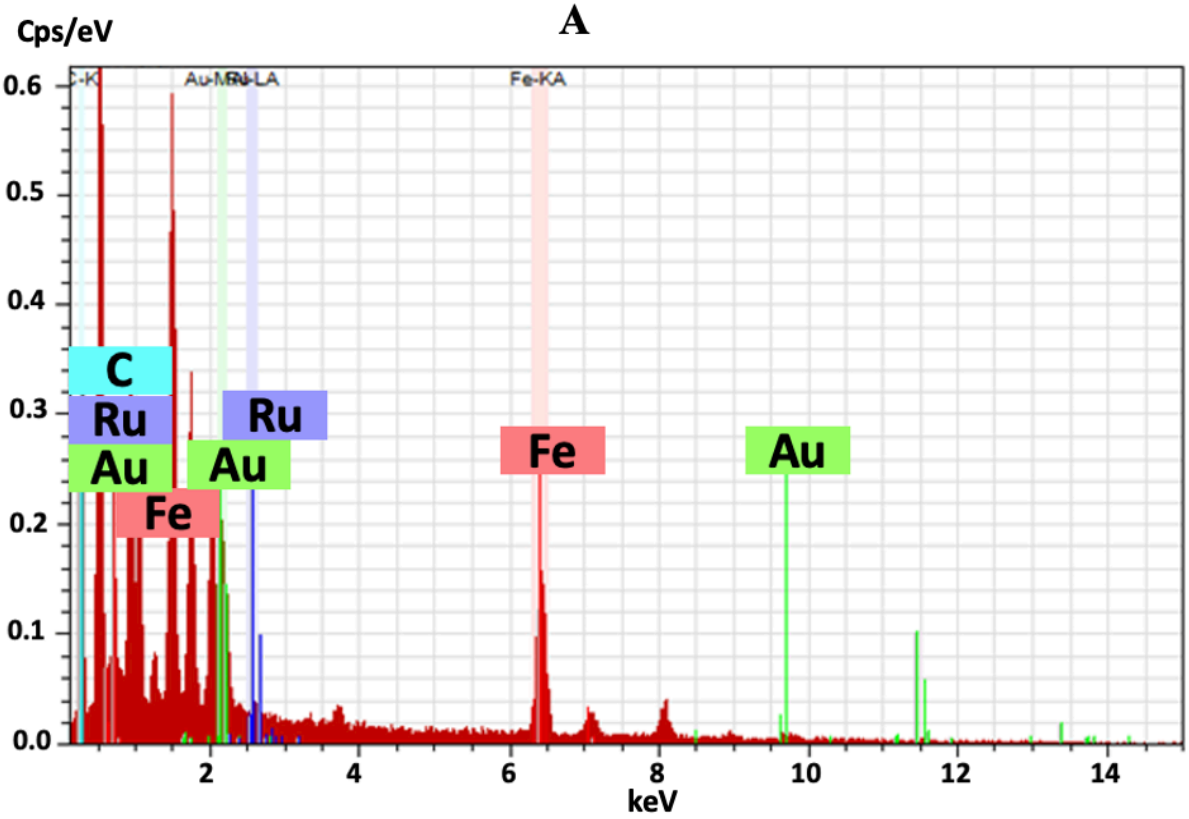

B

Element	C [ppm]
Fe	2418.00
Ru	685.50
Au	0.56

C

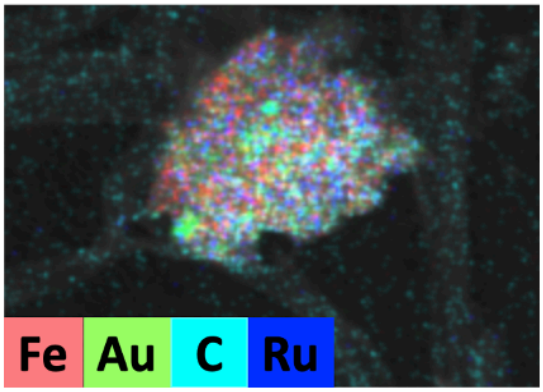

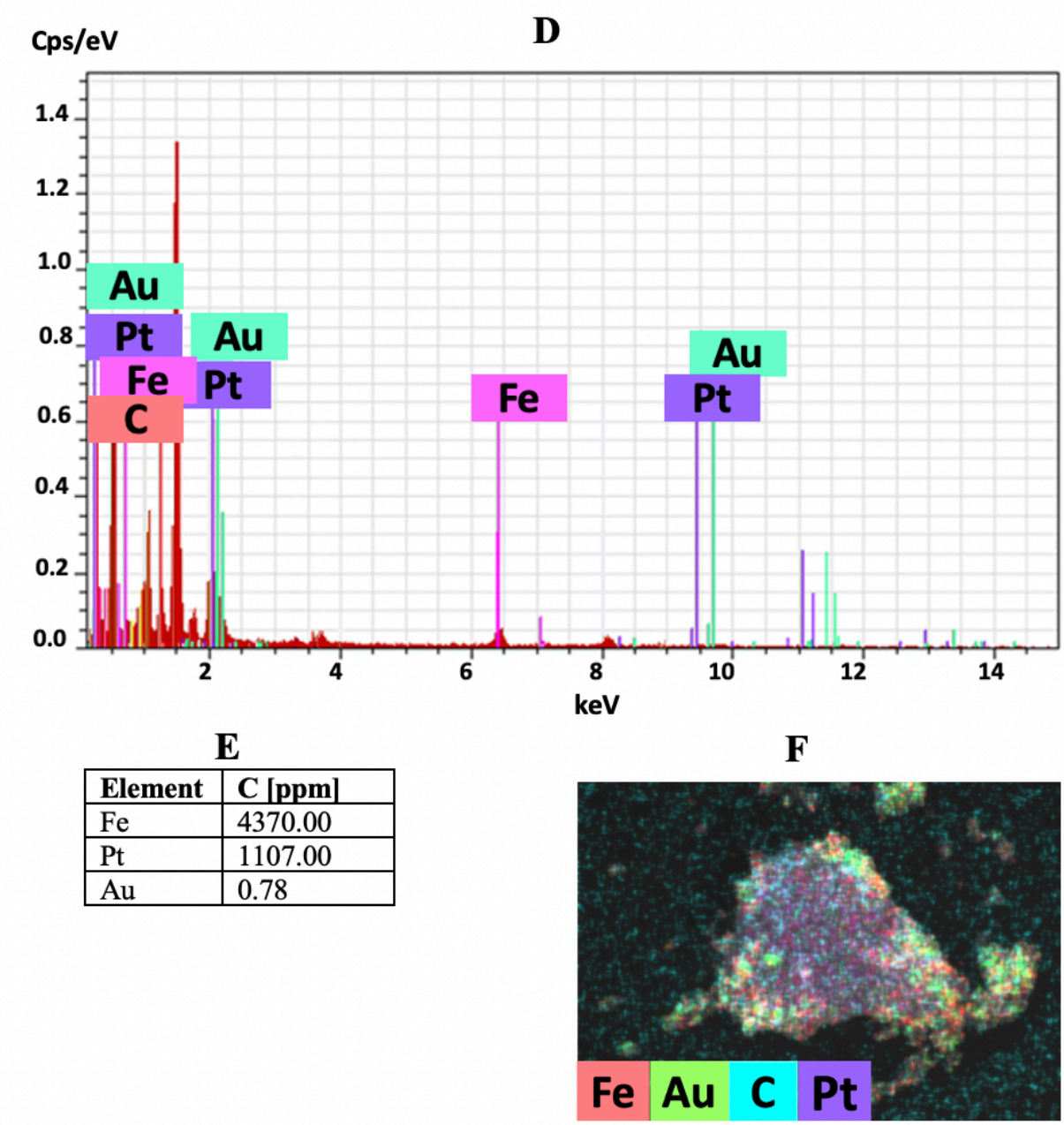

Element	C [ppm]
Fe	4370.00
Pt	1107.00
Au	0.78

*Figure 5. **A** - EDX spectroscopy-based elementary analysis of RuNPs/ABs sample; **B** - main elements concentration of RuNPs/ABs sample determined with EDXRF; **C** - EDX elementary mapping of RuNPs/ABs sample; **E** - EDX spectroscopy elementary analysis of RuNPs/ABs sample; **F** - main elements concentration of RuNPs/ABs sample determined with EDXRF; **G** - EDX elementary mapping of RuNPs/ABs sample.*

According to Figure 5 which represents EDX spectroscopy results, RuNPs/ABs conjugate sample containing Fe, Ru and Au, was relevant to metal precursors and iron oxide nanoseeds which were used for NPs synthesis. EDXRF analysis showed that RuNPs/ABs conjugate sample mostly contained Fe (2418.00 ppm). Such phenomenon could be explained with magnetic separation and the fact that the sample could contain not only trimetallic NPs but also unmodified iron oxide NPs. Magnetic field sample treatment not only separated non-

paramagnetic NPs but also helped to exchange solution in which such NPs are suspended. EDXRF-based determination of Ru (685.50 ppm) and Au (0.56 ppm) in analyzed sample proved a presence of such elements in synthesized NPs. EDX mapping analysis also detected the presence of mentioned elements in the examined sample. In the case of PtNPs/ABs conjugate sample, EDX spectroscopic analysis detected presence of Fe, Pt, and Au in the tested sample. EDXRF analysis showed concentration of Fe in Pt-containing sample which was almost twice higher (4370.00 ppm) than in Ru-containing sample. It was detected that concentration of Pt in the sample was equal to 1107.00 ppm. Presence of Pt same as presence of Ru corresponded for NPs catalytic activity. Concentrations of iron and gold precursors used during synthesis was the same for both types of multimetallic NPs. During multimetallic NPs synthesis Pt and Ru precursors were also used in the same concentration. According to EDXRF analysis, PtNPs/ABs conjugate samples contained more Fe in comparison to Ru-containing sample. Additionally, a higher level of element responsible of NPs catalytic activity was detected for Pt-containing NPs. Detection of Au in PtNPs/ABs conjugate samples finalized a verification of all three main metal presence in synthesized NPs. EDX elementary mapping showed the presence of all three Fe, Pt, and Au elements in the analyzed samples.

3.9. NLISA

3.9.1. Detection of ABs on NPs surface

To detect the presence of immobilized ABs on NPs surface TMB-based immunoassay was used. At the same time, nonspecific interactions of NPs/ABs conjugates with ABs and unmodified surface of PET MaxiSorp™ plates were examined. In the case of ABs presence on NPs surface NPs/ABs conjugate should interact with specific ABs immobilized on MaxiSorp™ plates surface. As a result of this interaction, NPs/ABs conjugates were immobilized on wells surfaces and not removed during the washing step, and catalyzed product formation. If NPs/ABs conjugates did not interact with non-specific ABs or with the unmodified surface of the MaxiSorp™ plate, they were removed during the washing step and did not take part in signal generation (Scheme 29).

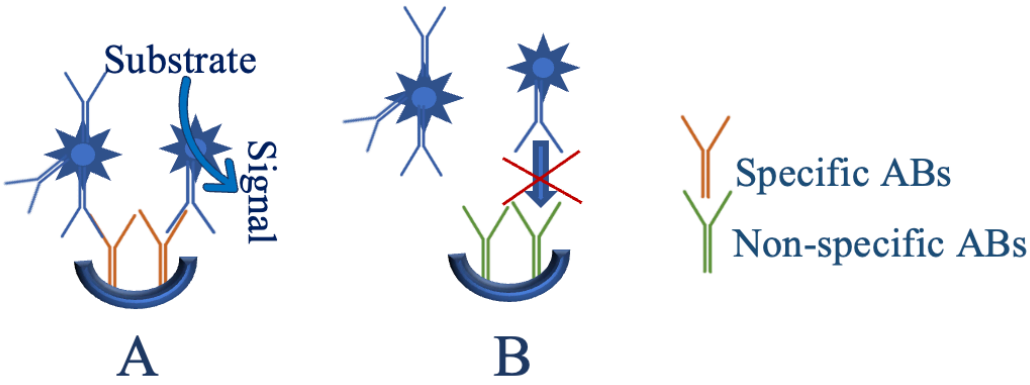

*Scheme 29. Interaction between NPs/ABs conjugates with specific(**A**) or nonspecific(**B**) ABs immobilized on the multi-well plates surface.*

NPs were conjugated with anti-human CRP ABs while surface of 96-well plate was modified with specific and nonspecific ABs. Part of wells in the plate was left unmodified to check the interaction of NPs/ABs conjugates with the bare surface of MaxiSorp^{TM} plate. For modification of the plate used in this experiment blocking buffer containing 3% of BSA in PBST was used.

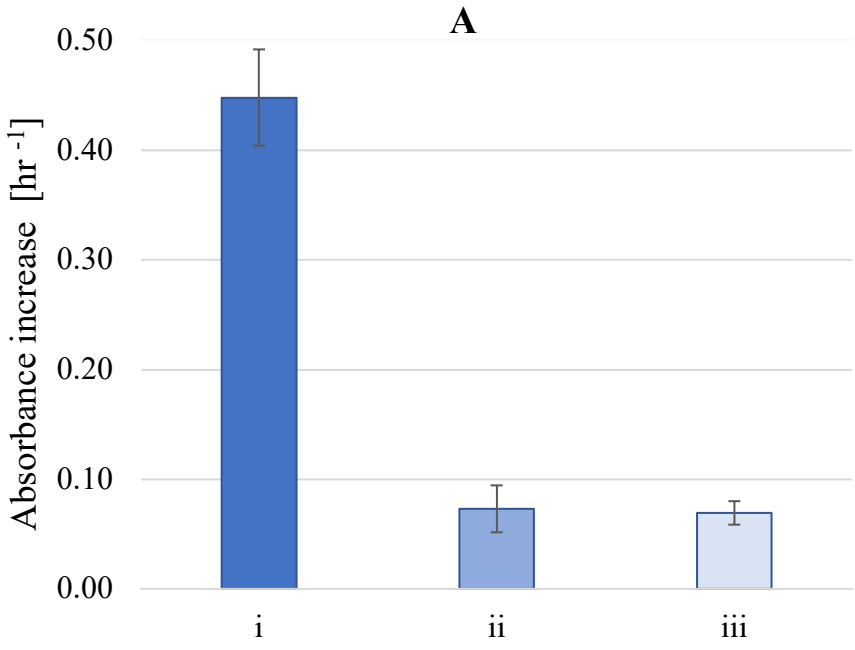

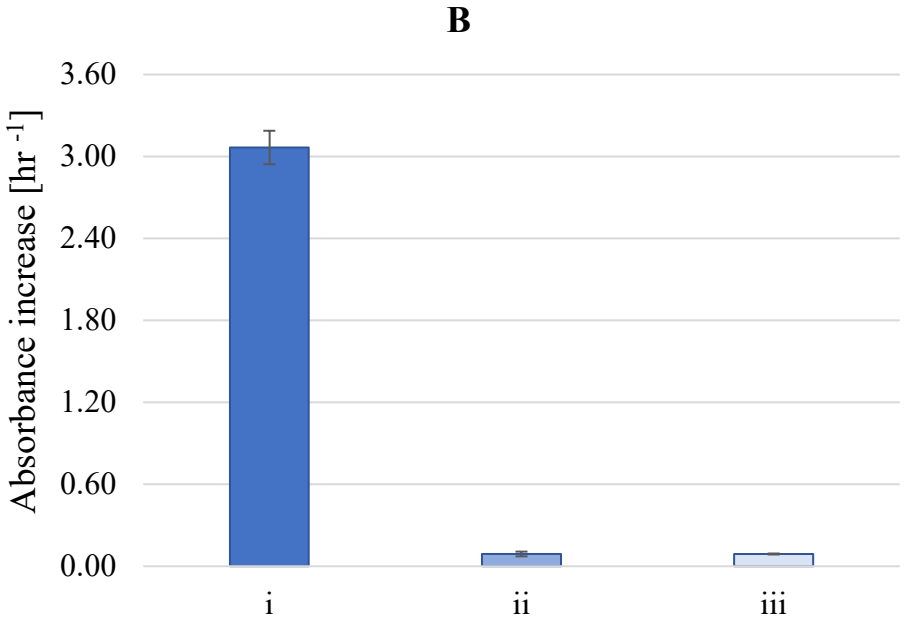

*Figure 6. Absorbance increase for samples containing RuNPs/ABs (**A**) or PtNPs/ABs (**B**) conjugates with specific **(i)** or non-specific **(ii)** ABs immobilized on MaxiSorp™ plates and unmodified surface of 96-well plates **(iii)**. Analytical signals were measured at 625 nm using TMB-based immunoassay. Each bar represents increase of absorbance average value from 5 measurements with error bars representing standard deviation.*

According to Figure 6, analytical signals derived from non-specific interaction of RuNPs/ABs conjugates with ABs (0.07 hr^{-1}) and unmodified surface of MaxiSorp™ plates (0.07 hr^{-1}) were lower than analytical signal derived from specific interaction; however, there still was a room for improvement. A similar difference of analytical signals was noticed for PtNPs/ABs conjugate results. The analytical signal for non-specific interaction of PtNPs/ABs conjugates and ABs immobilized on MaxiSorp™ plate was 0.10 hr^{-1} while analytical signal obtained from NPs/ABs conjugates interaction with unmodified surface of MaxiSorp™ was 0.09 hr^{-1}. High analytical signal detected for specific interaction of PtNPs/ABs conjugates with ABs immobilized in plate surface (3.07 hr^{-1}) confirmed successful modification of NPs with ABs. RuNPs/ABs conjugates showed lower catalytic activity (0.45 hr^{-1}) in comparison to PtNPs/ABs conjugates what coincided with a difference of activity of these catalysts examined in the solution (for more details, please see Chapter 3.7 above).

3.9.2. Optimalisation of blocking buffer content

To decrease non-specific interactions of NPs/ABs conjugates with unmodified surface of MaxiSorp™ or non-specific ABs, blocking buffers of different composition were used. In previous experiments blocking buffer containing 3% of BSA in PBST. Such blocking buffer usage led to comparatively high analytical signal derived from non-specific interactions

between NPs/ABs conjugates and surface of MaxiSorp™ plates. According to the existing literature, BSA (66.50 kDa) is commonly used as a blocking agent in ELISA protocols. BSA should prevent non-specific interaction with the plate surface by blocking free binding spaces which were left after plate modification with capture biomolecules. Nevertheless, BSA weakly binds to plate surface and can be easily removed with PBST buffer (Ahirwar *et al.*, 2015). To find more efficient blocking buffer, influence of composition of different blocking buffers on non-specific interaction was examined. Consequently, an alternative blocking agent casein was chosen. Casein phosphoprotein separated from bovine milk is another commonly used blocking agent in ELISA and western blots protocols. There is no information in the literature about binding of casein to plate surface or possibility to remove such protein with PBST. Additionally, casein (24.00 kDa) is smaller than BSA. It was presumed that smaller casein could take a vacant binding space left after BSA, and combination of casein with BSA or casein alone could help to decrease non-specific interactions. At the same time, different compositions of dilution buffer were checked. Table 7 shows combinations of buffers which were examined.

Table 7. Protein content of i-iii PBST buffer sets.

Buffer sets	**Protein content**	
	Blocking buffer	**Dilution buffer**
i	3% BSA	1% BSA
ii	1% BSA+1% casein	1% BSA + 1% casein
iii	3% casein	1% casein

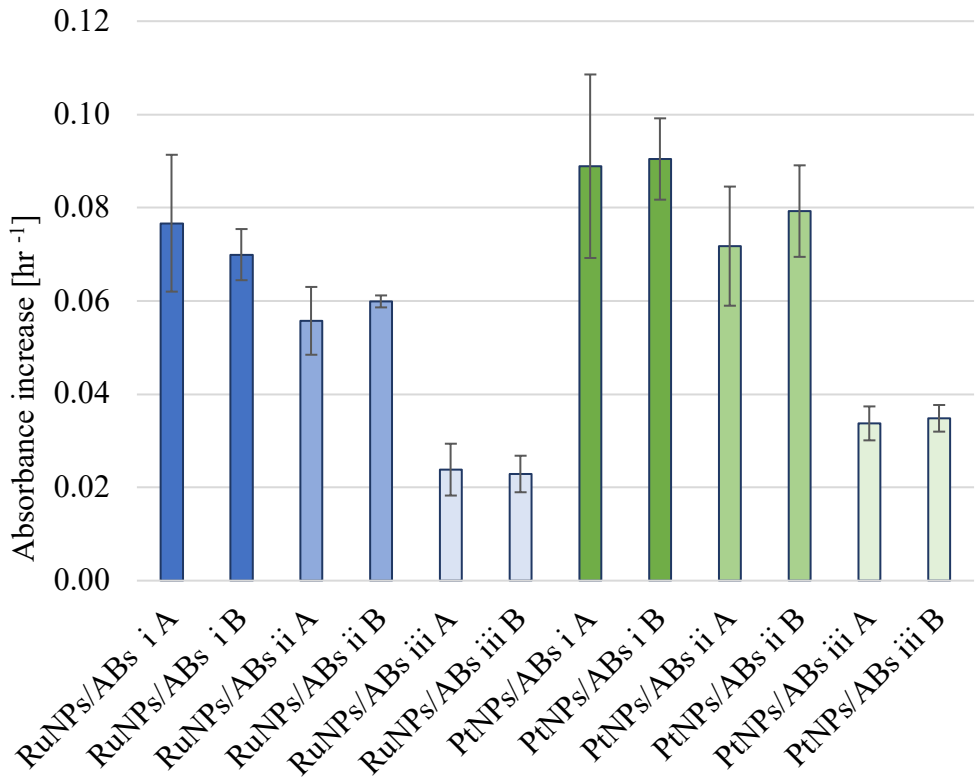

*Figure 7. Analytical signals (increase of absorbance) derived from non-specific interaction of NPs/ABs conjugates and ABs immobilized on multi-well plate surface (**A**) or bare surface of multi-well plate (**B**). (**i-iii**) stand for different buffers sets used for plate surface modification and conjugate mixture preparation. Detection was made at 625 nm with TMB-based immunoassay. Each bar represents increase of absorbance average value from 5 measurements with error bars representing standard deviation.*

According to Figure 7, the highest analytical signal for non-specific interaction for PtNPs/ABs conjugates was detected in the case when buffer set containing 3% of BSA was used. It amounted to 0.09 hr^{-1} for non-specific interaction with ABs immobilized on MaxiSorp™ plate surface and 0.09 hr^{-1} for interaction with unmodified surface of MaxiSorp™. Usage of buffer set ii (1% BSA + 1% casein) slightly decreased analytical signal obtained as a result of non-specific interaction with ABs (0.07 hr^{-1}) and with unmodified surface of multi-well plate (0.08 hr^{-1}) for the same type of NPs/ABs conjugates. The best result of non-specific interaction reduction of PtNPs/ABs conjugates was detected for buffer set iii (3% and 1% of casein) (0.03 hr^{-1} for non-specific interaction with ABs and 0.03 hr^{-1} for interaction with unmodified multi-well plate surface). Analytical signals derived from non-specific interactions of RuNPs/ABs conjugates were generally smaller than these observed in the case of PtNPs/ABs conjugates. Such difference could be explained with primary lower catalytic activity of RuNPs/ABs conjugates. Application of buffer set i for RuNPs/ABs conjugates showed the worst blocking function (0.08 hr^{-1} for non-specific ABs and 0.07 hr^{-1} for unmodified multi-well

surface). Similar to Pt-containing conjugates, buffer set ii decreased non-specific interaction of RuNPs/ABs conjugates with bare surface of multi-well plate (0.05 hr^{-1}) and non-specific ABs (0.06 hr^{-1}). The lowest non-specific interaction of RuNPs/ABs conjugates was detected in the case of application of buffer set iii (0.02 hr^{-1} for non-specific ABs and 0.02 hr^{-1} for unmodified multi-well plate surface). Based on the presented results, it was chosen to use the buffer containing 3% of casein in PBST as a blocking and the buffer containing 1% casein in PBST as a dilution buffer.

3.9.3. NPs/ABs conjugates-based antigen detection performed on multi-well plates

To check usability of NPs/ABs conjugates for antigen detection the surface of MaxiSorp™ plates was modified with specific polyclonal and monoclonal anti-human CRP ABs. According to the literature, monoclonal ABs are more sensitive and specific in comparison to polyclonal ABs. Polyclonal ABs are usually cheaper and easier to produce in comparison to monoclonal ABs. Depending on requirements, both types of mentioned ABs are used for biotests construction (Alhajj and Farhana, 2022). Therefore, it was decided to examine the influence of monoclonal and polyclonal ABs on antigen detection. NPs/ABs conjugates could interact with ABs immobilized on the surface of the multi-well plate only in the presence of antigen (Scheme 30).

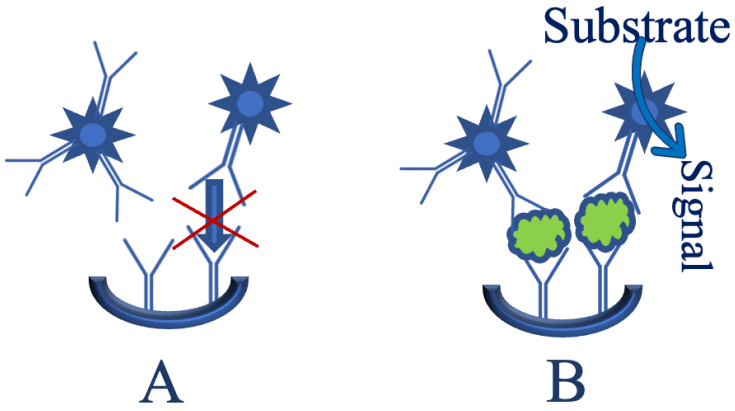

*Scheme 30. Antigen detection with NPs/ABs conjugates. **A** - sample containing no antigen; **B** - sample containing antigen.*

NPs/ABs conjugate interaction with antigen led to the creation of a complex. This complex interacted with antibody immobilized on the surface of multi-well plate. In the case when the formed complex could not be removed during the washing step, it participated in the analytical signal generation. Usability of NPs/ABs conjugates for antigen detection was checked with TMB-based immunoassay. One part of NPs/ABs conjugates was mixed with samples containing CRP (positive control), and another part was mixed only with dilution

buffer (negative control). Prepared samples were distributed into the wells unmodified or modified with polyclonal or monoclonal ABs.

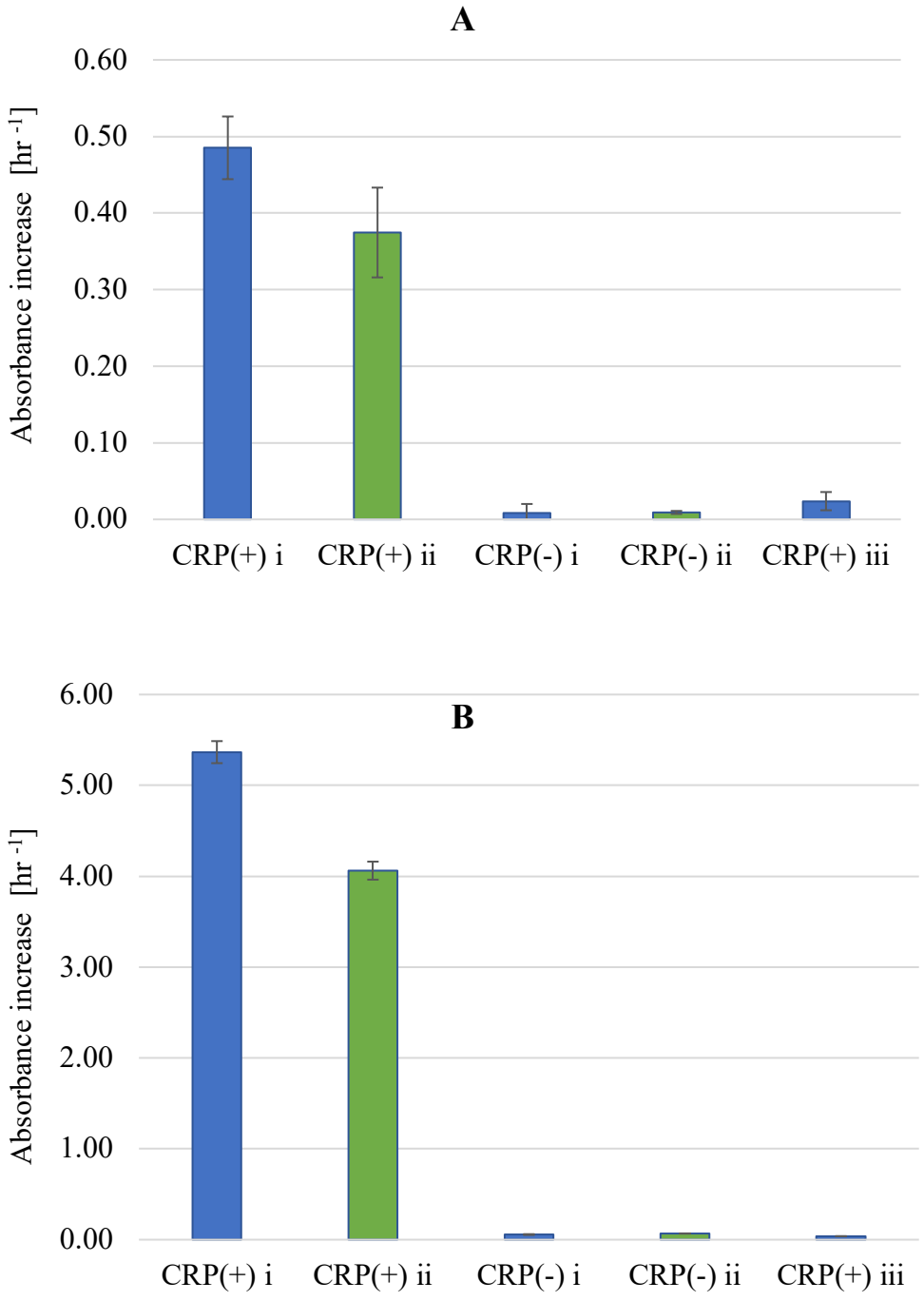

*Figure 8. Absorbance increase for the positive control (CRP (+)) or negative control (CRP(-)) samples containing RuNPs/ABs (**A**) or PtNPs/ABs (**B**) conjugates. In addition, graph shows the influence of ABs type (monoclonal **(i)** or polyclonal **(ii)** Ab) used for modification of MaxiSorp™ plate surface on analytical signal. Furthermore, non-specific interaction with unmodified surface of multi-well plate(iii) were checked. Detection was made at 625 nm with TMB-based immunoassay. Each bar represents increase of absorbance average value from 5 measurements with error bars representing standard deviation.*

According to Figure 8, the analytical signal derived from RuNPs/ABs conjugates was higher in the case of application of monoclonal ABs (0.49 hr^{-1}) than in the case of application of polyclonal ABs (0.36 hr^{-1}). The analytical signal generated due to non-specific interaction of samples containing only dilution buffer and NPs/ABs conjugates was much lower for wells modified with both types of ABs (0.01 hr^{-1} for monoclonal ABs and 0.01 hr^{-1} for polyclonal Abs) than analytical signal detected for samples containing 50 ng/ml of CRP. Non-specific interaction of the positive control sample containing the same type of NPs/ABs conjugates with unmodified multi-well plate was slightly higher (0.02 hr^{-1}) than interaction with modified plate surface. Such differences can be explained by ABs interaction with unblocked multiwell plate surface. In the case of PtNPs/ABs conjugates, higher analytical signal was detected for wells modified with monoclonal ABs (5.37 hr^{-1}) than for wells modified with polyclonal ABs (4.06 hr^{-1}). Analytical signal derived from non-specific interaction of negative control samples was lower (0.06 hr^{-1} for wells modified with monoclonal ABs and 0.07 hr^{-1} for wells modified with polyclonal ABs than analytical signal from specific interaction. Non-specific interaction of the positive control sample containing PtNPs/ABs conjugates resulted in the generated analytical signal equal to 0.04 hr^{-1}. The high analytical signal detected for samples containing CRP and NPs/ABs conjugates detected on wells modified with specific ABs proved that conjugates might be used for antigen detection.

3.9.4. Influence of NPs concentration and magnetic separation on analytical signal

Biological samples are usually complex and multicomponent. The presence of interferents can affect analytical signal generation and false results (both positive and negative, overestimated and underestimated) can be obtained. Magnetic separation allows removing of interferents from analyzed samples. At the same time, the volume of sample can be decreased thus increasing the analyte concentration. The mentioned magnetic separation benefits should improve the analytical parameters of antigen detection assays (Xu *et al.*, 2011). Scheme 31 shows a schematic concept of magnetic sample separation.

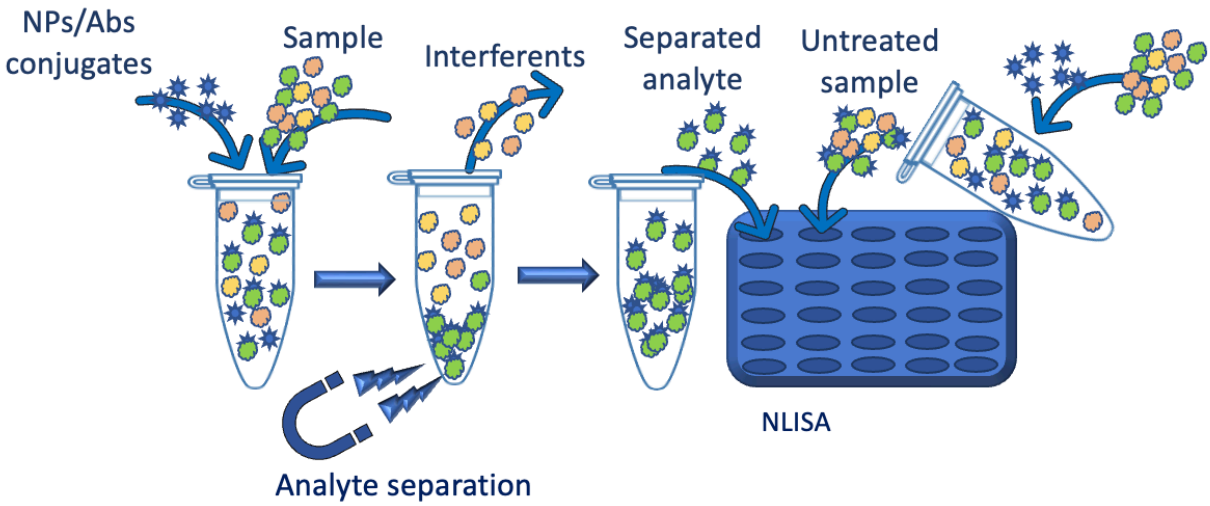

Scheme 31. Magnetic separation of sample components.

Influence of magnetic separation on generation of the analytical signal was examined in order to check a positive influence of sample magnetic premeasurement treatment. At the same time the influence of NPs/ABs conjugates concentration was examined with the TMB-based immunoassay. To optimize the concentration of NPs/ABs conjugates used for antigen detection influence of different NPs/ABs concentration (dilution) on the analytical signal was examined. The standard concentration of CRP antigen used for these experiments was 50 ng/ml prepared in dilution buffer. In all previously presented experiments NPs/ABs conjugates were diluted 40 times. During this experiment, NPs/ABs conjugates dilutions (20-100) were prepared and mixed with CRP first. Next, prepared samples (500 ul) were divided into two equal parts each. One set of sample compounds was separated in magnetic field generated using the neodymium magnet and resuspended in 250 ul of dilution buffer. Another set was used without any additional manipulation.

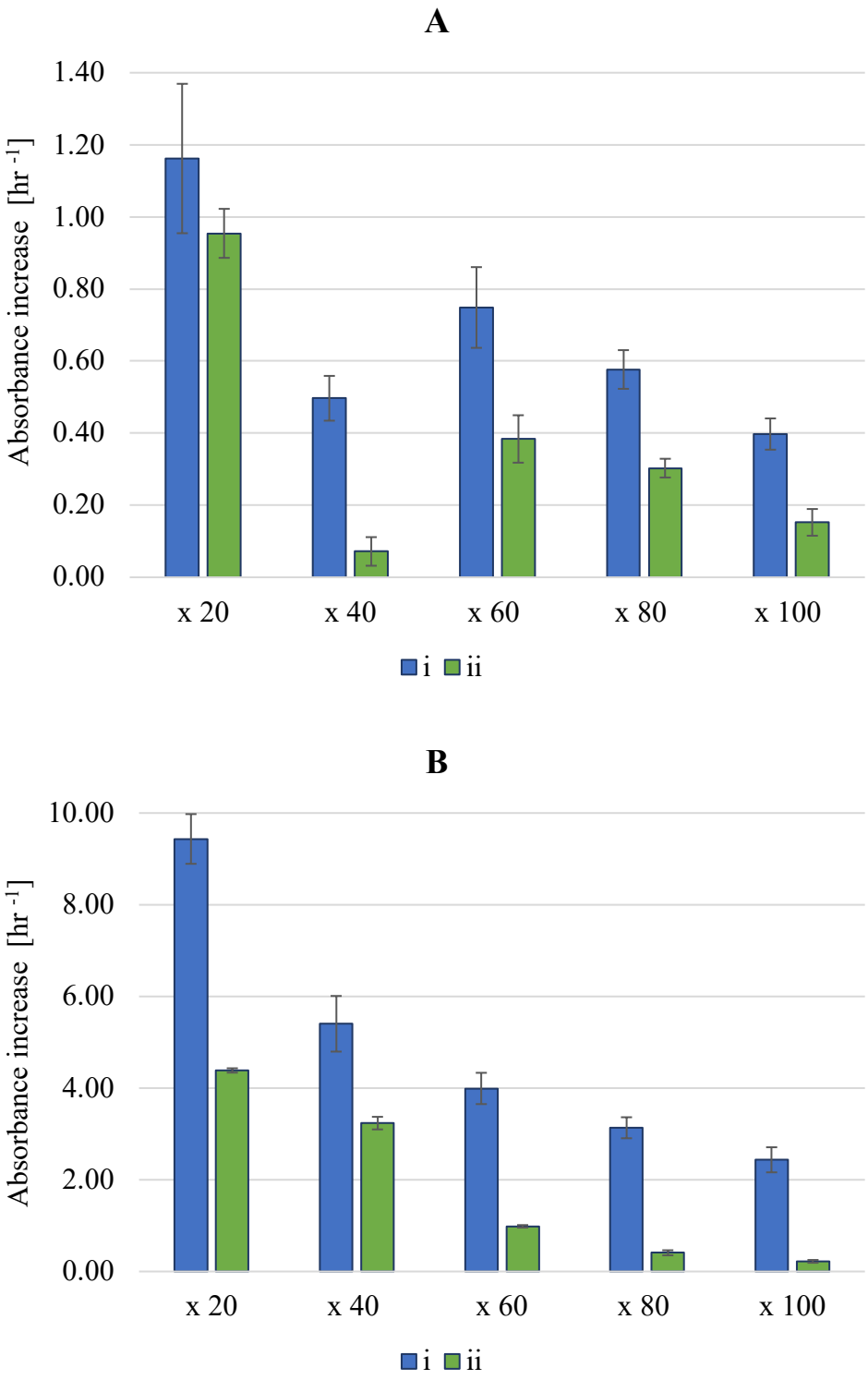

*Figure 9. Absorbance increase for samples derived from RuNPs/ABs (**A**) or PtNPs/ABs (**B**) separated in magnetic field (**i**) and non-separated samples (**ii**)). **x20, x40, x60, x80, x100** - different NPs/Ag conjugates concentration obtained via dilution Such analytical signals were detected at 625 nm using TMB-based immunoassay. Each bar represents increase of absorbance average value from 5 measurements with error bars representing standard deviation.*

According to the Figure 9, increase of PtNPs/ABs conjugate dilution decreased the analytical signal. Analytical signal from the sample separated in a magnetic field and containing 20 times diluted of PtNPs/ABs conjugates was almost two times higher (9.43 hr^{-1}) than analytical signal detected for the untreated sample (4.38 hr^{-1}). Analytical signal detected for untreated sample containing 100 times diluted NPs was 0.22 hr^{-1}, whereas the analytical signal for magnetically separated sample was 2.44 hr^{-1}. Similar to Pt-containing conjugates, the relation between analytical signal and NPs/ABs conjugates concentration was obtained for RuNPs/ABs conjugates. For all dilutions of Ru-containing conjugates analytical signals derived from magnetically separated samples were higher than for untreated samples. Diluting RuNPs/ABs conjugates 100 times lowered the analytical signal for magnetically separated positive control sample down to 0.40 hr^{-1}, and for not separated ones to 0.15 hr^{-1}. Increasing of conjugate concentration up to 20 times dilution of conjugate increase the analytical signal derived from the positive control samples up to 1.16 hr^{-1}. Analysis of presented result proved a positive effect of magnetic separation and sample preconcentration on analytical signal. Such results corroborated with the findings found in the literature (Ríos and Zougagh, 2016; Mukherjee *et al.*, 2022). In addition, it was found that there was a room for signal enhancement with increasing conjugate concentration.

3.9.5. Influence of incubation time on analytical signal

Currently, one of the main biotest development tendencies is the reduction of analysis time. According to the literature, standard ELISA assay duration is around 1.5 h (Engvall and Perlmann, 1971; Minic and Zivkovic, 2021). Running time of NLISA assay used and described in Chapters 3.9.1 - 3.9.4 of this work was 35 min. 30 min incubation of sample on multi-well plate was the longest step of NLISA assay. Another 5 minutes were used for sample separation, washing step, addition of substrate and signal measurement. The room for improvement was found in the reduction of time required for the incubation step. For such experiment NPs/ABs conjugates were mixed with the positive control samples (i) containing 50 ng/ml of CRP and negative control samples (ii) containing no antigen.

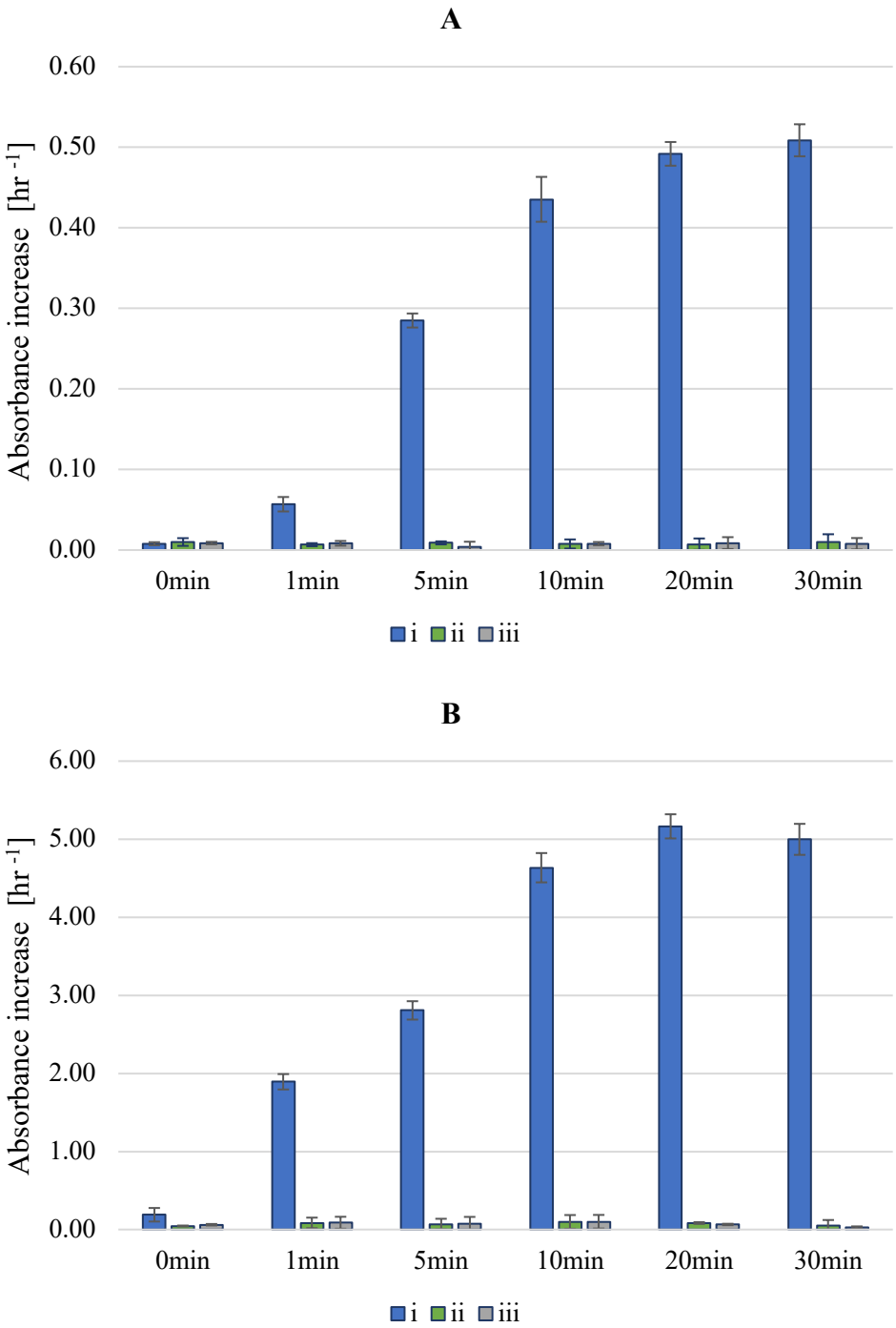

*Figure 10. Absorbance increase derived from the positive (**i**) or negative (**ii**) control RuNPs/ABs (**A**) or PtNPs/ABs (**B**) conjugates samples incubated at t=0, 1, 5, 10, 20 or 30 min on wells modified with CRP specific ABs. (**iii**) - analytical signal obtained from the positive control samples incubated under the same time condition on non-modified wells. Such analytical signals were measured at 625 nm using TMB-based immunoassay. Each bar represents increase of absorbance average value from 5 measurements with error bars representing standard deviation.*

According to Figure 10, the analytical signal for PtNPs/ABs conjugates measured directly after preparation (with no incubation) was 0.01 hr^{-1} for the positive control sample and

0.01 hr^{-1} for negative control samples placed in wells modified with analyte-specific Abs. Analytical signal measured for the same type of the positive control sample placed in unmodified wells was also 0.01 hr^{-1}. After the incubation of RuNPs/ABs conjugates containing the positive control samples in wells modified with ABs, which lasted 1 minute, enhanced analytical signal of 0.05 hr^{-1} was measured. Increasing of incubation time up to 5 min improved the analytical signal almost 6 times so it reached 0.28 hr^{-1} for the positive control samples containing RuNPs/ABs conjugates. Incubation of the sample for 10, 20 and 30 min led to comparatively same level of analytical signal (0.44 hr^{-1}, 0.49 hr^{-1} and 0.51 hr^{-1}, respectively). Analytical signal measured immediately after addition of RuNPs/ABs conjugate containing positive control sample into wells modified with ABs was close to zero, which was identical to the same sample incubated in unmodified wells. Analytical signal measured at t=0 for negative control sample containing RuNPs/ABs conjugate added into ABs modified wells amounted to 0.01 hr^{-1}. Similar to the PtNPs/ABs conjugate-containing sample, increased incubation time for RuNPs/ABs conjugate-containing positive control sample respectively enhanced the analytical signal. Analytical signals derived from the positive control samples incubated 10, 20 and 30 min on wells modified with antibodies were close to each other (4.63 hr^{-1}, 5.16 hr^{-1} and 5.00 hr^{-1}). Taking into account similarity of experimental results for samples incubated 10, 20 and 30 min, test execution time can be decreased down to 15 min for both types of NPs/ABs conjugates without significant negative influence on analytical signal. Obtained results allowed to classify the presented NLISA as a rapid test in comparison to classical ELISA (Engvall and Perlmann, 1971; Minic and Zivkovic, 2021).

Table 8 represents information about execution time of different nanomaterial-based NLISA described in the literature and developed in this work.

Table 8. Time of execution of different nanomaterial-based NLISA described in literature and developed in this work.

Nanomaterial	**NLISA analysis time**	**Recourse (literature)**
Quantum dots (QD)	60-150 min	(Luo *et al.*, 2012)
Au NP	5 min	(Ming *et al.*, 2014)
QD labelled magnetic beads	60-180 min	(Yang *et al.*, 2014)
QD	5 min	(Zhang *et al.*, 2015)
Eu-NPs	18 min	(Huttunen *et al.*, 2016)
Citicoline BSA AuNPs- conjugate	45 min	(Xie *et al.*, 2020)
NPs/ABs conjugate	**15-30 min**	This work

According to Table 8, CRP analysis can be done in 5-180 min using NLISA tests. NPs/ABs conjugate-based NLISA developed in this work can be executed in 15 min; therefore, in comparison to NLISA presented in literature such test can be qualified as a rapid one.

3.9.6. Influence of interferents on the measured analytical signal

The presence of interferents in biological samples can affect assays result due to competition with an analyte, interaction with conjugates and a receptor layer. Other mechanisms of interaction are also possible. To imitate biological sample content and check developed NLISA selectivity, different interferents were added to the positive (samples containing CRP) and negative controls (samples containing no CRP). The influence of interferents presence on analytical signal was examined with TMB-based immunoassay. As interfering agents, human immunoglobulin G (IgG), human serum albumin (HSA), troponin I (TnI) and plasma thromboplastin complex (PTC), in concentrations of 100 ng/ml, were chosen. All prepared samples were incubated in wells modified with CRP-specific Abs.

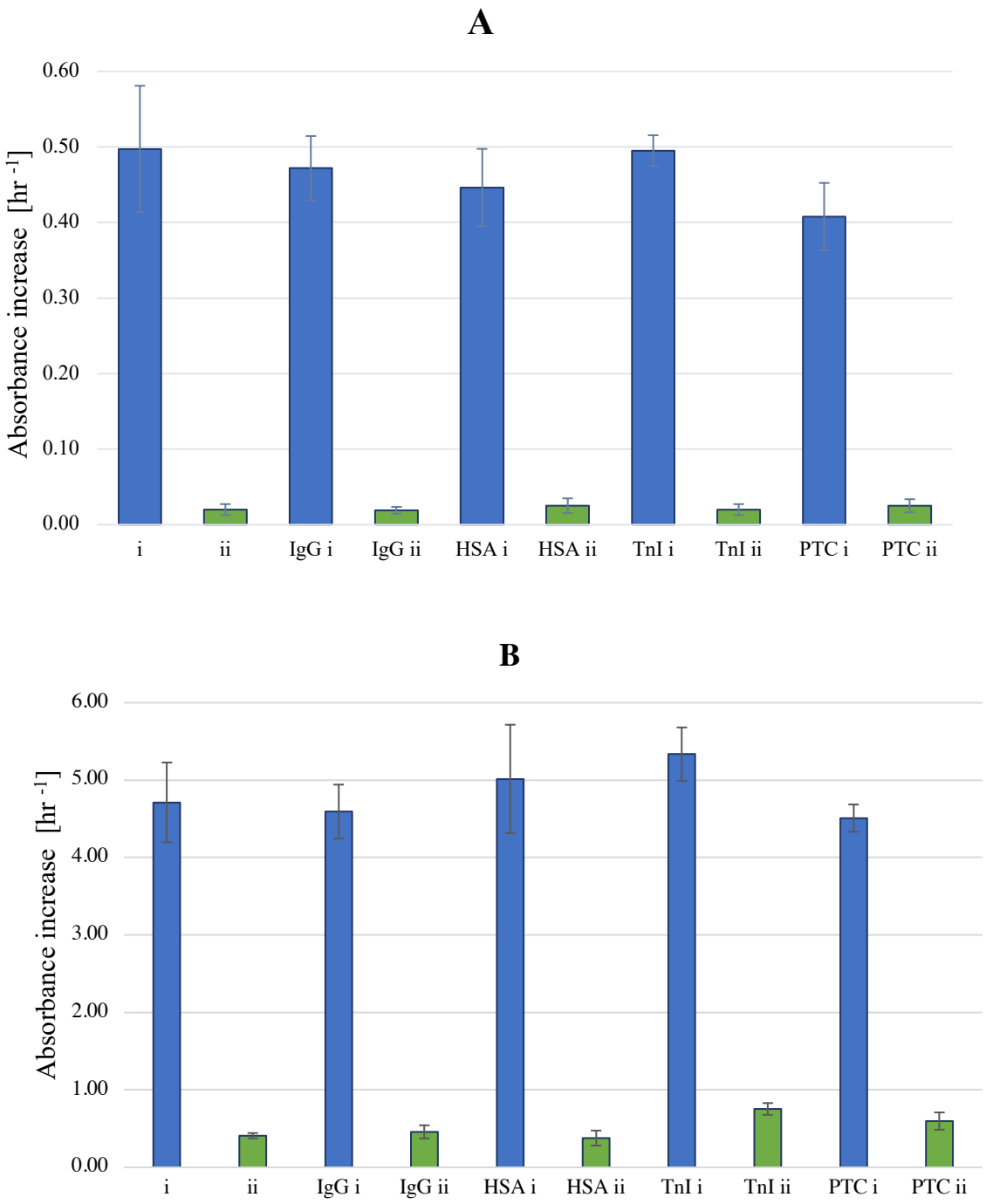

*Figure 11. Absorbance increase derived from the positive control samples (**i**) and negative control samples (**ii**) containing RuNPs/ABs (**A**) or PtNPs/ABs (**B**) conjugates and interferents (IgG, HAS, TnI and PTC). Such analytical signals were detected at 625 nm using TMB-based immunoassay Each bar represents increase of absorbance average value from 5 measurements with error bars representing standard deviation.*

According to Figure 11, the addition of different interferents to RuNPs/ABs conjugate containing samples influenced the analytical signal in comparatively same way. The presence of TnI in both positive and negative control PtNPs/ABs conjugate containing sample was reflected with the highest analytical signals (5.34 hr^{-1} for positive control sample and 0.75 hr^{-1}

for negative control sample) in comparison to samples that contained other types of interferents. The addition of IgG, HSA and PTC did not introduce significant changes to experimental results in comparison to results which were obtained for the positive control sample containing only CRP and PtNPs/ABs conjugate. The lowest analytical signal was detected for RuNPs/ABs conjugate containing positive control sample in the presence of PTC (0.41 hr^{-1}). Signal decrease could be explained by the PTC competition with CRP for interaction with ABs immobilized on a plate surface or unblocked protein binding spots. The addition of IgG, HSA and TnI did not introduce significant changes to experimental results in comparison to results which were obtained for the positive control sample containing only CRP and RuNPs/ABs conjugate. Same as it was described for Ru-containing samples, analytical signals detected for almost all types of interferents addition to PtNPs/ABs conjugate containing samples were on comparatively same level. According to obtained results interferent addition did not introduce a significant effect on the analytical result thus it could be ignored.

3.9.7. Analytical parameters of NPs/ABs conjugate-based NLISA

Optimized conditions of the NLISA test allowed evaluation of the analytical performance and sensitivity of NPs/ABs conjugate-based NLISA. For this purpose, calibration curves were prepared based on different concentrations of CRP (from 0.02 ng/ml to 500 ng/ml). In order to compare the sensitivity and linear range of the immunoassay based on magnetic nanozymes with classical ELISA labels, the analytical parameters of the analogous immunoassay based on usage of HRP/ABs conjugates were also determined.

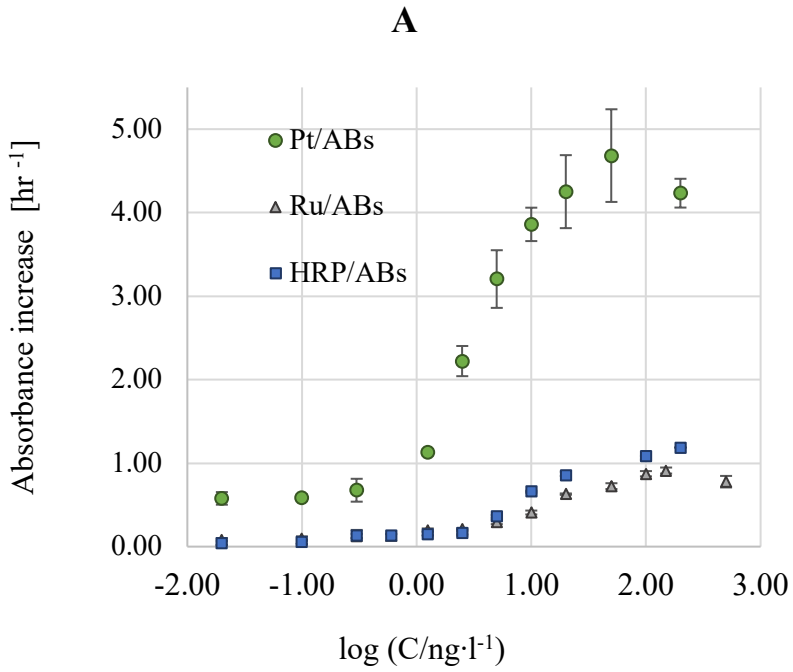

B

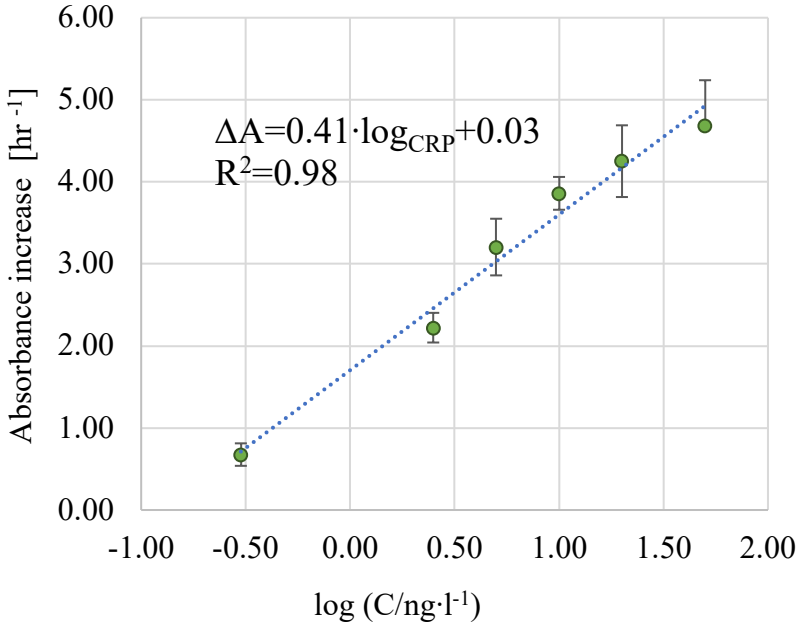
6.00
5.00
4.00
3.00
2.00
1.00
0.00
Absorbance increase [hr -1]
ΔA=0.41·logCRP+0.03
R2=0.98
-1.00
-0.50
0.00
0.50
1.00
1.50
2.00
log (C/ng·l-1)

C

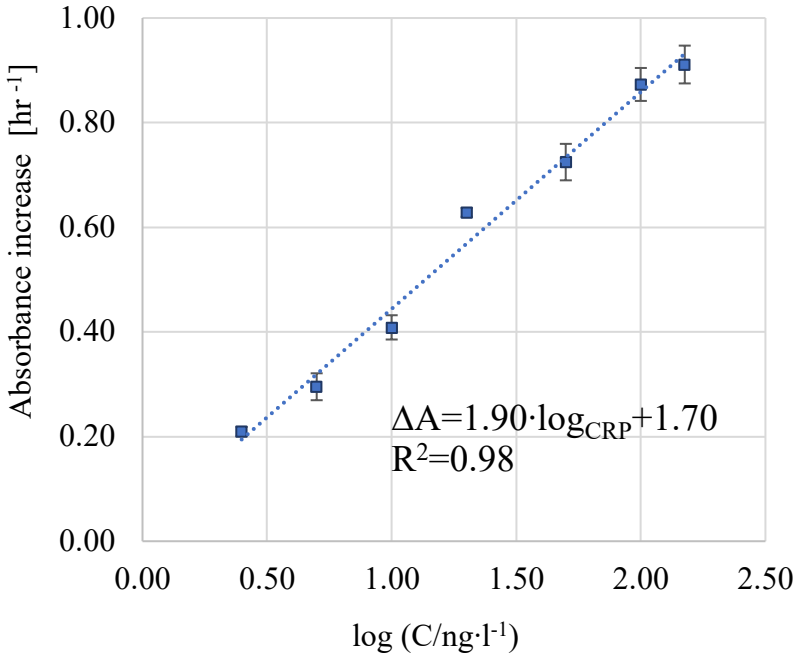
1.00
0.80
0.60
0.40
0.20
0.00
Absorbance increase [hr -1]
ΔA=1.90·logCRP+1.70
R2=0.98
0.00
0.50
1.00
1.50
2.00
2.50
log (C/ng·l-1)

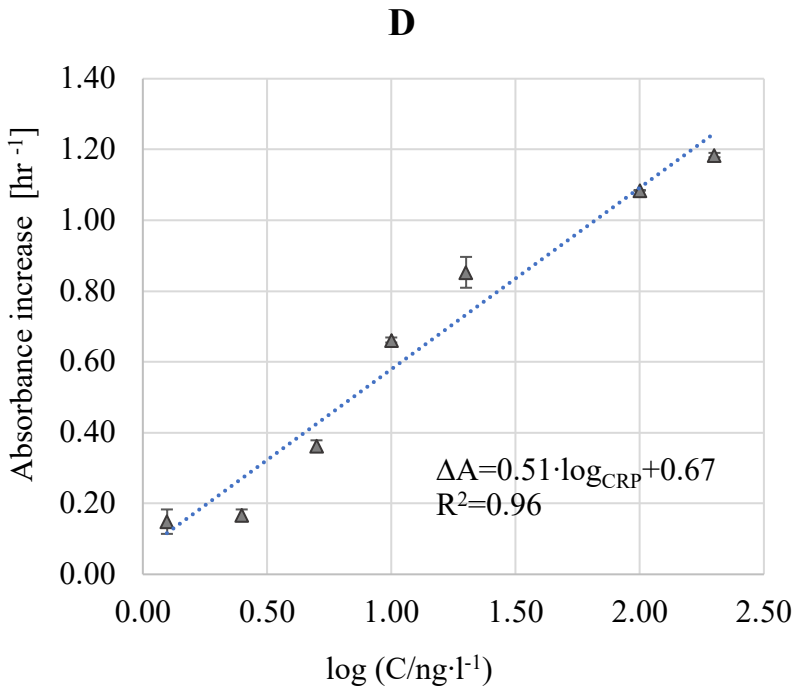

*Figure 12. **A** - calibration curves for CRP (obtained using PtNPs/ABs, RuNPs/ABs and HRP/ABs-based conjugates) and sensitivity (the slopes of regression equation for CRP made with RuNPs/ABs (**B**), PtNPs/ABs (**C**), and HRP/ABs (**D**) conjugates. Each point represents absorbance average value detected at 625 nm for 4 independent measurements with error bars representing standard deviation. Mentioned experiment was with TMB-based immunoassay.*

According to Figure 12, in all cases analytically useful dose-response curves were obtained with a good linear relation between the analytical signals and analyte concentrations. Correlation coefficients R^2 for the PtNPs/ABs conjugate-based NLISA was 0.98 and R^2=0.99 for the RuNPs/ABs conjugate-based NLISA. In the case of HRP/ABs conjugate-based ELISA R^2 was equal to 0.96. The limit of detection (LOD) was calculated according to the rule of triple blank criterion. The LOD of PtNPs/ABs conjugates-based NLISA (LOD=0.34 ng/ml) significantly exceeded the sensitivity and detection limit of HRP/ABs conjugates-based ELISA (LOD=1.72 ng/ml), while the use of RuNPs/ABs conjugates-based NLISA led to similar analytical parameters (LOD=1.67 ng/ml). Nevertheless, the detection limit of CRP at the level below 1 ng/ml and the linear range of at least two log units comfortably meet the requirements for tests for highly sensitive determination of CRP at diagnostically significant levels (Nehring, Goyal and Patel, 2022). Analytical parameter comparison of NLISA test presented in this work with other recently reported CRP nanomaterial-based assays is shown in Table 9.

Table 9. LOD of nanomaterial-based tests presented in literature and NPs/ABs conjugate-based assays developed in this work.

Nanomaterial	**LOD**	**Recourse (literature)**
QD	60 ng/ml	(Luo *et al.*, 2012)
Au NP	$12 \cdot 10^3$ ng/ml	(Ming *et al.*, 2014)
QD labelled magnetic beads	1 ng/ml	(Yang *et al.*, 2014)
QD	790 ng/ml	(Zhang *et al.*, 2015)
Eu-NPs	30 ng/ml	(Huttunen *et al.*, 2016)
Citicoline BSA AuNPs-conjugate	$8 \cdot 10^{-3}$ ng/ml	(Xie *et al.*, 2020)
RuNPs/ABs conjugates	**1.67 ng/ml**	This work
PtNPs/ABs conjugates	**0.34 ng/ml**	This work
HRP/ABs conjugates	**1.72 ng/ml**	This work

According to Table 9, NLISA assays reported in literature over the last decade were characterised with LOD in a range from $8 \cdot 10^{-3}$ to $12 \cdot 10^3$ ng/ml. In comparison to NLISA examples reported in literature PtNPs/ABs conjugates-based assay can be qualified as one of the most sensitive CRP detection tests.

3.10. NPs/ABs conjugates-based biotest performed on open PES bioreactors

According to the main dissertation topic, NPs/ABs conjugates usage in biotest was planned in order to construct a multifunctional microfluidic chip for antigen detection. PES flexible foil was chosen as a material for the open bioreactors construction due to well-known methodology of surface modification and history of the successful application in microfluidic chips construction. Compared to multiwell plates, the application of flexible PES foil as a surface for open bioreactors increased possible geometry combinations of assay construction and applicability for biotests, paving the way for miniaturization and, as a result, expanding the applicability of NPs-based antigen analysis (Azeem *et al.*, 2021). To test the usability of PES foil in NPs-based antigen detection a simple construction of open bioreactor was chosen. On the surface of PES foil a hydrophobic mask was introduced to create physical boundaries for bioreactors. Such construction allowed a single bioreactor to contain up to 30 ul of a solution.

3.10.1. Interaction between specific and nonspecific ABs immobilized on flexible PES bioreactors and NPs/ABs conjugates

The same experimental strategy as for detection of ABs presence on NPs surface and examination of non-specific interaction made on 96-well plates was used for tests using open bioreactors constructed on PES foils.

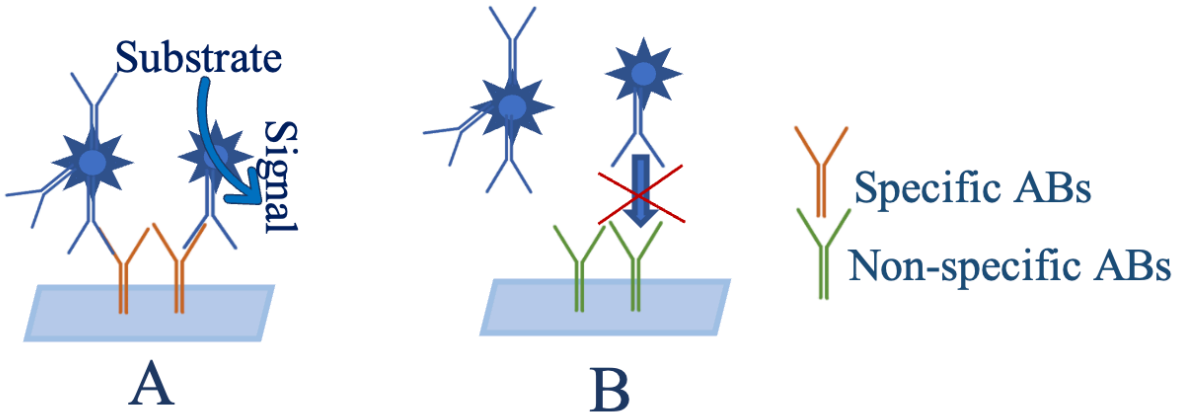

*Scheme 32. Interaction between specific (**A**) and non-specific (**B**) ABs immobilized on flexible PES foil surface and NPs/ABs conjugates.*

Scheme 32 represents the analytical signal generation as a result of interaction between NPs/ABs conjugates and antibody immobilized on the flexible PES foil.

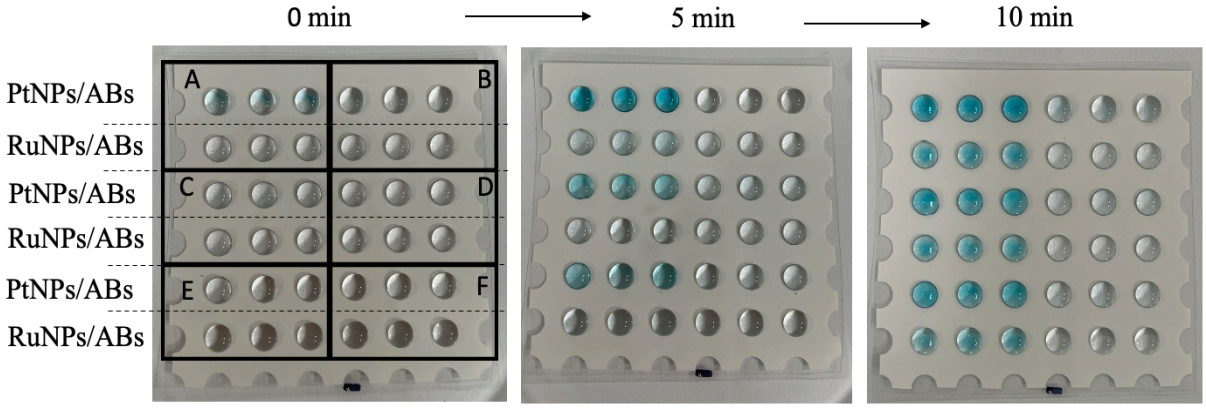

*Image 4. Coloured product formation catalyzed by NPs/ABs conjugates at t=0, 5 and 10 min incubations on flexible PES foil open bioreactors. Field **A** – product formation resulting from interactions between PtNPs/ABs or RuNPs/ABs conjugates with specific ABs immobilized on flexible PES foil open bioreactors. Field **B** - product formation resulting from interactions between nonspecific ABs immobilized on flexible PES foil open bioreactors and PtNPs/ABs or RuNPs/ABs conjugates. Field **C** (modified with specific monoclonal ABs) - product formation resulting from interactions between PtNPs/ABs or RuNPs/ABs conjugates for the positive control sample. Field **D** (modified with specific monoclonal ABs) - product formation resulting from interactions between PtNPs/ABs or RuNPs/ABs conjugates for negative control. Field **E** (modified with specific monoclonal ABs) - product formation resulting from interactions between Fe/Pt/Au NPs or Fe/Ru/Au NPs for the positive control sample. Field **F** (modified with specific monoclonal ABs) - product formation resulting from interactions between PtNPs/ABs or RuNPs/ABs conjugates for negative control sample.*

Image 4 represents the product generation catalyzed by NPs/ABs conjugates. On the surface of reactors within the field A ABs specific to ABs in conjugates were immobilized. The surface of the field B was modified with non-specific ABs for NPs/ABs conjugates. PtNPs/ABs containing solution were placed in the first line of bioreactors. In the second bioreactors line RuNPs/ABs conjugates solution were placed. After 10 minutes of incubation solutions containing formed coloured product were transferred into 96-well plate and the absorbance was measured. Collected solutions did not contain conjugates and once they were removed from bioreactors surface, the product formation catalyzed with NPs was stopped.

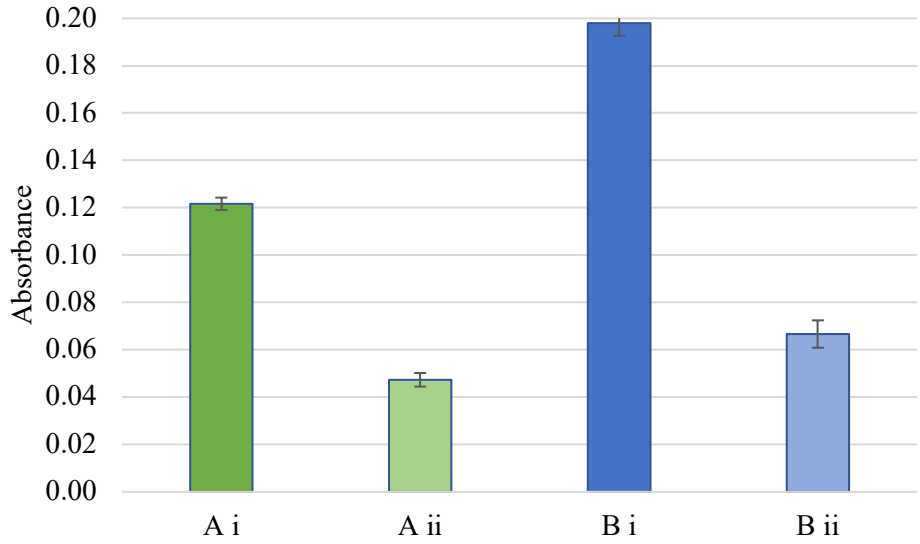

*Figure 13. Absorbance of solutions containing product formed as a result of RuNPs/ABs(**A**) or PtNPs/ABs(**B**) conjugates specific (**i**) or non-specific (**ii**) interactions with ABs immobilized on surface of bioreactors. Analytical signal measured at 625 nm obtained using TMB-based immunoassay. Each bar represents absorbance average value from 3 measurements with error bars representing standard deviation.*

According to Figure 13, the analytical signal derived from specific interactions between Pt/ABs conjugates and ABs immobilized on bioreactors surface was around 3 times higher (0.198) than analytical signal derived from non-specific interaction (0.60). In the case of RuNPs/ABs conjugates, the specific interaction generated the analytical signal around three times higher (0.12) than non-specific interaction (0.05). Analytical signal derived from PtNPs/ABs conjugates was higher for specific interaction in comparison to RuNPs/ABs conjugates. At the same time, both types of NPs/ABs conjugates showed comparatively same level of non-specific interaction.

3.10.2. NPs-based antigen detection using flexible PES bioreactors

On the fields E-F two tests were carried out simultaneously. The usability of NPs/ABs conjugate for antigen detection and influence of specific ABs type immobilized on bioreactor surface on analytical signal were tested within the mentioned fields. The bioreactor surfaces of fields C and D were modified with monoclonal anti-human CRP ABs whereas the surface of fields E and F were modified with polyclonal anti-human CRP ABs. On bioreactors within C and E fields the solution of NPs previously incubated with CRP was applied. Samples added on bioreactors within fields D and F were not incubated with CRP. The same mechanism as it was described for test caried out on 96-well plates was used to examine the usability of NPs/ABs conjugates for CRP detection on PES foils. CRP as antigen had to bind to NPs/ABs conjugates surface and then was recognized with specific ABs immobilized on bioreactors surface (Scheme 33).

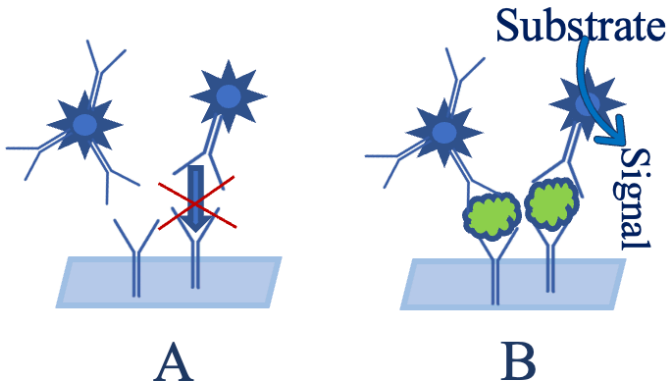

*Scheme 33. Antigen detection with NPs/ABs conjugates. **A** - sample containing no antigen; **B** - sample containing antigen with specific ABs immobilized on flexible PET foil surface.*

In the case of antigen absence NPs/ABs conjugates did not have chance to interact with bioreactors surface and were removed during the washing step.

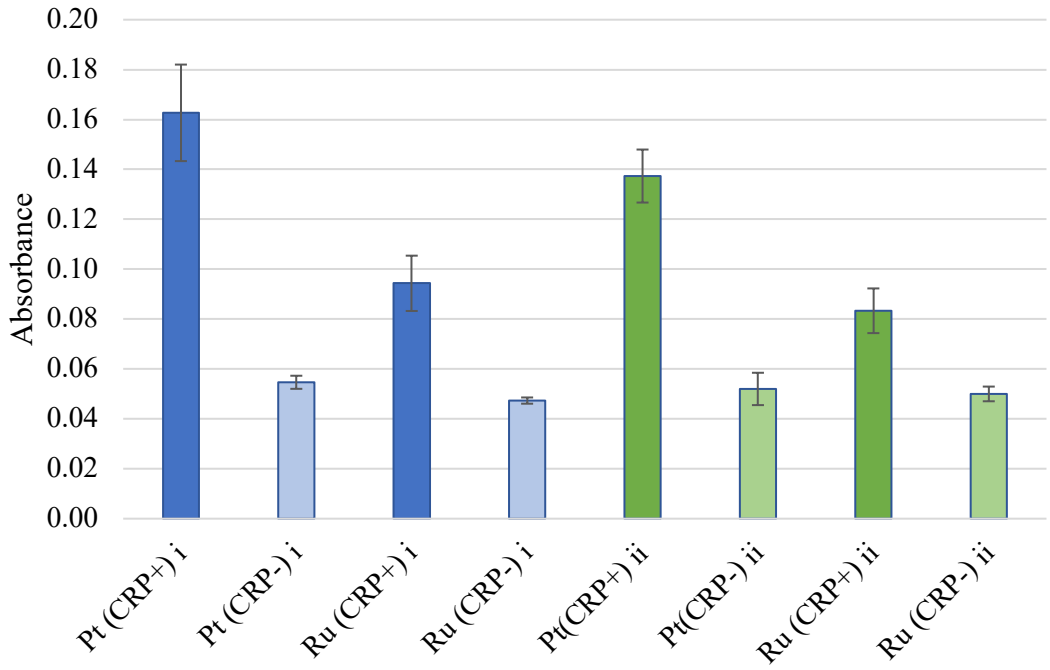

*Figure 14. Absorbance measured at 625 nm derived from the positive control (**CRP (+)**) or negative control (**CRP (-)**) samples containing RuNPs/ABs(**Ru**) or PtNPs/ABs(**Pt**) incubated in bioreactors modified with monoclonal (**i**) or polyclonal (**ii**) ABs. Such experiment was carried out with TMB-based immunoassay. Each bar represents absorbance average value from 5 measurements with error bars representing standard deviation.*

As shown on Figure 14, for test fields modified with monoclonal ABs, analytical signal for sample of PtNPs/ABs conjugates incubated with CRP was almost three times higher (0.15) than for the sample of the same conjugates which was not incubated with CRP (0.06). For the test performed on bioreactors modified with polyclonal ABs analytical signal derived from samples incubated with CRP was also higher (0.15) than for the samples with no CRP added (0.05). In the case of RuNPs/ABs conjugates used in the test carried out on bioreactors modified with monoclonal ABs, the analytical signal for samples containing CRP was almost twice higher (0.08) than for the samples with no CRP added (0.05). In the case of the test carried out on bioreactors modified with polyclonal ABs, analytical signal for samples containing RuNPs/ABs conjugates and CRP was slightly higher (0.09) than for samples with no CRP (0.05). According to the literature, monoclonal antibodies should show higher selectivity and sensitivity for antigen recognition what in theory can influence the analytical signal (Alhajj and Farhana, 2022). According to Figure 15, analytical signals for both types of NPs/ABs incubated with CRP were higher for bioreactors modified with monoclonal ABs than for the ones modified with polyclonal ABs. For PtNPs/ABs conjugates incubated with CRP analytical signal generated in the case of bioreactors modified with monoclonal ABs was 0.16 and for bioreactors modified with polyclonal ABs it amounted to 0.14. For the same bioreactors types analytical

signals obtained for RuNPs/ABs conjugates were 0.09 for the bioreactors modified with monoclonal ABs and 0.08 for the bioreactors modified with polyclonal ABs. Analytical signals derived from non-specific interaction between two types of NPs/ABs conjugates and bioreactors modified with polyclonal and monoclonal ABs were virtually at the same level. Taking into account higher signal originated from monoclonal ABs usage, such ABs type was used for bioreactors modification for further tests.

3.10.3. Analytical parameters of CRP detection performed on PES bioreactors

To prove that PES bioreactors together with NPs/ABs conjugates could be used as an analytical biotest, experiments leading to the determination of signal dependence on analyte concentration were performed.

Taking into account the higher analytical signal obtained for samples with Pt/ABs conjugates, such NPs/ABs conjugates were used in tests for calibration curve preparation. To compare a nanomaterial-based assay with natural enzyme-based assay HRP/ABs conjugates were also used. Similarly to the results obtained for tests carried out on MaxiSorp™ plates, tests carried out on PES bioreactors displayed a linear correlation between analytical signal and logarithm of analyte concentration (Figure 15).

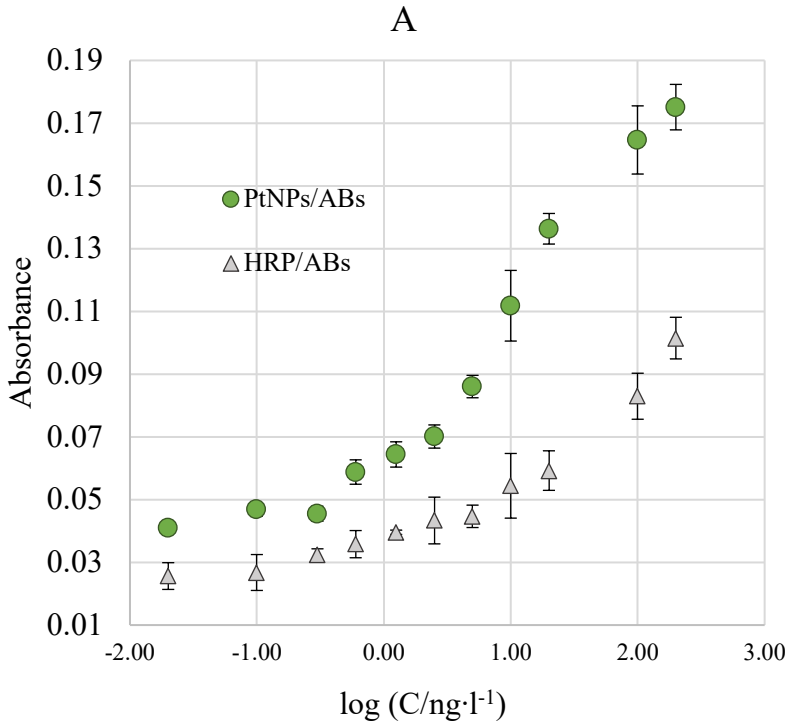

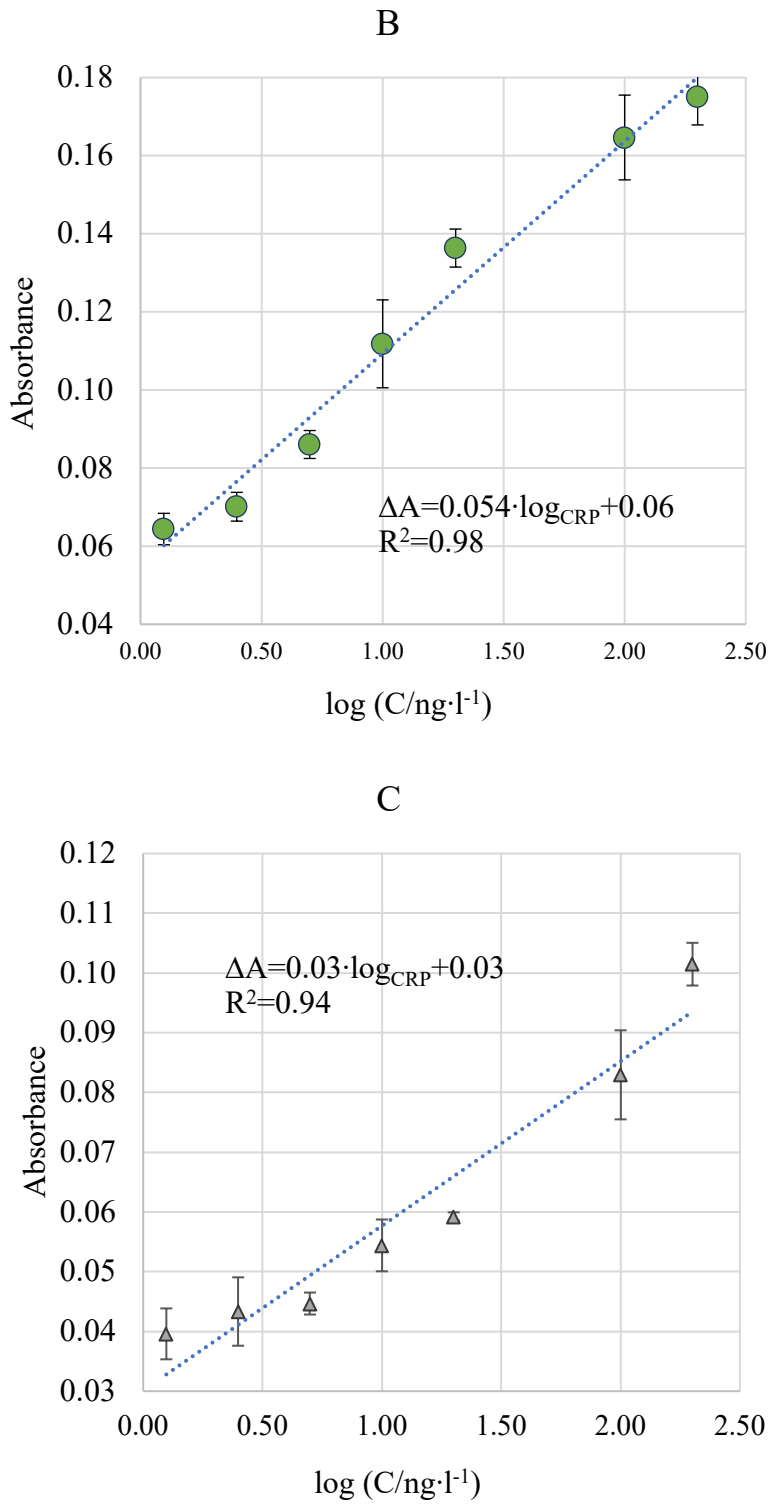

*Figure 15. **A** - calibration curves for CRP (obtained using PtNPs/ABs and HRP/ABs-based conjugates) and sensitivity (the slopes of regression equation for CRP made with PtNPs/ABs (**B**), and HRP/ABs (**C**) conjugates. Each point represents absorbance average value detected at 625 nm for 4 independent measurements.*

Linear relationship between absorbance and analyte concentration obtained for PtNPs/ABs conjugate-based tests performed on PES-based open bioreactors covered diagnostically useful range of CRP concentration (Nehring, Goyal and Patel, 2022). LOD was calculated according to the rule of triple blank criterion. The LOD of PtNPs/ABs conjugates-based CRP detection tests (LOD=0.60 ng/ml) were significantly lower than detection limit of HRP/ABs conjugates-based ELISA (LOD=3.18 ng/ml). In addition, PtNPs/ABs conjugates-based assays were characterized with higher sensitivity in comparison to natural enzyme-based test. According to the fact that PtNPs/ABs tests performed on open PES bioreactors were characterised with the detection limit lower than 1 ng/ml and displayed a wide linear range, such tests could be qualified as sensitive CRP determination assays. No examples of PES usage as bioreactors surface in nanomaterials-based CRP tests were reported in literature, so NPs-based assays described in this work were compared to nanomaterial-based immunoadsorption assays (Table 10).

Table 10. LOD of nanomaterials-based tests presented in literature and NPs/ABs conjugate-based assays developed in this work.

Name	**LOD**	**Recourse (literature)**
QD	60 ng/ml	(Luo *et al.*, 2012)
Au NP	$12 \cdot 10^3$ ng/ml	(Ming *et al.*, 2014)
QD labelled magnetic beads	1 ng/ml	(Yang *et al.*, 2014)
QD	790 ng/ml	(Zhang *et al.*, 2015)
Eu-NPs	30 ng/ml	(Huttunen *et al.*, 2016)
Citicoline BSA AuNPs-conjugate	$8 \cdot 10^{-3}$ ng/ml	(Xie *et al.*, 2020)
RuNPs/ABs conjugates*	1.67 ng/ml	This work
PtNPs/ABs conjugates*	0.34 ng/ml	This work
HRP/ABs conjugates*	1.72 ng/ml	This work
PtNPs/ABs conjugates#	**0.60 ng/ml**	This work
HRP/ABs conjugates#	**3.18 ng/ml**	This work
*-tests performed on MaxiSorp™ plates; #-tests performed on PES open bioreactors		

According to information in the Table 10, PtNPs/ABs conjugate-based tests carried out using PES-based open bioreactors were less sensitive and characterized with higher LOD in comparison to the tests based on the same conjugates type performed on MaxiSorp™ plates. Nevertheless, such tests showed better parameters than natural enzyme-based assays and can still be classified as highly sensitive CRP detection tests.

3.11. NPs/ABs conjugates-based multifunctional microfluidic system for antigen detection

After promising result which were obtained for antigen detection with NPs/ABs conjugates using PES-based bioreactors, PES foils were used to create microfluidic multifunctional cassette chips. In addition to microfluidic multifunctional cassette, it was decided to manufacture a magnetic separation module. Magnetic separation module together with microfluidic cassettes were combined to create a prototype model system for antigen detection.

3.11.1. Microfluidic cassette construction concept

The main task of the microfluidic cassette was to combine sample separation, its preconcentration and analytical reaction in one. The microfluidic cassette consisted of several main parts:

- the chamber for magnetic separation;
- the microreactor chamber with the antibody immobilized on the surface;
- the chamber for spectrophotometric detection.

Scheme 34 shows a block diagram of the microfluidic cassette chip.

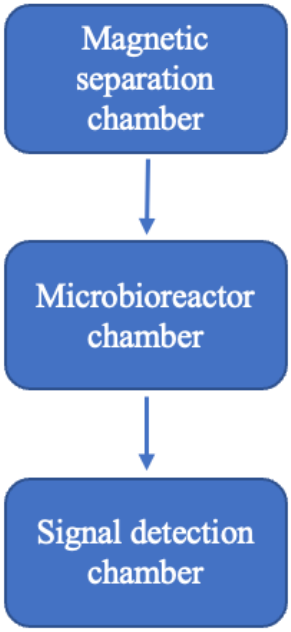

Scheme 34. Block diagram of the microfluidic cassette chip functional parts.

In order to combine this concept of a microfluidic cassette with the selected construction material in the form of foil, it was necessary to design the cassette in a multi-layer form. Such cassette consisted of six layers made of alternating hydrophilic polyester film and double-sided adhesive film. In addition, cassette overlay facilitating the handling was mounted on the microfluidic surface. The overlay containing reservoir of the detection chamber and connectors for peristaltic pump tubing.

The initial condition was the thickness of the available polyester films, which was about 100 um. This, in turn, determined the maximum height of the microstructures, exceeding which could result in their collapse. The dimensions of the microreactor were also determined taking into account the experience obtained during the participation in the ImDiag project. The width of the microreactor (at its widest point) was about 1.94 mm, while its length was about 13 mm. Therefore, the total volume of the microreactor was 1.89 ul.

Layer 1 of the microfluidic cassette was made of a double-sided hydrophilic PES film. No microfluidic structures were fabricated on this layer (Scheme 35).

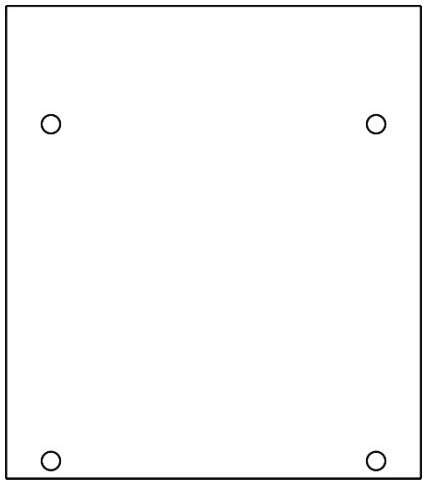

Scheme 35. Layer 1 structural elements.

Although this layer had no microfluidic structures, it nevertheless played a very important role in the entire microfluidic cassette. The upper part was, among others, the bottom of the microbioreactor on the surface of which ABs was immobilized. In addition, layer 1 played a role as the bottom of the detection chamber. This layer was covered from the top with layer 2 made of double-sided adhesive foil (Scheme 36).

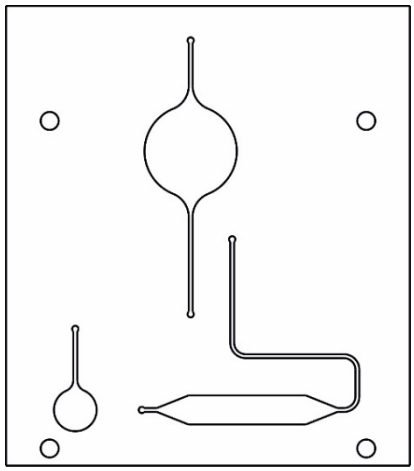

Scheme 36. Layer 2 structural elements.

The main elements of layer 2 were magnetic separation chamber and flow microreactor. Each part had its own inlet and outlet connected via microchannels. The magnetic separation chamber, microreactor and the flow microstructures on this layer were connected to layer 3 made of a hydrophilic film. Layer 3 contained separation chamber, microbioreactor and flow microstructures (Scheme 37).

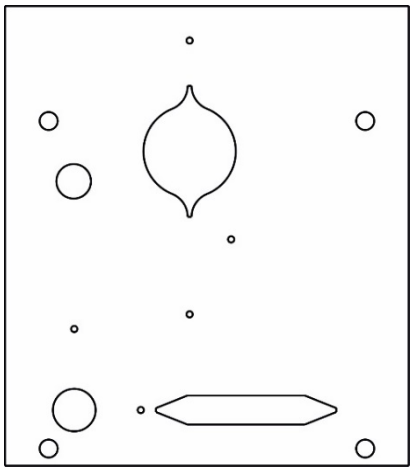

Scheme 37. Layer 3 and 4 structural elements.

The main role of layer 3 was to increase volumes of chambers (by increasing their height) and to prevent their collapse. Layer 4 was made of double-sided adhesive foil and contained the same structural elements as layer 3. Layer 4 was connected to layer 5 made of hydrophilic foil to lower part of the cassette.

Layer 5 serves as a top sealing surface for the microbioreactor along with flow microstructures (Scheme 38).

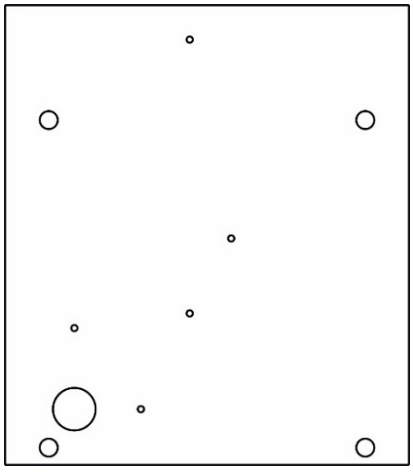

Scheme 38. Layer 5 and 6 structural elements.

The layer 6 of the cassette was made of double-sided adhesive, containing the same structural elements as layer 5 and functioned to connect the main part of the cassette (layers 1-5) with the PMMA overlay. PMMA overlay contained reservoir of the detection chamber and connectors for peristaltic pump tubing (Image 5).

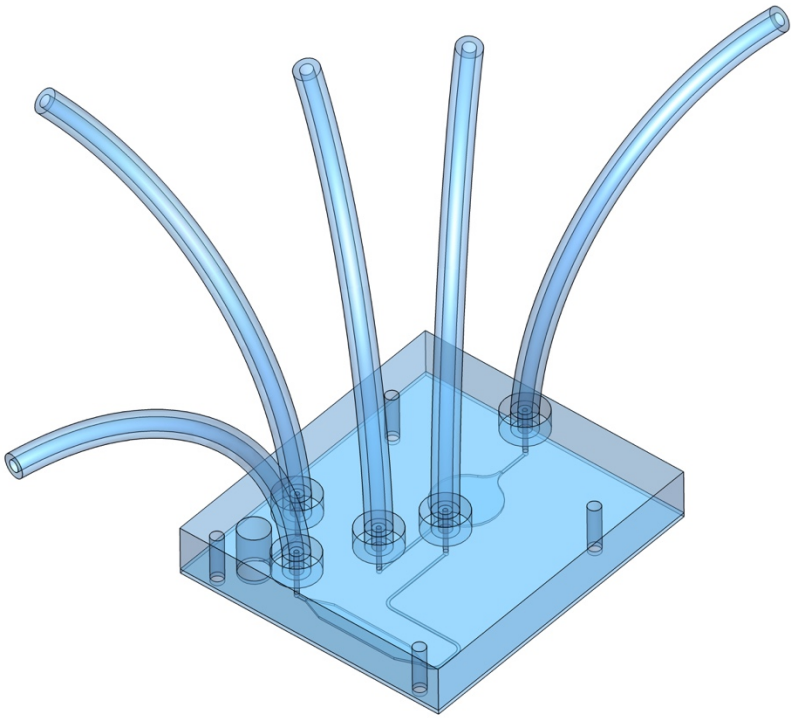

Image 5. 3D model of cassette overlay with connected tubings.

3.11.2. Magnetic separation module construction conception

Construction of magnetic separation module allowed to work with three microfluidic cassettes on the same time (Image 6).

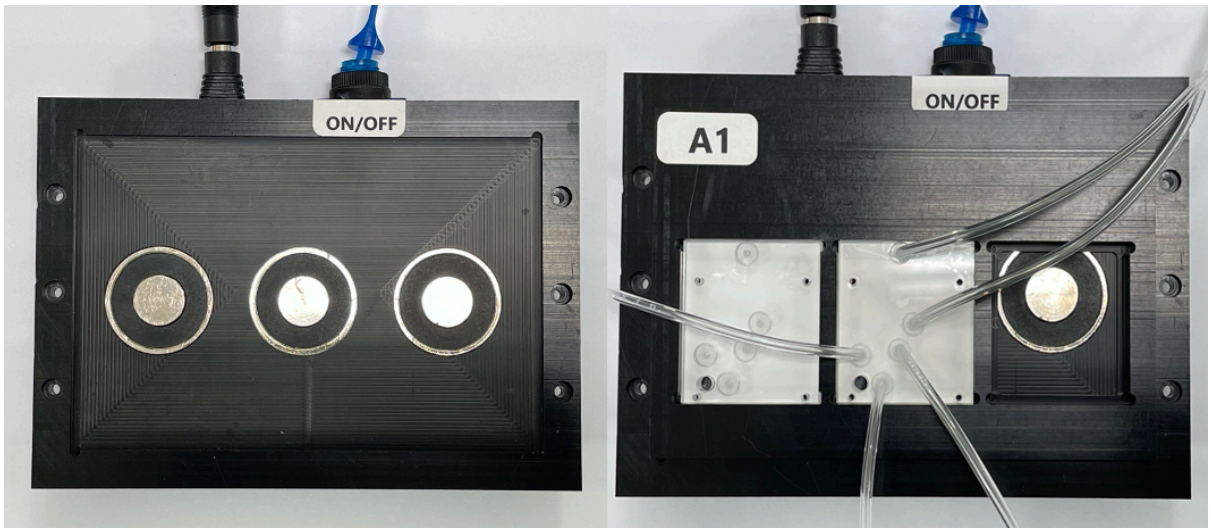

Image 6. ***Left*** *-photo of stationary part of the magnetic separation module;* ***Right*** *– photo of stationary part with portable holder and installed microfluidic cassettes.*

Switchable electromagnets mounted in stationary part of the module were located directly under the magnetic separation chamber of microfluidic cassette and allowed to generate magnetic field on purpose. Separation chamber also allowed to preconcentrate the sample as

NPs/ABs complexes were entrapped in the magnetic field and resuspended in the smaller volume of the dilution buffer in comparison to what the primary volume of sample was. Microbioreactor was isolated from the magnetic separation chamber and was in contact only with the pre-treated sample without interferents. Not immobilized NPs were removed from microbioreactor before substrate mixture was added to such part of the microfluidic cassette. Substrate mixture than was contacted with catalytically active NPs only in the microbioreactor and when substrate solution was removed from microbioreactor and introduced to detection chamber, the formation of the coloured product was stopped. Such manipulation allowed to delay the analytical signal measurement by the time needed to remove microfluidic tubing and place the holder with microfluidic cassettes to the multi-well spectrophotometer. Image 7 represents a module of portable holder with installed microfluidic cassettes.

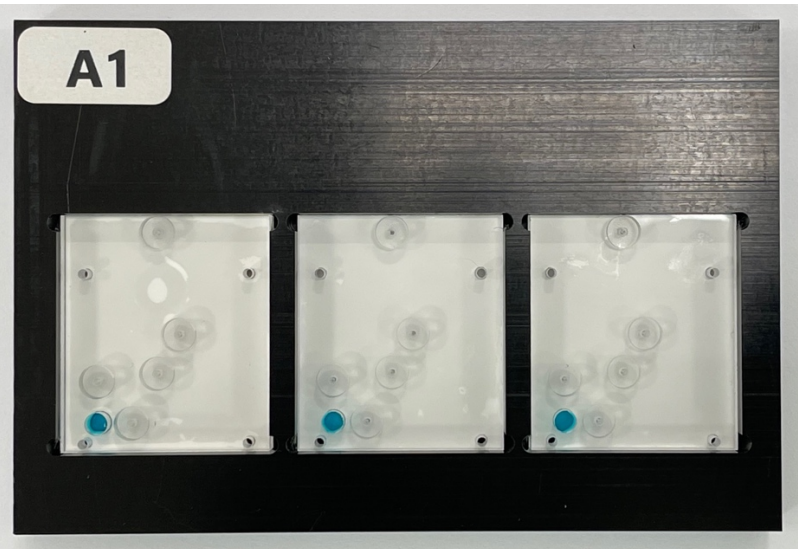

Image 7. Picture of portable holder with installed microfluidic cassettes.

Locations of detection chambers were compatible with N 1, N 10 and N 19 wells of 384-well plate what made possible to use multi-well spectrophotometer for analytical signal measurement without additional modification of detection equipment.

3.11.3. Examination of NPs/ABs interactions with microfluidic cassette

To investigate specific and nonspecific interaction of PtNPs/ABs conjugates with microfluidic cassettes, two types of chips were used. The first type contained microbioreactor modified with monoclonal anti-rabbit ABs specific to PtNPs/ABs conjugates. The surface of the second type of microbioreactors was modified with non-specific ABs produced in goat. The assumption was made that NPs/ABs conjugates should not express nonspecific interactions with internal microfluidic cassette parts. Only NPs/ABs interaction with magnetic field and

microbioreactor modified with specific ABs was expected. In such experiments a sample containing 20 times diluted NPs/ABs conjugates in dilution buffer was used.

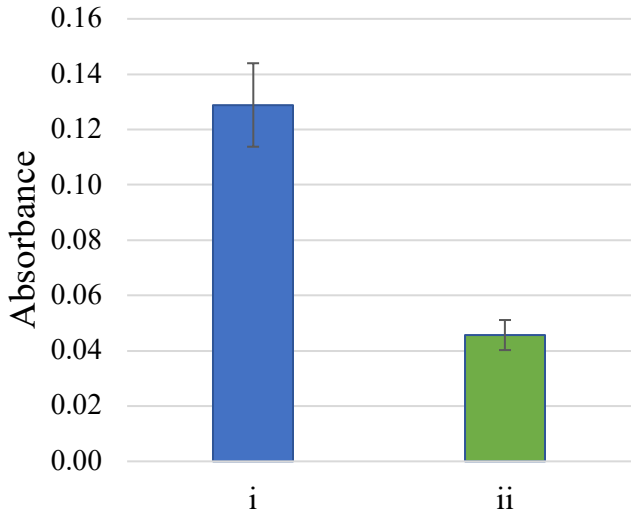

*Figure16. Absorbance measured at 625 nm derived from specific **(i)** and non-specific **(ii)** interaction of PtNPs/ABs conjugates with microfluidic cassette chip. Each bar represents absorbance average value from 5 measurements with error bars representing standard deviation.*

According to Figure 16 analytical signal derived from specific interaction of NPs/ABs conjugates was higher more than twice (0.13) than analytical signal form non-specific interaction (0.05). Such difference between analytical signals opens the opportunity to use such microfluidic cassette chips for antigen determination.

3.11.4. Antigen detection with microfluidic cassette chip

Microfluidic cassette chips were also used for analyses of different antigen concentration. For such experiment samples of different concentrations (from 0 to 500 ng/ml) of CRP and 20 times diluted PtNPs/ABs conjugates were used.

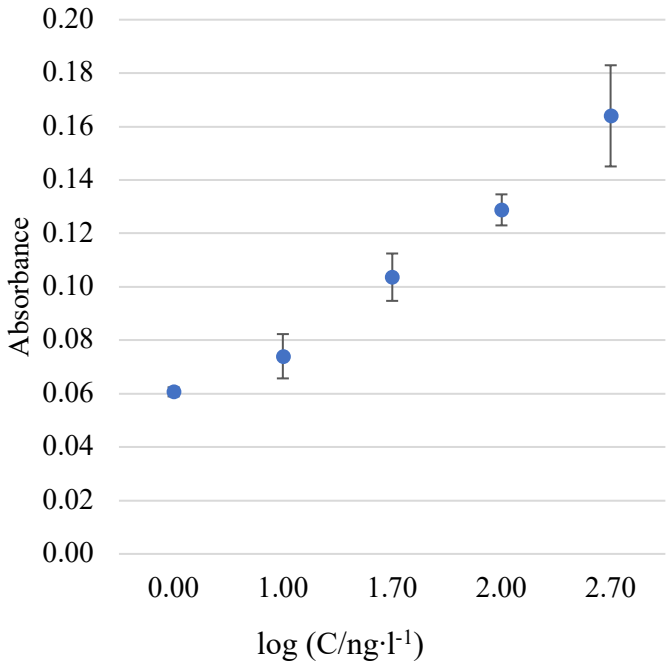

Figure 17. Absorbance measured at 625 nm for samples containing different concentration of CRP and PtNPs/ABs conjugates. Such experiment was done with TMB-based immunoassay. Each point represents absorbance average value from 5 measurements with error bars representing standard deviation.

Figure 17 represents analytical signals obtained for samples of different concentrations of CRP (0-500 ng/ml). According to Figure 19 analytical signal increased when increasing the CRP concentration. Such influence of analyte concentration on analytical signal proved that developed microfluidic cassette chips have high potential to be used for determination this analyte in samples. Prototype point-of-care devices for CRP determination described in literature were constructed according to different concept and various analytical techniques were used for signal generation and analysis.

In 2009, Brundenburg with his team presented a point-of-care device for CRP detection based on use of polymer biochips. Biochips presented by Brundenburg were manufactured with PMMA and contained optical elements required for signal measurement. The signal detection was based on total internal reflection fluorescence technique. Despite the simplicity of biochip construction, such biotest required unique equipment for analytical signal detection (Brandenburg *et al.*, 2009). Another research group developed an optical-fibre-based device for CRP detection. According to the authors, such system could be used for analyte determination and was based on chemiluminescence measurement (Nie *et al.*, 2020). Mou's research group presented nanomaterial-based chemiluminescent immunoassay for CRP detection. Analytical signal of such assay was generated using specifically developed charge-coupled camera (Mou

et al., 2021). Electrochemical CRP detection devices are also represented in literature (Pohanka, 2019; Amouzadeh Tabrizi and Acedo, 2022). Detection of analytical signal derived from microfluidic cassette chips presented in this dissertation work does not require any specific equipment due to compatibility with ordinary multiwell spectrophotometer. Commercialized point-of-care devices for CRP determination also usually require their own specific system of analytical signal detection. Moreover, same as the prototypes described in the literature, commercial point-of-care tests do not possess the in-built sample separation and preconcentration systems. Microfluidic cassette system developed as a part of this dissertation work was characterized with simple manufacturing and was multifunctional (sample separation, preconcentration and analytical reaction maintenance). Moreover, the presented microfluidic cassette chip has a room for further development and improvement. Some of these improvements, for example, concern an amplification of the analytical signal. The author of this work admits that increase of magnetic field strength can help to entrap a higher number of NPs which take part in analytical signal generation. Furthermore, increase of bioreactor surface covered with bioreceptors carry the potential to increase an analytical product formation via immobilization of higher number of NPs/ABs conjugates.

4. Summary and conclusions

This work for the first time presents the NPs in which paramagnetic properties are combined with enhanced peroxidase-like activity and ability to create conjugates with ABs. Such nanomaterials were used for highly sensitive detection of antigen in NLISA assays performed on MaxiSorp^{TM} plates and open PES bioreactors. In addition, the proof-of-concept point-of-care microfluidic cassette for antigen detection was successfully developed. Several experiments were carried out to achieve a stated results. First of all, different types of monometallic and multimetallic NPs were synthetized using various reducing agent of different concentrations. The peroxidase-like activity of synthesized NPs was examined in the presence of different HRP substrates in a wide range of pH. Catalytic activity mechanism of chosen NPs was investigated. Influence of multimetallic NPs/ABs conjugates synthesis and surface modification on nanozyme activity was examined. Specific and nonspecific interactions of synthesized conjugates with ABs, analyte and unmodified surface of polystyrene and PES were examined. A separate investigation was carried out to determine an influence of ABs type used for polystyrene and PES surface modification on analytical signal originated from immunotest prepared on such substrates. Magnetic separation and NPs dilution influence on analytical signal was duly examined. Buffer content influence on nonspecific interaction with modified and unmodified surface of polystyrene was tested. Working parameters of developed RuNPs/ABs and PtNPs/ABs conjugate-based NLISA performed on MaxiSorp^{TM} plates and PES bioreactors were compared with HRP/ABs conjugate-based ELISA and nanomaterial-based CRP determination immunoassays presented in the literature.

CRP detection device was developed and manufactured. It consists of microfluidic cassette chip compatible with multiwell plate spectrophotometer and magnetic separation module.

Based on the results obtained and presented in this doctoral thesis, the following conclusions can be drawn:

- Metal composition as well as type and concentration of reducing agent have an influence on stability, morphology and, as a result, on multimetallic NPs catalytic activity;
- It was confirmed that Ru-containing NPs can release ions and display heterogenic and homogenic mechanisms of catalytic activity. The combination of these two mechanisms may result in increased catalytic activity, which is important for the catalysts used in the assays;

- Synthesis steps and surface modification can influence multimetallic NPs catalytic activity. Introduction of Ru or Pt significantly increase catalytic activity of Fe_3O_4 nanocubes. Au decoration together with PEG stabilization decreased catalytic activity of obtained NPs. Introduction of conjugation-active groups decreased NPs catalytic activity due to blocking of active sites on NPs surface or entrapment of ions. ABs immobilization on NPs surface decreased NPs activity even further. Nevertheless, it was detected that final NPs/ABs conjugate activity is significantly higher than primary activity of Fe_3O_4 nanocubes;
- Higher catalytic activity of PtNPs/ABs conjugates was detected in comparison to RuNPs/ABs conjugates;
- It was proven that synthesized NPs/ABs conjugates can specifically interact with the analyte and specific ABs. Such experimental results allowed to use NPs/ABs conjugates in more advanced experiments of CRP determination;
- Buffer content selection is an important step for the elimination of unspecific interaction of NPs/ABs conjugates with a plate surface. Examination of different buffer content showed that 3% casein in blocking buffer and 1% of same protein in dilution buffer can help to minimize unspecific interactions of NPs/ABs conjugates with a plate surface. In contrast, BSA presence increased analytical signal for negative control sample almost three-fold in comparison to the results obtained when using casein;
- The positive influence of polyclonal ABs usage was confirmed for PS and PES surface modification on analytical tests signals performed on such substrates; Magnetic separation and sample preconcentration enhanced the analytical signal in comparison to analytical signal obtained from untreated samples. Such manipulations allowed to minimize interferents influence. In addition, sample preconcentration could help to perform analysis highly diluted samples; Additional room for improvement was found for NLISA analytical signal amplification as a function of conjugate concentration;
- Analysis time of NPs/ABs conjugates-based assays can be decreased to 15 min without any negative influence on analytical parameters of mentioned test;
- It was confirmed that the developed NLISA assay is highly specific and the presence of interferents in the analyzed sample had no visible negative effect on analytical signal level;

- According to analytical parameters given in Table 11 all PtNPs/ABs conjugate-based assays developed in this work can be classified as highly sensitive CRP determination tests in comparison to other nanomaterial-based assays.

Table 11. Analytical parameters and analysis time of nanomaterials-based tests presented in literature and NPs/ABs conjugate-based assays developed in this work.

Name	**LOD**	**Analysis time**	**Recourse (literature)**
QD	60 ng/ml	60-150 min	(Luo *et al.*, 2012)
Au NP	$12 \cdot 10^3$ ng/ml	5 min	(Ming *et al.*, 2014)
QD labelled magnetic beads	1 ng/ml	60-180 min	(Yang *et al.*, 2014)
QD	790 ng/ml	5 min	(Zhang *et al.*, 2015)
Eu-NPs	30 ng/ml	18 min	(Huttunen *et al.*, 2016)
Citicoline BSA AuNPs- conjugate	$8 \cdot 10^{-3}$ ng/ml	45 min	(Xie *et al.*, 2020)
RuNPs/ABs conjugates*	**1.67 ng/ml**	**15-30 min**	**This work**
PtNPs/ABs conjugates*	**0.34 ng/ml**	**15-30 min**	**This work**
HRP/ABs conjugates*	**1.72 ng/ml**	**15-30 min**	**This work**
PtNPs/ABs conjugates#	**0.60 ng/ml**	**30 min**	**This work**
HRP/ABs conjugates#	**3.18 ng/ml**	**30 min**	**This work**
*-tests performed on MaxiSorp™ plates; #-tests performed on PES open bioreactors			

- The developed microfluidic cassette chip can be classified as proof-of-concept point-of-care due to the promising results obtained for determination of wide range of CRP levels (from 0 to 500 ng/ml). The correlation of analytical signal obtained for microfluidic cassette chip and analyte concentration was observed.

The experiments carried out within this doctoral project are interdisciplinary and combined elements of chemistry, biotechnology, and materials engineering. Experimental results allowed for the formulation of conclusions that contain a source of knowledge for further considerations on the use of multimetallic multifunctional NPs in antigen detection assays and development of nanomaterial-based biosensors and biotests. Furthermore, this work is a starting point for the development of the new analytically useful lab-on-a-chip microsystems that can

be used in the future as diagnostic point-of-care devices for fast and sensitive determination of disease biomarkers.

5. Bibliography

Abdel-Lateef, M.A. (2022) 'Utilization of the peroxidase-like activity of silver nanoparticles nanozyme on o-phenylenediamine/H_2O_2 system for fluorescence detection of mercury (II) ions', *Scientific Reports*, 12(1), p. 6953. doi:10.1038/s41598-022-10779-8.

Abdi, A. *et al.* (2022) 'Smart water injection', in *Chemical Methods*. Elsevier, pp. 313–356. doi:10.1016/B978-0-12-821931-7.00008-0.

Abhijith, K.S., Ragavan, K. V. and Thakur, M.S. (2013) 'Gold nanoparticles enhanced chemiluminescence – a novel approach for sensitive determination of aflatoxin-B1', *Analytical Methods*, 5(18), p. 4838. doi:10.1039/c3ay40694f.

Abid, N. *et al.* (2022) 'Synthesis of nanomaterials using various top-down and bottom-up approaches, influencing factors, advantages, and disadvantages: A review', *Advances in Colloid and Interface Science*, 300, p. 102597. doi:10.1016/j.cis.2021.102597.

Abid, S.A. *et al.* (2020) 'Antibacterial and cytotoxic activities of cerium oxide nanoparticles prepared by laser ablation in liquid', *Environmental Science and Pollution Research*, 27(24), pp. 30479–30489. doi:10.1007/s11356-020-09332-9.

Adair, J.H., Suvaci, E. and Sindel, J. (2001) 'Surface and colloid chemistry', in *Encyclopedia of Materials: Science and Technology*. Elsevier, pp. 1–10. doi:10.1016/B0-08-043152-6/01622-3.

Adeniyi, O., Sicwetsha, S. and Mashazi, P. (2020) 'Nanomagnet-silica nanoparticles decorated with Au@Pd for enhanced peroxidase-like activity and colorimetric glucose sensing', *ACS Applied Materials & Interfaces*, 12(2), pp. 1973–1987. doi:10.1021/acsami.9b15123.

Aghahosseini, H. *et al.* (2021) 'Ag–Pd alloy immobilized on semi-heterogeneous support as a novel highly efficient artificial nitroreductase: experimental design optimization and kinetic study', *Catalysis Letters*, 151(5), pp. 1262–1272. doi:10.1007/s10562-020-03418-2.

Ahirwar, R. *et al.* (2015) 'BSA blocking in enzyme-linked immunosorbent assays is a non-mandatory step: a perspective study on mechanism of BSA blocking in common ELISA protocols', *RSC Advances*, 5(121), pp. 100077–100083. doi:10.1039/C5RA20750A.

Ahmad, A., Senapati, S., Khan, M. Islam, *et al.* (2003) 'Extracellular Biosynthesis of Monodisperse Gold Nanoparticles by a Novel Extremophilic Actinomycete, Thermomonospora sp.', *Langmuir*, 19(8), pp. 3550–3553. doi:10.1021/la026772l.

Ai, L. *et al.* (2022) 'One-pot corrosive synthesis of Ru-Fe_3O_4 heterostructure: A localized photothermal electrocatalyst towards accelerated water splitting', *Colloids and Surfaces A: Physicochemical and Engineering Aspects*, 651. doi:10.1016/j.colsurfa.2022.129767.

Al-Radadi, N.S. (2019) 'Green synthesis of platinum nanoparticles using Saudi's Dates extract and their usage on the cancer cell treatment', *Arabian Journal of Chemistry*, 12(3), pp. 330–349. doi:10.1016/j.arabjc.2018.05.008.

Albrecht, H.O. (1928) 'Über die chemiluminescenz des aminophthalsäurehydrazids', *Zeitschrift für Physikalische Chemie*, 136U(1), pp. 321–330. doi:10.1515/zpch-1928-13625.

Alhajj, M. and Farhana, A. (2022) 'Enzyme Linked Immunosorbent', *StatPearls Publishing*. PMID: 32310382

Alkilany, A.M. *et al.* (2014) 'Colloidal stability of citrate and mercaptoacetic acid capped gold nanoparticles upon lyophilization: effect of capping ligand attachment and type of cryoprotectants', *Langmuir*, 30(46), pp. 13799–13808. doi:10.1021/la504000v.

Alvarado-Ramírez, L. *et al.* (2021) 'Enzyme (single and multiple) and nanozyme biosensors: recent developments and their novel applications in the water-food-health nexus', *Biosensors*, 11(11), p. 410. doi:10.3390/bios11110410.

Amourizi, F., Dashtian, K. and Ghaedi, M. (2020) 'Developing a new colorimetric bioassay for iodide determination based on gold supported iridium peroxidase catalysts', *New Journal of Chemistry*, 44(14), pp. 5588–5597. doi:10.1039/C9NJ06310B.

Amouzadeh Tabrizi, M. and Acedo, P. (2022) 'Highly sensitive RNA-based electrochemical aptasensor for the determination of C-reactive protein using carbon nanofiber-chitosan modified screen-printed electrode', *Nanomaterials*, 12(3), p. 415. doi:10.3390/nano12030415.

An, C. *et al.* (2011) 'Study on Ag–Pd bimetallic nanoparticles for electrocatalytic reduction of benzyl chloride', *Electrochemistry Communications*, 13(12), pp. 1413–1416. doi:10.1016/j.elecom.2011.08.049.

António, M., Vitorino, R. and Daniel-da-Silva, A.L. (2021) 'Gold nanoparticles-based assays for biodetection in urine', *Talanta*, 230, p. 122345. doi:10.1016/j.talanta.2021.122345.

Anu Mary Ealia, S. and Saravanakumar, M.P. (2017) 'A review on the classification, characterisation, synthesis of nanoparticles and their application', *IOP Conference Series: Materials Science and Engineering*, 263, p. 032019. doi:10.1088/1757-899X/263/3/032019.

Aramesh, M. *et al.* (2017) 'Conformal nanocarbon coating of alumina nanocrystals for biosensing and bioimaging', *Carbon*, 122, pp. 422–427. doi:10.1016/j.carbon.2017.06.101.

Arends, I.W.C.E., Kodama, T. and Sheldon, R.A. (2004) 'Oxidation using ruthenium catalysts', *Topics in Organometallic Chemistry*, pp. 277–320. doi:10.1007/b94652.

Artioli, G., Angelini, I. and Polla, A. (2008) 'Crystals and phase transitions in protohistoric glass materials', *Phase Transitions*, 81(2–3), pp. 233–252. doi:10.1080/01411590701514409.

Asgharnasl, S. *et al.* (2020) 'Preparation of a novel magnetic bionanocomposite based on factionalized chitosan by creatine and its application in the synthesis of polyhydroquinoline, 1,4-dyhdropyridine and 1,8-dioxo-decahydroacridine derivatives', *International Journal of Biological Macromolecules*, 144, pp. 29–46. doi:10.1016/j.ijbiomac.2019.12.059.

Avci Duman, Y. (2021) 'Three phase partitioning of plant peroxidases', in *Three Phase Partitioning*. Elsevier, pp. 155–174. doi:10.1016/B978-0-12-824418-0.00007-2.

Axet, M.R. and Philippot, K. (2020) 'Catalysis with colloidal Ruthenium nanoparticles', *Chemical Reviews*, 120(2), pp. 1085–1145. doi:10.1021/acs.chemrev.9b00434.

Azeem, I. *et al.* (2021) 'Binding enhancements of antibody functionalized natural and synthetic fibers', *RSC Advances*, 11(48), pp. 30353–30360. doi:10.1039/D1RA04645D.

Baghdadi, A.M. *et al.* (2022) 'Structural refinement and antimicrobial activity of aluminum oxide nanoparticles', *Journal of the Ceramic Society of Japan*, 130(3), p. 21140. doi:10.2109/jcersj2.21140.

Behravan, M. *et al.* (2019) 'Facile green synthesis of silver nanoparticles using Berberis vulgaris leaf and root aqueous extract and its antibacterial activity', *International Journal of Biological Macromolecules*, 124, pp. 148–154. doi:10.1016/j.ijbiomac.2018.11.101.

Benzerara, K. *et al.* (2011) 'Significance, mechanisms and environmental implications of microbial biomineralization', *Comptes Rendus Geoscience*, 343(2–3), pp. 160–167. doi:10.1016/j.crte.2010.09.002.

Bloch, K. *et al.* (2021) 'Bacteriogenic Platinum nanoparticles for application in nanomedicine', *Frontiers in Chemistry*, 9. doi:10.3389/fchem.2021.624344.

Bocarsly, A.B. and Niangar, E.V. (2009) 'Fuel cells – proton-exchange membrane fuel cells. Membranes: Elevated Temperature', in *Encyclopedia of Electrochemical Power Sources*. Elsevier, pp. 724–733. doi:10.1016/B978-044452745-5.00232-X.

Bordet, A. *et al.* (2020) 'Molecular control of the catalytic properties of rhodium nanoparticles in supported ionic liquid phase (SILP) Systems', *ACS Catalysis*, 10(23), pp. 13904–13912. doi:10.1021/acscatal.0c03559.

Bovaird, J.H., Ngo, T.T. and Lenhoff, H.M. (1982) 'Optimizing the o-phenylenediamine assay for horseradish peroxidase: effects of phosphate and pH, substrate and enzyme concentrations, and stopping reagents.', *Clinical chemistry*, 28(12), pp. 2423–6. Available at: http://www.ncbi.nlm.nih.gov/pubmed/6754137.

Boverhof, D.R. *et al.* (2015) 'Comparative assessment of nanomaterial definitions and safety evaluation considerations', *Regulatory Toxicology and Pharmacology*, 73(1), pp. 137–150. doi:10.1016/j.yrtph.2015.06.001.

Bradley, R.C., Arking, A. and Beers, D.S. (1960) 'Secondary positive ion-emission from Platinum', *The Journal of Chemical Physics*, 33(3), pp. 764–769. doi:10.1063/1.1731256.

Brandenburg, A. *et al.* (2009) 'Integrated point of care testing system based on low cost polymer biochips', *SPIE BiOS* p. 716902. doi:10.1117/12.808160.

Brandenburg, K. and Moll, H. (1984) 'The terephthalate dosimeter for γ-, X- and β-radiation: dependence on dose and dose rate', *Radiation Physics and Chemistry (1977)*, 23(4), pp. 431–434. doi:10.1016/0146-5724(84)90132-8.

Breslow, R. and Overman, L.E. (1970) '"Artificial enzyme" combining a metal catalytic group and a hydrophobic binding cavity', *Journal of the American Chemical Society*, 92(4), pp. 1075–1077. doi:10.1021/ja00707a062.

Brun, N., Mazerolles, L. and Pernot, M. (1991) 'Microstructure of opaque red glass containing copper', *Journal of Materials Science Letters*, 10(23), pp. 1418–1420. doi:10.1007/BF00735696.

Cao, G.-J. *et al.* (2017) 'Mimicking horseradish peroxidase and oxidase using ruthenium nanomaterials', *RSC Advances*, 7(82), pp. 52210–52217. doi:10.1039/C7RA10370K.

Chaudhury, K. *et al.* (2013) 'Mitigation of endometriosis using regenerative cerium oxide nanoparticles', *Nanomedicine: Nanotechnology, Biology and Medicine*, 9(3), pp. 439–448. doi:10.1016/j.nano.2012.08.001.

Chen, H. *et al.* (2006) 'One-step preparation and characterization of PDDA-protected gold nanoparticles', *Polymer*, 47(2), pp. 763–766. doi:10.1016/j.polymer.2005.11.034.

Chen, H., Wang, Y. and Dong, S. (2007) 'An effective hydrothermal route for the synthesis of multiple pdda-protected noble-metal nanostructures', *Inorganic Chemistry*, 46(25), pp. 10587–10593. doi:10.1021/ic7009572.

Chen, J. *et al.* (2009) 'Shape-controlled synthesis of platinum nanocrystals for catalytic and electrocatalytic applications', *Nano Today*, 4(1), pp. 81–95. doi:10.1016/j.nantod.2008.09.002.

Chen, Y.-S. *et al.* (2020) 'Fluorescence quenchers manipulate the peroxidase-like activity of gold-based nanomaterials', *ACS Omega*, 5(38), pp. 24487–24494. doi:10.1021/acsomega.0c02956.

Chen, Y. *et al.* (2021) 'Thermal atomization of platinum nanoparticles into single atoms: an effective strategy for engineering high-performance nanozymes', *Journal of the American Chemical Society*, 143(44), pp. 18643–18651. doi:10.1021/jacs.1c08581.

Chen, Z. *et al.* (2018) 'Enzyme mimicry for combating bacteria and biofilms', *Accounts of Chemical Research*, 51(3), pp. 789–799. doi:10.1021/acs.accounts.8b00011.

Chen, Z. *et al.* (2007) 'A sensitive immunosensor using colloidal gold as electrochemical label', *Talanta*, 72(5), pp. 1800–1804. doi:10.1016/j.talanta.2007.02.020.

Choukourov, A. *et al.* (2021) 'Residual- and linker-free metal/polymer nanofluids prepared by direct deposition of magnetron-sputtered Cu nanoparticles into liquid PEG', *Journal of Molecular Liquids*, 336, p. 116319. doi:10.1016/j.molliq.2021.116319.

Chu, Z. *et al.* (2019) 'Ultrasmall Au–Ag alloy nanoparticles: protein-directed synthesis, biocompatibility, and x-ray computed tomography imaging', *ACS Biomaterials Science & Engineering*, 5(2), pp. 1005–1015. doi:10.1021/acsbiomaterials.8b01176.

Cui, M. *et al.* (2017) 'Facile synthesis of iridium nanoparticles with superior peroxidase-like activity for colorimetric determination of H_2O_2 and xanthine', *Sensors and Actuators B: Chemical*, 243, pp. 203–210. doi:10.1016/j.snb.2016.11.145.

Culliford, B.J. and Nickolls, L.C. (1964) 'The benzidine test: a critical review', *Journal of forensic sciences*, 9(1), pp. 175–91. Available at: http://www.ncbi.nlm.nih.gov/pubmed/14113938.

Dadigala, R. *et al.* (2022) 'Effective fabrication of cellulose nanofibrils supported Pd nanoparticles as a novel nanozyme with peroxidase and oxidase-like activities for efficient dye degradation', *Journal of Hazardous Materials*, 436, p. 129165. doi:10.1016/j.jhazmat.2022.129165.

Das, B. *et al.* (2021) 'Nanozymes in point-of-care diagnosis: An Emerging Futuristic Approach for Biosensing', *Nano-Micro Letters*, 13(1), p. 193. doi:10.1007/s40820-021-00717-0.

Das, B. and Patra, S. (2017) 'Antimicrobials', *Nanostructures for Antimicrobial Therapy*. Elsevier, pp. 1–22. doi:10.1016/B978-0-323-46152-8.00001-9.

Dasaratrao Sawle, B. *et al.* (2008) 'Biosynthesis and stabilization of Au and Au–Ag alloy nanoparticles by fungus, Fusarium semitectum', *Science and Technology of Advanced Materials*, 9(3), p. 035012. doi:10.1088/1468-6996/9/3/035012.

Demirkan, B. *et al.* (2020) 'Palladium supported on polypyrrole/reduced graphene oxide nanoparticles for simultaneous biosensing application of ascorbic acid, dopamine, and uric acid', *Scientific Reports*, 10(1), p. 2946. doi:10.1038/s41598-020-59935-y.

Deng, L., Nguyen, M.T. and Yonezawa, T. (2018) 'Sub-2 nm single-crystal pt nanoparticles via sputtering onto a liquid polymer', *Langmuir*, 34(8), pp. 2876–2881. doi:10.1021/acs.langmuir.7b04274.

Ding, J. *et al.* (2016) 'Au–Pt alloy nanoparticles site-selectively deposited on $CaIn_2S_4$ nanosteps as efficient photocatalysts for hydrogen production', *Journal of Materials Chemistry A*, 4(32), pp. 12630–12637. doi:10.1039/C6TA04468A.

Dong, C. *et al.* (2018) 'Size-dependent activity and selectivity of carbon dioxide photocatalytic reduction over platinum nanoparticles', *Nature Communications*, 9(1), p. 1252. doi:10.1038/s41467-018-03666-2.

Dong, J. *et al.* (2014) 'Co_3O_4 Nanoparticles with multi-enzyme activities and their application in immunohistochemical assay', *ACS Applied Materials & Interfaces*, 6(3), pp. 1959–1970. doi:10.1021/am405009f.

Doroszkowski, A. (1999) 'The physical chemistry of dispersion', in *Paint and Surface Coatings*. Elsevier, pp. 198–242. doi:10.1533/9781855737006.198.

Drozd, M. *et al.* (2016) 'Revisiting catechol derivatives as robust chromogenic hydrogen donors working in alkaline media for peroxidase mimetics', *Analytica Chimica Acta*, 948, pp. 80–89. doi:10.1016/j.aca.2016.10.027.

Eberhardt, D. *et al.* (2018) 'Templated growth of pd nanoparticles using sputtering deposition process and its catalytic activities', *Journal of Nanoscience and Nanotechnology*, 18(3), pp. 2075–2078. doi:10.1166/jnn.2018.13973.

Eid, K., Wang, H. and Wang, L. (2017) 'Nanoarchitectonic metals', in *Supra-Materials Nanoarchitectonics*. Elsevier, pp. 135–171. doi:10.1016/B978-0-323-37829-1.00006-7.

Eivazzadeh-Keihan, R. *et al.* (2021) 'Functionalized magnetic nanoparticles for the separation and purification of proteins and peptides', *TrAC Trends in Analytical Chemistry*, 141, p. 116291. doi:10.1016/j.trac.2021.116291.

El-Sayed, I.H., Huang, X. and El-Sayed, M.A. (2005) 'Surface plasmon resonance scattering and absorption of anti-EGFR antibody conjugated gold nanoparticles in cancer diagnostics: applications in oral cancer', *Nano Letters*, 5(5), pp. 829–834. doi:10.1021/nl050074e.

Emerson, E. (1943) 'The condensation of aminoantipyrine. A new color test for phenolic compounds', *The Journal of Organic Chemistry*, 08(5), pp. 417–428. doi:10.1021/jo01193a004.

Engvall, E. and Perlmann, P. (1971) ‘Enzyme-linked immunosorbent assay (ELISA) quantitative assay of immunoglobulin G’, *Immunochemistry*, 8(9), pp. 871–874. doi:10.1016/0019-2791(71)90454-X.

Eom, N. *et al.* (2021) ‘General trends in core–shell preferences for bimetallic nanoparticles’, *ACS Nano*, 15(5), pp. 8883–8895. doi:10.1021/acsnano.1c01500.

Fan, L. *et al.* (2018) ‘A novel AuNP-based glucose oxidase mimic with enhanced activity and selectivity constructed by molecular imprinting and O_2 -containing nanoemulsion embedding’, *Advanced Materials Interfaces*, 5(22), p. 1801070. doi:10.1002/admi.201801070.

Fang, X., Mark, G. and von Sonntag, C. (1996) ‘OH radical formation by ultrasound in aqueous solutions Part I: the chemistry underlying the terephthalate dosimeter’, *Ultrasonics Sonochemistry*, 3(1), pp. 57–63. doi:10.1016/1350-4177(95)00032-1.

Faust, B.C. and Allen, J.M. (1993) ‘Aqueous-phase photochemical formation of hydroxyl radical in authentic cloudwaters and fogwaters’, *Environmental Science & Technology*, 27(6), pp. 1221–1224. doi:10.1021/es00043a024.

Fenton, H.J.H. (1894) ‘LXXIII.—Oxidation of tartaric acid in presence of iron’, *J. Chem. Soc., Trans.*, 65, pp. 899–910. doi:10.1039/CT8946500899.

Ferrer Flegeau, E. *et al.* (2011) ‘Autocatalysis for C–H Bond Activation by Ruthenium(II) Complexes in Catalytic Arylation of Functional Arenes’, *Journal of the American Chemical Society*, 133(26), pp. 10161–10170. doi:10.1021/ja201462n.

Fontana, L.A. *et al.* (2019) ‘Peroxidase activity of new mixed-valence cobalt complexes with ligands derived from pyridoxal’, *Applied Organometallic Chemistry*, 33(7). doi:10.1002/aoc.4903.

Freestone, I. *et al.* (2007) ‘The Lycurgus Cup — A Roman nanotechnology’, *Gold Bulletin*, 40(4), pp. 270–277. doi:10.1007/BF03215599.

Frens, G. (1972) ‘Particle size and sol stability in metal colloids’, *Kolloid-Zeitschrift und Zeitschrift für Polymere*, 250(7), pp. 736–741. doi:10.1007/BF01498565.

Fu, B. *et al.* (2020) ‘A simple ultrasensitive electrochemical sensor for simultaneous determination of homovanillic acid and vanillylmandelic acid in human urine based on MWCNTs-Pt nanoparticles as peroxidase mimics’, *Journal of Electroanalytical Chemistry*, 866, p. 114165. doi:10.1016/j.jelechem.2020.114165.

Furst, A., Berlo, R.C. and Hooton, S. (1965) ‘Hydrazine as a reducing agent for organic compounds (Catalytic hydrazine reductions)’, *Chemical Reviews*, 65(1), pp. 51–68. doi:10.1021/cr60233a002.

Gao, B., Morison, G.K. and Kundur, P. (1992) ‘Voltage stability evaluation using modal analysis’, *IEEE Power Engineering Review*, 12(11), p. 41. doi:10.1109/MPER.1992.161430.

Gao, L. *et al.* (2007) ‘Intrinsic peroxidase-like activity of ferromagnetic nanoparticles’, *Nature Nanotechnology*, 2(9), pp. 577–583. doi:10.1038/nnano.2007.260.

Garg, B., Bisht, T. and Ling, Y.-C. (2015) ‘Graphene-based nanomaterials as efficient

peroxidase mimetic catalysts for biosensing applications: An overview', *Molecules*, 20(8), pp. 14155–14190. doi:10.3390/molecules200814155.

Gauvreau, V. *et al.* (2004) 'Engineering surfaces for bioconjugation: Developing strategies and quantifying the extent of the reactions', *Bioconjugate Chemistry*, 15(5), pp. 1146–1156. doi:10.1021/bc049858u.

Gavrilenko, E.A. *et al.* (2019) 'Comparative study of physicochemical and antibacterial properties of zno nanoparticles prepared by laser ablation of Zn target in water and air', *Materials*, 12(1), p. 186. doi:10.3390/ma12010186.

Germer, T.A., Zwinkels, J.C. and Tsai, B.K. (2014) 'Theoretical concepts in spectrophotometric measurements', in, pp. 11–66. doi:10.1016/B978-0-12-386022-4.00002-9.

Gleu, K. and Pfannstiel, K. (1936) 'Über 3-Aminophthalsäure-hydrazid', *Journal für Praktische Chemie*, 146(5–7), pp. 137–150. doi:10.1002/prac.19361460504.

Goon, I.Y. *et al.* (2009) 'Fabrication and dispersion of gold-shell-protected magnetite nanoparticles: Systematic control using polyethyleneimine', *Chemistry of Materials*, 21(4), pp. 673–681. doi:10.1021/cm8025329.

Green, N. (1963) 'Avidin. 1. The use of biotin for kinetic studies and for assay', *Biochemical Journal*, 89(3), pp. 585–591. doi:10.1042/bj0890585.

Green, N.M. (1975) 'Avidin', in, pp. 85–133. doi:10.1016/S0065-3233(08)60411-8.

Gu, S. *et al.* (2020) 'Mechanism of the oxidation of 3,3′,5,5′-tetramethylbenzidine catalyzed by peroxidase-like Pt nanoparticles immobilized in spherical polyelectrolyte brushes: A kinetic study', *ChemPhysChem*, 21(5), pp. 450–458. doi:10.1002/cphc.201901087.

Guan, B.Y. *et al.* (2016) 'A universal cooperative assembly-directed method for coating of mesoporous TiO_2 nanoshells with enhanced lithium storage properties', *Science Advances*, 2(3). doi:10.1126/sciadv.1501554.

Guilbault, G.G., Brignac, P.J. and Juneau, M. (1968) 'Substrates for the fluorometric determination of oxidative enzymes', *Analytical Chemistry*, 40(8), pp. 1256–1263. doi:10.1021/ac60264a027.

Guillén, G.G. *et al.* (2017) 'Effects of ablation energy and post-irradiation on the structure and properties of titanium dioxide nanomaterials', *Applied Surface Science*, 405, pp. 183–194. doi:10.1016/j.apsusc.2017.01.282.

Guo, Y., Fu, X. and Peng, Z. (2018) 'Controllable synthesis of MoS_2 nanostructures from monolayer flakes, few-layer pyramids to multilayer blocks by catalyst-assisted thermal evaporation', *Journal of Materials Science*, 53(11), pp. 8098–8107. doi:10.1007/s10853-018-2103-0.

Guo, Z.-X., Li, L. and Shen, H.-X. (1999) 'Study and analytical application of bromopyrogallol red as a hydrogen donor substrate for peroxidase', *Analytica Chimica Acta*, 379(1–2), pp. 63–68. doi:10.1016/S0003-2670(98)00625-4.

Gupta, P.K., Son, S.E. and Seong, G.H. (2021) 'Functionalized ultra-fine bimetallic PtRu alloy

nanoparticle with high peroxidase-mimicking activity for rapid and sensitive colorimetric quantification of C-reactive protein', *Microchimica Acta*, 188(4), p. 119. doi:10.1007/s00604-021-04775-4.

Han, L. *et al.* (2015) 'Au@Ag heterogeneous nanorods as nanozyme interfaces with peroxidase-like activity and their application for one-pot analysis of glucose at nearly neutral pH', *ACS Applied Materials & Interfaces*, 7(26), pp. 14463–14470. doi:10.1021/acsami.5b03591.

Hansen, C.H. *et al.* (2017) 'Nanoswitch-linked immunosorbent assay (NLISA) for fast, sensitive, and specific protein detection', *Proceedings of the National Academy of Sciences*, 114(39), pp. 10367–10372. doi:10.1073/pnas.1708148114.

Harvey, J.N. *et al.* (2019) 'Scope and Challenge of Computational Methods for Studying Mechanism and Reactivity in Homogeneous Catalysis', *ACS Catalysis*, 9(8), pp. 6803–6813. doi:10.1021/acscatal.9b01537.

Hassanpour, P. *et al.* (2018) 'Biomedical applications of aluminium oxide nanoparticles', *Micro & Nano Letters*, 13(9), pp. 1227–1231. doi:10.1049/mnl.2018.5070.

Hatamie, A. *et al.* (2015) 'Zinc oxide nanostructure-modified textile and its application to biosensing, photocatalysis, and as antibacterial material', *Langmuir*, 31(39), pp. 10913–10921. doi:10.1021/acs.langmuir.5b02341.

He, S.-B. *et al.* (2014) 'Synthesis and peroxidase-like activity of salt-resistant platinum nanoparticles by using bovine serum albumin as the scaffold', *ChemCatChem*, 6(6), pp. 1543–1548. doi:10.1002/cctc.201400011.

He, S. Bin *et al.* (2014) 'Synthesis and peroxidase-like activity of salt-resistant platinum nanoparticles by using bovine serum albumin as the scaffold', *ChemCatChem*, 6(6), pp. 1543–1548. doi:10.1002/cctc.201400011.

He, W. *et al.* (2010) 'Design of AgM bimetallic alloy nanostructures (M = Au, Pd, Pt) with tunable morphology and peroxidase-like activity', *Chemistry of Materials*, 22(9), pp. 2988–2994. doi:10.1021/cm100393v.

Hein, C.D., Liu, X.-M. and Wang, D. (2008) 'Click chemistry, a powerful tool for pharmaceutical sciences', *Pharmaceutical Research*, 25(10), pp. 2216–2230. doi:10.1007/s11095-008-9616-1.

Hierrezuelo, J. *et al.* (2010) 'Electrostatic stabilization of charged colloidal particles with adsorbed polyelectrolytes of opposite charge', *Langmuir*, 26(19), pp. 15109–15111. doi:10.1021/la102912u.

Hock, N. *et al.* (2022) 'Thiolated nanoparticles for biomedical applications: mimicking the workhorses of our body', *Advanced Science*, 9(1), p. 2102451. doi:10.1002/advs.202102451.

Hola, K. *et al.* (2015) 'Tailored functionalization of iron oxide nanoparticles for MRI, drug delivery, magnetic separation and immobilization of biosubstances', *Biotechnology Advances*, 33(6), pp. 1162–1176. doi:10.1016/j.biotechadv.2015.02.003.

Hormozi Jangi, A.R., Hormozi Jangi, M.R. and Hormozi Jangi, S.R. (2020) 'Detection

mechanism and classification of design principles of peroxidase mimic based colorimetric sensors: A brief overview', *Chinese Journal of Chemical Engineering*, 28(6), pp. 1492–1503. doi:10.1016/j.cjche.2020.01.020.

Hsu, C.-L. *et al.* (2016) 'Immobilization of aptamer-modified gold nanoparticles on BiOCl nanosheets: Tunable peroxidase-like activity by protein recognition', *Biosensors and Bioelectronics*, 75, pp. 181–187. doi:10.1016/j.bios.2015.08.049.

Hu, X., Zhou, L. and Gao, C. (2011) 'Hyperbranched polymers meet colloid nanocrystals: a promising avenue to multifunctional, robust nanohybrids', *Colloid and Polymer Science*, 289(12), pp. 1299–1320. doi:10.1007/s00396-011-2457-1.

Huang, L. *et al.* (2018) 'Diverse applications of TMB-based sensing probes', *Organic & Biomolecular Chemistry*, 16(31), pp. 5667–5676. doi:10.1039/C8OB01364K.

Huang, R. and Liu, R. (2017) 'Efficient in situ growth of platinum nanoclusters on the surface of Fe<inf>3</inf>O<inf>4</inf> for the detection of latent fingermarks', *Journal of Materials Science*, 52(23), pp. 13455–13465. doi:10.1007/s10853-017-1475-x.

Huang, Y., Ren, J. and Qu, X. (2019) 'Nanozymes: Classification, catalytic mechanisms, activity regulation, and applications', *Chemical Reviews*, 119(6), pp. 4357–4412. doi:10.1021/acs.chemrev.8b00672.

Hünig, S. (1964) 'Über zweistufige Redoxsysteme, I', *Justus Liebigs Annalen der Chemie*, 676(1), pp. 32–35. doi:10.1002/jlac.19646760105.

Huttunen, R.J. *et al.* (2016) 'Residual nanoparticle label immunosensor for wash-free C-reactive protein detection in blood', *Biosensors and Bioelectronics*, 83, pp. 54–59. doi:10.1016/j.bios.2016.04.036.

I Almalah, H., A Alzahrani, H. and S Abdelkader, H. (2019) 'Green synthesis of silver nanoparticles using cinnamomum zylinicum and their synergistic effect against multi-drug resistance bacteria', *Journal of Nanotechnology Research*, 01(02). doi:10.26502/jnr.2688-8521008.

Ijaz, I. *et al.* (2020) 'Detail review on chemical, physical and green synthesis, classification, characterizations and applications of nanoparticles', *Green Chemistry Letters and Reviews*, 13(3), pp. 223–245. doi:10.1080/17518253.2020.1802517.

Israel, L.L. *et al.* (2020) 'Magnetic iron oxide nanoparticles for imaging, targeting and treatment of primary and metastatic tumors of the brain', *Journal of Controlled Release*, 320, pp. 45–62. doi:10.1016/j.jconrel.2020.01.009.

Ivanova, P. *et al.* (2021) 'Nanoparticles of chosen noble metals as reactive oxygen species scavengers', *Nanotechnology*, 32(5), p. 055704. doi:10.1088/1361-6528/abc19f.

Jazayeri, M.H. *et al.* (2016) 'Various methods of gold nanoparticles (GNPs) conjugation to antibodies', *Sensing and Bio-Sensing Research*, 9, pp. 17–22. doi:10.1016/j.sbsr.2016.04.002.

Jeevanandam, J. *et al.* (2018) 'Review on nanoparticles and nanostructured materials: history, sources, toxicity and regulations', *Beilstein Journal of Nanotechnology*, 9, pp. 1050–1074. doi:10.3762/bjnano.9.98.

Jha, A.K., Prasad, K. and Kulkarni, A.R. (2009) 'Synthesis of TiO_2 nanoparticles using microorganisms', *Colloids and Surfaces B: Biointerfaces*, 71(2), pp. 226–229. doi:10.1016/j.colsurfb.2009.02.007.

Jha, A.K., Prasad, Kamlesh and Prasad, K. (2009) 'A green low-cost biosynthesis of Sb_2O_3 nanoparticles', *Biochemical Engineering Journal*, 43(3), pp. 303–306. doi:10.1016/j.bej.2008.10.016.

Jiang, B. *et al.* (2018) 'Standardized assays for determining the catalytic activity and kinetics of peroxidase-like nanozymes', *Nature Protocols*, 13(7), pp. 1506–1520. doi:10.1038/s41596-018-0001-1.

Josephy, P.D., Eling, T. and Mason, R.P. (1982) 'The horseradish peroxidase-catalyzed oxidation of 3,5,3',5'-tetramethylbenzidine. Free radical and charge-transfer complex intermediates.', *The Journal of biological chemistry*, 257(7), pp. 3669–75. Available at: http://www.ncbi.nlm.nih.gov/pubmed/6277943.

Kainthan, R.K. *et al.* (2006) 'Biocompatibility testing of branched and linear polyglycidol', *Biomacromolecules*, 7(3), pp. 703–709. doi:10.1021/bm0504882.

Kannan, R. *et al.* (2022) 'Advance molecular tools to detect plant pathogens', in *Biopesticides*. Elsevier, pp. 401–416. doi:10.1016/B978-0-12-823355-9.00008-0.

Karakuzu, O. *et al.* (2019) 'Amplex red assay for measuring hydrogen peroxide production from caenorhabditis elegans', *Bio-protocol*, 9(21). doi:10.21769/BioProtoc.3409.

Karoui, R. (2018) 'Spectroscopic technique: Fluorescence and ultraviolet-visible (UV-Vis) Spectroscopies', in *Modern Techniques for Food Authentication*. Elsevier, pp. 219–252. doi:10.1016/B978-0-12-814264-6.00007-4.

Karpova, E. V. *et al.* (2021) 'Core–shell nanozymes "Artificial Peroxidase": Stability with superior catalytic properties', *The Journal of Physical Chemistry Letters*, 12(23), pp. 5547–5551. doi:10.1021/acs.jpclett.1c01200.

Karyakin, A.A. *et al.* (2000) 'Oriented Immobilization of Antibodies onto the Gold Surfaces via Their Native Thiol Groups', *Analytical Chemistry*, 72(16), pp. 3805–3811. doi:10.1021/ac9907890.

Khade, B.S. *et al.* (2021) 'Adsorption of α-amylase and starch on porous zinc oxide nanosheet: Biophysical study', *Food Biophysics*, 16(2), pp. 280–291. doi:10.1007/s11483-021-09669-9.

Khan, A. *et al.* (2016) 'A chemical reduction approach to the synthesis of copper nanoparticles', *International Nano Letters*, 6(1), pp. 21–26. doi:10.1007/s40089-015-0163-6.

Khatami, M. *et al.* (2018) 'Core@shell nanoparticles: Greener synthesis using natural plant products', *Applied Sciences*, 8(3), p. 411. doi:10.3390/app8030411.

Khurana, K., Rathee, N. and Jaggi, N. (2020) 'Deposition of uniform plasmonic Ag nanoparticles by in-situ substrate heating using thermal evaporator', in, p. 090006. doi:10.1063/5.0001691.

Kim, M. *et al.* (2017) 'Synthesis of nanoparticles by laser ablation: A Review', *KONA Powder*

and Particle Journal, 34, pp. 80–90. doi:10.14356/kona.2017009.

Kim, M., Ko, S.M. and Nam, J.-M. (2016) 'Dealloying-based facile synthesis and highly catalytic properties of Au core/porous shell nanoparticles', *Nanoscale*, 8(22), pp. 11707–11717. doi:10.1039/C6NR01321J.

Kim, M.S. *et al.* (2017) 'Pt-Decorated Magnetic Nanozymes for Facile and Sensitive Point-of-Care Bioassay', *ACS Applied Materials & Interfaces*, 9(40), pp. 35133–35140. doi:10.1021/acsami.7b12326.

Kim, T.K. *et al.* (2014) 'Multi-core MgO NPs@C core–shell nanospheres for selective CO 2 capture under mild conditions', *New J. Chem.*, 38(4), pp. 1606–1610. doi:10.1039/C4NJ00067F.

Kolb, H.C., Finn, M.G. and Sharpless, K.B. (2001) 'Click Chemistry: Diverse Chemical Function from a Few Good Reactions', *Angewandte Chemie International Edition*, 40(11), pp. 2004–2021. doi:10.1002/1521-3773(20010601)40:11<2004::AID-ANIE2004>3.3.CO;2-5.

Kong, J. *et al.* (2021) 'One-pot synthesis of AuAgPd trimetallic nanoparticles with peroxidase-like activity for colorimetric assays', *Analytical and Bioanalytical Chemistry*, 413(21), pp. 5383–5393. doi:10.1007/s00216-021-03514-1.

Kraynov, A. and E., T. (2011) 'Concepts for the Stabilization of Metal Nanoparticles in Ionic Liquids', in *Applications of Ionic Liquids in Science and Technology*. InTech. doi:10.5772/22111.

Krieg, R. and Halbhuber, K.-J. (2010) 'Detection of endogenous and immuno-bound peroxidase - The status Quo in histochemistry', *Progress in Histochemistry and Cytochemistry*, 45(2), pp. 81–139. doi:10.1016/j.proghi.2009.11.001.

Kudeyarov, Y.A. *et al.* (2017) 'Analysis of Methods and Means of Measuring Catalytic Activity of Biologically and Chemically Active Substances', *Measurement Techniques*, 60(3), pp. 291–296. doi:10.1007/s11018-017-1188-1.

Kumar, A. *et al.* (2008) 'Silver-nanoparticle-embedded antimicrobial paints based on vegetable oil', *Nature Materials*, 7(3), pp. 236–241. doi:10.1038/nmat2099.

Kumar, A.P. *et al.* (2022) 'Synthesis of Magnetically Recoverable Ru/Fe_3O_4 Nanocomposite for Efficient Photocatalytic Degradation of Methylene Blue', *Journal of Cluster Science*, 33(3), pp. 853–865. doi:10.1007/s10876-021-02149-7.

Kumar, S., Aaron, J. and Sokolov, K. (2008) 'Directional conjugation of antibodies to nanoparticles for synthesis of multiplexed optical contrast agents with both delivery and targeting moieties', *Nature Protocols*, 3(2), pp. 314–320. doi:10.1038/nprot.2008.1.

Kurdekar, A.D. *et al.* (2018) 'Streptavidin-conjugated gold nanoclusters as ultrasensitive fluorescent sensors for early diagnosis of HIV infection', *Science Advances*, 4(11). doi:10.1126/sciadv.aar6280.

Kwon, G.S. and Kataoka, K. (1995) 'Block copolymer micelles as long-circulating drug vehicles', *Advanced Drug Delivery Reviews*, 16(2–3), pp. 295–309. doi:10.1016/0169-409X(95)00031-2.

Lan, J. *et al.* (2014) 'Colorimetric determination of sarcosine in urine samples of prostatic carcinoma by mimic enzyme palladium nanoparticles', *Analytica Chimica Acta*, 825, pp. 63–68. doi:10.1016/j.aca.2014.03.040.

Landry, M.J. *et al.* (2017) 'Surface-plasmon-mediated hydrogenation of carbonyls catalyzed by silver nanocubes under visible light', *ACS Catalysis*, 7(9), pp. 6128–6133. doi:10.1021/acscatal.7b02128.

Le, T.C. *et al.* (2019) 'Janus particles: recent advances in the biomedical applications', *International Journal of Nanomedicine*, Volume 14, pp. 6749–6777. doi:10.2147/IJN.S169030.

Lee, K.S., Price, E.O. and Land, J.E. (1956) 'A Spectrophotometric investigation of the niobium pyrogallol complex 1', *Journal of the American Chemical Society*, 78(7), pp. 1325–1327. doi:10.1021/ja01588a017.

Lengke, M.F., Fleet, M.E. and Southam, G. (2006) 'Morphology of gold nanoparticles synthesized by filamentous cyanobacteria from gold(i)−thiosulfate and gold(III)−chloride complexes', *Langmuir*, 22(6), pp. 2780–2787. doi:10.1021/la052652c.

Leonhardt, U. (2007) 'Invisibility cup', *Nature Photonics*, 1(4), pp. 207–208. doi:10.1038/nphoton.2007.38.

Lewandowska, H., Wójciuk, K. and Karczmarczyk, U. (2021) 'Metal nanozymes: new horizons in cellular homeostasis regulation', *Applied Sciences*, 11(19), p. 9019. doi:10.3390/app11199019.

Li, C.-L. *et al.* (2012) 'Peroxidase mimicking DNA–gold nanoparticles for fluorescence detection of the lead ions in blood', *The Analyst*, 137(22), p. 5222. doi:10.1039/c2an35599j.

Li, L. *et al.* (2022) 'Platinum janus nanoparticles as peroxidase mimics for catalytic immunosorbent assay', *ACS Applied Nano Materials*, 5(1), pp. 1397–1407. doi:10.1021/acsanm.1c03944.

Li, S. *et al.* (2022) 'One-pot synthesis of a peroxidase-like nanozyme and its application in visual assay for tyrosinase activity', *Talanta*, 239, p. 123088. doi:10.1016/j.talanta.2021.123088.

Li, W. *et al.* (2015) 'BSA-stabilized Pt nanozyme for peroxidase mimetics and its application on colorimetric detection of mercury(II) ions', *Biosensors and Bioelectronics*, 66, pp. 251–258. doi:10.1016/j.bios.2014.11.032.

Li, X. *et al.* (2011) 'Biosynthesis of nanoparticles by microorganisms and their applications', *Journal of Nanomaterials*, 2011, pp. 1–16. doi:10.1155/2011/270974.

Li, X. *et al.* (2014) 'Catalytic activity of shaped platinum nanoparticles for hydrogenation: a kinetic study', *Catalysis Science & Technology*, 4(9), p. 3290. doi:10.1039/C4CY00580E.

Li, X. *et al.* (2018) 'Three hidden talents in one framework: a terephthalic acid-coordinated cupric metal–organic framework with cascade cysteine oxidase- and peroxidase-mimicking activities and stimulus-responsive fluorescence for cysteine sensing', *Journal of Materials Chemistry B*, 6(39), pp. 6207–6211. doi:10.1039/C8TB02167H.

Liang, M. and Yan, X. (2019) 'Nanozymes: From new concepts, mechanisms, and standards to applications', *Accounts of Chemical Research*, 52(8), pp. 2190–2200. doi:10.1021/acs.accounts.9b00140.

Lim, B. *et al.* (2009) 'Pd-Pt bimetallic nanodendrites with high activity for oxygen reduction', *Science*, 324(5932), pp. 1302–1305. doi:10.1126/science.1170377.

Lin, D. *et al.* (2021) 'Circulating tumor cells: biology and clinical significance', *Signal Transduction and Targeted Therapy*, 6(1), p. 404. doi:10.1038/s41392-021-00817-8.

Lin, S. *et al.* (2018) 'Nanozymes for biomedical sensing applications', in *Biomedical Applications of Functionalized Nanomaterials*. Elsevier, pp. 171–209. doi:10.1016/B978-0-323-50878-0.00007-0.

Lin, X.-Q. *et al.* (2015) 'Platinum nanoparticles/graphene-oxide hybrid with excellent peroxidase-like activity and its application for cysteine detection', *The Analyst*, 140(15), pp. 5251–5256. doi:10.1039/C5AN00809C.

Lin, X., O'Reilly Beringhs, A. and Lu, X. (2021) 'Applications of nanoparticle-antibody conjugates in immunoassays and tumor imaging', *The AAPS Journal*, 23(2), p. 43. doi:10.1208/s12248-021-00561-5.

Lin, Y.-C. *et al.* (2022) 'Multimodal bioimaging using nanodiamond and gold hybrid nanoparticles', *Scientific Reports*, 12(1), p. 5331. doi:10.1038/s41598-022-09317-3.

Liu, H., Huang, Z. and Liu, C. (2022) 'Development of a horseradish peroxidase-Fenton-like system for the degradation of sulfamethazine under weak acid condition', *Environmental Science and Pollution Research*, 29(8), pp. 12065–12074. doi:10.1007/s11356-021-16681-6.

Liu, S.G. *et al.* (2018) 'A fluorescence and colorimetric dual-mode assay of alkaline phosphatase activity via destroying oxidase-like CoOOH nanoflakes', *Journal of Materials Chemistry B*, 6(18), pp. 2843–2850. doi:10.1039/C7TB03275G.

Liu, W.-J. *et al.* (2006) 'Novel method for the preparation of core–shell nanoparticles with movable Ag core and polystyrene loop shell', *Journal of Solid State Chemistry*, 179(4), pp. 1253–1258. doi:10.1016/j.jssc.2006.01.042.

Liu, Y. *et al.* (2020) 'Palladium-based nanomaterials for cancer imaging and therapy', *Theranostics*, 10(22), pp. 10057–10074. doi:10.7150/thno.45990.

Liu, Z.L. *et al.* (2004) 'Synthesis of magnetite nanoparticles in W/O microemulsion', *Journal of Materials Science*, 39(7), pp. 2633–2636. doi:10.1023/B:JMSC.0000020046.68106.22.

Llobat-Estelles, M., Sevillano-Cabeza, A. and Medina-Escriche, J. (1986) 'Kinetic-catalytic determination of cobalt by oxidation of Pyrogallol Red by hydrogen peroxide', *The Analyst*, 111(2), p. 193. doi:10.1039/an9861100193.

Logan, N. *et al.* (2020) 'Amalgamated gold-nanoalloys with enhanced catalytic activity for the detection of mercury ions (Hg_2^+) in seawater samples', *Nano Research*, 13(4), pp. 989–998. doi:10.1007/s12274-020-2731-y.

Long, N.V. *et al.* (2011) 'Shape-controlled synthesis of Pt–Pd core–shell nanoparticles

exhibiting polyhedral morphologies by modified polyol method', *Acta Materialia*, 59(7), pp. 2901–2907. doi:10.1016/j.actamat.2011.01.033.

Lopez, M. (2014) 'Combined in situ Hybridization/Immunohistochemistry (ISH/IH) on Free-floating Vibratome Tissue Sections', 4(18). doi:10.21769/BioProtoc.1243.

Lu, F. *et al.* (2014) 'Plant-mediated synthesis of Ag–Pd alloy nanoparticles and their application as catalyst toward selective hydrogenation', *ACS Sustainable Chemistry & Engineering*, 2(5), pp. 1212–1218. doi:10.1021/sc500034r.

Luo, C., Zhang, Y. and Wang, Y. (2005) 'Palladium nanoparticles in poly(ethyleneglycol): the efficient and recyclable catalyst for Heck reaction', *Journal of Molecular Catalysis A: Chemical*, 229(1–2), pp. 7–12. doi:10.1016/j.molcata.2004.10.039.

Luo, Y. *et al.* (2012) 'Sensitive and rapid quantification of C-reactive protein using quantum dot-labeled microplate immunoassay', *Journal of Translational Medicine*, 10(1), p. 24. doi:10.1186/1479-5876-10-24.

Lv, M. *et al.* (2021) 'Improved quantification of immune-gold labeling and its use to compare the distribution of cellular factors among sub-chloroplast compartments', *Micron*, 145, p. 103060. doi:10.1016/j.micron.2021.103060.

Ma, X. *et al.* (2008) 'Palladium nanoparticles in polyethylene glycols: Efficient and recyclable catalyst system for hydrogenation of olefins', *Catalysis Communications*, 9(1), pp. 70–74. doi:10.1016/j.catcom.2007.05.028.

Mahmoodi, A., Ghoranneviss, M. and Asgary, S. (2017) 'Effect of different sputtering time on the formation of copper and copper oxide nano particles by magnetron sputtering system', *Journal of Structural Chemistry*, 58(6), pp. 1245–1250. doi:10.1134/S0022476617060245.

Mahmoudi, T. *et al.* (2021) '(Nano)tag–antibody conjugates in rapid tests', *Journal of Materials Chemistry B*, 9(27), pp. 5414–5438. doi:10.1039/D1TB00571E.

Mahmudunnabi, R.G. *et al.* (2020) 'Nanozyme-based electrochemical biosensors for disease biomarker detection', *The Analyst*, 145(13), pp. 4398–4420. doi:10.1039/D0AN00558D.

Malathi, S. *et al.* (2014) 'One pot green synthesis of Ag, Au and Au–Ag alloy nanoparticles using isonicotinic acid hydrazide and starch', *Carbohydrate Polymers*, 111, pp. 734–743. doi:10.1016/j.carbpol.2014.04.105.

Manea, F. *et al.* (2004) 'Nanozymes: Gold-Nanoparticle-based transphosphorylation catalysts', *Angewandte Chemie International Edition*, 43(45), pp. 6165–6169. doi:10.1002/anie.200460649.

Marklund, S. and Marklund, G. (1974) 'Involvement of the superoxide anion radical in the autoxidation of pyrogallol and a convenient assay for superoxide dismutase', *European Journal of Biochemistry*, 47(3), pp. 469–474. doi:10.1111/j.1432-1033.1974.tb03714.x.

Marques, A.C. *et al.* (2020) 'Functionalizing nanoparticles with cancer-targeting antibodies: A comparison of strategies', *Journal of Controlled Release*, 320, pp. 180–200. doi:10.1016/j.jconrel.2020.01.035.

Matthews, R.W. (1980) 'The radiation chemistry of the terephthalate dosimeter', *Radiation Research*, 83(1), p. 27. doi:10.2307/3575256.

Mattox, D.M. (2002) 'Physical vapor deposition (PVD) processes', *Metal Finishing*, 100, pp. 394–408. doi:10.1016/S0026-0576(02)82043-8.

McCarthy, M.B. and White, R.E. (1983) 'Functional differences between peroxidase compound I and the cytochrome P-450 reactive oxygen intermediate.', *The Journal of biological chemistry*, 258(15), pp. 9153–8. Available at: http://www.ncbi.nlm.nih.gov/pubmed/6874682.

Meder, F. *et al.* (2016) 'Labeling the Structural integrity of nanoparticles for advanced in situ tracking in bionanotechnology', *ACS Nano*, 10(4), pp. 4660–4671. doi:10.1021/acsnano.6b01001.

Menazea, A.A. (2020) 'Femtosecond laser ablation-assisted synthesis of silver nanoparticles in organic and inorganic liquids medium and their antibacterial efficiency', *Radiation Physics and Chemistry*, 168, p. 108616. doi:10.1016/j.radphyschem.2019.108616.

Miao, Z. *et al.* (2020) 'Ultrasmall rhodium nanozyme with RONS scavenging and photothermal activities for anti-inflammation and antitumor Theranostics of colon diseases', *Nano Letters*, 20(5), pp. 3079–3089. doi:10.1021/acs.nanolett.9b05035.

Mie, G. (1908) 'Beiträge zur Optik trüber Medien, speziell kolloidaler Metallösungen', *Annalen der Physik*, 330(3), pp. 377–445. doi:10.1002/andp.19083300302.

MIFUNE, M. *et al.* (2000) 'Peroxidase-like activity of glass-beads modified with metal-porphines and their analytical applications.', *Analytical Sciences*, 16(11), pp. 1121–1125. doi:10.2116/analsci.16.1121.

Ming, C. *et al.* (2014) 'Rapid and quantitative detection of C-reactive protein using quantum dots and immunochromatographic test strips', *International Journal of Nanomedicine*, p. 5619. doi:10.2147/IJN.S74751.

Minic, R. and Zivkovic, I. (2021) 'Optimization, Validation and Standardization of ELISA', in *Norovirus*. IntechOpen. doi:10.5772/intechopen.94338.

Miranda, R.R., Sampaio, I. and Zucolotto, V. (2022) 'Exploring silver nanoparticles for cancer therapy and diagnosis', *Colloids and Surfaces B: Biointerfaces*, 210, p. 112254. doi:10.1016/j.colsurfb.2021.112254.

Mo, S. *et al.* (2016) 'Increasing entropy for colloidal stabilization', *Scientific Reports*, 6(1), p. 36836. doi:10.1038/srep36836.

Mochizuki, M. *et al.* (2002) 'Kinetic analysis and mechanistic aspects of autoxidation of catechins', *Biochimica et Biophysica Acta (BBA) - General Subjects*, 1569(1–3), pp. 35–44. doi:10.1016/S0304-4165(01)00230-6.

Mohanty, J.. *et al.* (1997) 'A highly sensitive fluorescent micro-assay of H_2O_2 release from activated human leukocytes using a dihydroxyphenoxazine derivative', *Journal of Immunological Methods*, 202(2), pp. 133–141. doi:10.1016/S0022-1759(96)00244-X.

Mostafa, A.M. *et al.* (2017) 'Synthesis of cadmium oxide nanoparticles by pulsed laser ablation

in liquid environment', *Optik*, 144, pp. 679–684. doi:10.1016/j.ijleo.2017.06.065.

Motamedi-sedeh, F. *et al.* (2022) 'Carboxymethyl chitosan bounded iron oxide nanoparticles and gamma-irradiated avian influenza subtype H9N2 vaccine to development of immunity on mouse and chicken', *Veterinary Medicine and Science*, 8(2), pp. 626–634. doi:10.1002/vms3.680.

Mou, L. *et al.* (2021) 'Point-of-care immunoassays with tunable detection range for detecting infection in intensive care unit', *CCS Chemistry*, 3(5), pp. 1562–1572. doi:10.31635/ccschem.020.202000331.

Mu, J. *et al.* (2012) 'Intrinsic peroxidase-like activity and catalase-like activity of Co_3O_4 nanoparticles', *Chemical Communications*, 48(19), p. 2540. doi:10.1039/c2cc17013b.

Muhammed Shameem, P. V., Mekala, L. and Senthil Kumar, M. (2017) 'Exchange bias induced by the spin glass-like surface spins in sputter deposited Fe_3O_4 Thin Films', *IEEE Transactions on Magnetics*, 53(11), pp. 1–5. doi:10.1109/TMAG.2017.2703884.

Mukherjee, A. *et al.* (2022) 'Role of magnetic nanoparticles in development of biosensors for viral infection diagnostics', in *Advanced Biosensors for Virus Detection*. Elsevier, pp. 189–202. doi:10.1016/B978-0-12-824494-4.00002-3.

Mukherjee, P. *et al.* (2001) 'Bioreduction of $AuCl_4^-$ ions by the fungus, *Verticillium sp*. and surface trapping of the gold nanoparticles formed', *Angewandte Chemie International Edition*, 40(19), p. 3585. doi:10.1002/1521-

Mukherjee, P. *et al.* (2002) 'Extracellular Synthesis of Gold Nanoparticles by the Fungus Fusarium oxysporum', *ChemBioChem*, 3(5), p. 461. doi:10.1002/1439-7633(20020503)3:5<461::AID-CBIC461>3.0.CO;2-X.

Nair, B. and Pradeep, T. (2002) 'Coalescence of nanoclusters and formation of submicron crystallites assisted by lactobacillus strains', *Crystal Growth & Design*, 2(4), pp. 293–298. doi:10.1021/cg0255164.

Nam, N.H. and Luong, N.H. (2019) 'Nanoparticles: synthesis and applications', in *Materials for Biomedical Engineering*. Elsevier, pp. 211–240. doi:10.1016/B978-0-08-102814-8.00008-1.

Nanda Kumar, D., Chandrasekaran, N. and Mukherjee, A. (2018) 'Horseradish peroxidase-mediated in situ synthesis of silver nanoparticles: application for sensing of mercury', *New Journal of Chemistry*, 42(16), pp. 13763–13769. doi:10.1039/C8NJ02083C.

Nangia, Y. *et al.* (2012) 'Palladium@gold bimetallic nanostructures as peroxidase mimic for development of sensitive fluoroimmunoassay', *Analytica Chimica Acta*, 751, pp. 140–145. doi:10.1016/j.aca.2012.09.005.

Nasir, M. *et al.* (2017) 'An overview on enzyme-mimicking nanomaterials for use in electrochemical and optical assays', *Microchimica Acta*, 184(2), pp. 323–342. doi:10.1007/s00604-016-2036-8.

Nath, I., Chakraborty, J. and Verpoort, F. (2016) 'Metal organic frameworks mimicking natural enzymes: a structural and functional analogy', *Chemical Society Reviews*, 45(15), pp. 4127–

4170. doi:10.1039/C6CS00047A.

Navalón, S. and García, H. (2016) 'Nanoparticles for Catalysis', *Nanomaterials*, 6(7), p. 123. doi:10.3390/nano6070123.

Nehring, S.M., Goyal, A. and Patel, B.C. (2022) 'C Reactive Protein', *StatPearls*. PMID: 28722873.

Neikov, O.D. (2009) 'Mechanical crushing and grinding', in *Handbook of Non-Ferrous Metal Powders*. Elsevier, pp. 47–62. doi:10.1016/B978-1-85617-422-0.00002-1.

Ni, B. and Wang, X. (2015) 'Face the edges: catalytic active sites of nanomaterials', *Advanced Science*, 2(7), p. 1500085. doi:10.1002/advs.201500085.

Nichols, G. *et al.* (2002) 'A review of the terms agglomerate and aggregate with a recommendation for nomenclature used in powder and particle characterization', *Journal of Pharmaceutical Sciences*, 91(10), pp. 2103–2109. doi:10.1002/jps.10191.

NIE, D.-X., SHI, G.-Y. and YU, Y.-Y. (2016) 'Fe_3O_4 magnetic nanoparticles as peroxidase mimetics used in colorimetric determination of 2,4-Dinitrotoluene', *Chinese Journal of Analytical Chemistry*, 44(2), pp. 179–185. doi:10.1016/S1872-2040(16)60902-7.

Nie, F. *et al.* (2020) 'Trimetallic PdCuAu nanoparticles for temperature sensing and fluorescence detection of H_2O_2 and Glucose', *Frontiers in Chemistry*, 8. doi:10.3389/fchem.2020.00244.

Nie, R. *et al.* (2020) 'A portable pencil-like immunosensor for point-of-care testing of inflammatory biomarkers', *Analytical and Bioanalytical Chemistry*, 412(13), pp. 3231–3239. doi:10.1007/s00216-020-02582-z.

Niu, Z. and Li, Y. (2014) 'Removal and utilization of capping agents in nanocatalysis', *Chemistry of Materials*, 26(1), pp. 72–83. doi:10.1021/cm4022479.

Nour, S., Bolandi, B. and Imani, R. (2020) 'Nanotechnology in gene therapy for musculoskeletal regeneration', in *Nanoengineering in Musculoskeletal Regeneration*. Elsevier, pp. 105–136. doi:10.1016/B978-0-12-820262-3.00004-9.

Okyem, S. *et al.* (2021) 'High-Affinity Points of interaction on antibody allow synthesis of stable and highly functional antibody–Gold nanoparticle conjugates', *Bioconjugate Chemistry*, 32(8), pp. 1753–1762. doi:10.1021/acs.bioconjchem.1c00261.

Oluwatosin Abegunde, O. *et al.* (2019) 'Overview of thin film deposition techniques', *AIMS Materials Science*, 6(2), pp. 174–199. doi:10.3934/matersci.2019.2.174.

Ostovari Moghaddam, A. *et al.* (2018) 'Synthesis of bornite Cu_5FeS_4 nanoparticles via high energy ball milling: Photocatalytic and thermoelectric properties', *Powder Technology*, 333, pp. 160–166. doi:10.1016/j.powtec.2018.04.023.

Otis, G., Ejgenberg, M. and Mastai, Y. (2021) 'Solvent-free mechanochemical synthesis of ZnO nanoparticles by high-energy ball milling of ε-$Zn(OH)_2$ Crystals', *Nanomaterials*, 11(1), p. 238. doi:10.3390/nano11010238.

Otsuka, H., Nagasaki, Y. and Kataoka, K. (2003) 'PEGylated nanoparticles for biological and pharmaceutical applications', *Advanced Drug Delivery Reviews*, 55(3), pp. 403–419. doi:10.1016/S0169-409X(02)00226-0.

Page Faulk, W. and Malcolm Taylor, G. (1971) 'Communication to the editors', *Immunochemistry*, 8(11), pp. 1081–1083. doi:10.1016/0019-2791(71)90496-4.

Pal, G., Rai, P. and Pandey, A. (2019) 'Green synthesis of nanoparticles: A greener approach for a cleaner future', *Green Synthesis, Characterization and Applications of Nanoparticles*. Elsevier, pp. 1–26. doi:10.1016/B978-0-08-102579-6.00001-0.

Palchoudhury, S. *et al.* (2010) 'Platinum attachments on iron oxide nanoparticle surfaces', *Journal of Applied Physics*, 107(9), p. 3904. doi:10.1063/1.3355899.

Panferov, V.G. *et al.* (2020) 'Urchin peroxidase-mimicking Au@Pt nanoparticles as a label in lateral flow immunoassay: impact of nanoparticle composition on detection limit of Clavibacter michiganensis', *Microchimica Acta*, 187(5), p. 268. doi:10.1007/s00604-020-04253-3.

Parzuchowski, P.G. *et al.* (2020) 'Hyperbranched poly(ether-siloxane)s containing ammonium groups: synthesis, characterization and catalytic activity', *Polymers*, 12(4), p. 856. doi:10.3390/polym12040856.

Pate, K. and Safier, P. (2016) 'Chemical metrology methods for CMP quality', *Advances in Chemical Mechanical Planarization (CMP)*. Elsevier, pp. 299–325. doi:10.1016/B978-0-08-100165-3.00012-7.

Pawlonka, J. *et al.* (2014) 'An application of microemulsion method for synthesis of copper-zinc materials', *Annales UMCS, Chemia*, 68(1–2). doi:10.2478/umcschem-2013-0009.

Paździoch-Czochra, M. and Wideńska, A. (2002) 'Spectrofluorimetric determination of hydrogen peroxide scavenging activity', *Analytica Chimica Acta*, 452(2), pp. 177–184. doi:10.1016/S0003-2670(01)01455-6.

Pietrzak, M. and Ivanova, P. (2021) 'Bimetallic and multimetallic nanoparticles as nanozymes', *Sensors and Actuators B: Chemical*, 336, p. 129736. doi:10.1016/j.snb.2021.129736.

Pohanka, M. (2019) 'Piezoelectric immunosensor for the determination of c- reactive protein', *International Journal of Electrochemical Science*, pp. 8470–8478. doi:10.20964/2019.09.02.

Pokropivny, V.V. and Skorokhod, V.V. (2007) 'Classification of nanostructures by dimensionality and concept of surface forms engineering in nanomaterial science', *Materials Science and Engineering: C*, 27(5–8), pp. 990–993. doi:10.1016/j.msec.2006.09.023.

Powell, M.E.A. and Smith, M.J.H. (1954) 'The determination of serum acid and alkaline phosphatase activity with 4-aminoantipyrine (A.A.P.)', *Journal of Clinical Pathology*, 7(3), pp. 245–248. doi:10.1136/jcp.7.3.245.

Prati, L. *et al.* (2011) 'Ru modified Au catalysts for the selective oxidation of aliphatic alcohols', *Catalysis Science and Technology*, 1(9), pp. 1624–1629. doi:10.1039/c1cy00218j.

Ray, A. and Mitra, A.K. (2017) 'Nanotechnology in intracellular trafficking, imaging, and delivery of therapeutic agents', in *Emerging Nanotechnologies for Diagnostics, Drug Delivery*

and Medical s. Elsevier, pp. 169–188. doi:10.1016/B978-0-323-42978-8.00008-5.

Ren, X. *et al.* (2022) 'Nanozymes-recent development and biomedical applications', *Journal of Nanobiotechnology*, 20(1), p. 92. doi:10.1186/s12951-022-01295-y.

Reverberi, A. Pietro *et al.* (2019) 'Green synthesis of silver nanoparticles by low-energy wet bead milling of metal spheres', *Materials*, 13(1), p. 63. doi:10.3390/ma13010063.

Ríos, Á. and Zougagh, M. (2016) 'Recent advances in magnetic nanomaterials for improving analytical processes', *TrAC Trends in Analytical Chemistry*, 84, pp. 72–83. doi:10.1016/j.trac.2016.03.001.

Rodrigues, T.S., da Silva, A.G.M. and Camargo, P.H.C. (2019) 'Nanocatalysis by noble metal nanoparticles: controlled synthesis for the optimization and understanding of activities', *Journal of Materials Chemistry A*, 7(11), pp. 5857–5874. doi:10.1039/C9TA00074G.

Roucoux, A., Schulz, J. and Patin, H. (2002) 'Reduced transition metal colloids: a novel family of reusable catalysts?', *Chemical Reviews*, 102(10), pp. 3757–3778. doi:10.1021/cr010350j.

Sadeghi, P. *et al.* (2021) 'Lateral flow assays (LFA) as an alternative medical diagnosis method for detection of virus species: The intertwine of nanotechnology with sensing strategies', *TrAC Trends in Analytical Chemistry*, 145, p. 116460. doi:10.1016/j.trac.2021.116460.

Sápi, A. *et al.* (2021) 'Metallic nanoparticles in heterogeneous catalysis', *Catalysis Letters*, 151(8), pp. 2153–2175. doi:10.1007/s10562-020-03477-5.

Sathe, T.M. and Dhoble, A.S. (2017) 'A review on recent advancements in photovoltaic thermal techniques', *Renewable and Sustainable Energy Reviews*, 76, pp. 645–672. doi:10.1016/j.rser.2017.03.075.

Schaming, D. and Remita, H. (2015) 'Nanotechnology: from the ancient time to nowadays', *Foundations of Chemistry*, 17(3), pp. 187–205. doi:10.1007/s10698-015-9235-y.

Seku, K. *et al.* (2022) 'An efficient biosynthesis of palladium nanoparticles using Bael gum and evaluation of their catalytic and antibacterial activity', *International Journal of Biological Macromolecules*, 209, pp. 912–922. doi:10.1016/j.ijbiomac.2022.04.070.

Semaltianos, N.G. (2016) 'Nanoparticles by laser ablation of bulk target materials in liquids', in *Handbook of Nanoparticles*. Cham: Springer International Publishing, pp. 67–92. doi:10.1007/978-3-319-15338-4_1.

Shahid-ul-Islam *et al.* (2019) 'Multifunctional finishing of cellulosic fabric via facile, rapid in-situ green synthesis of AgNPs using pomegranate peel extract biomolecules', *Sustainable Chemistry and Pharmacy*, 12, p. 100135. doi:10.1016/j.scp.2019.100135.

Shanmugasundaram, T. *et al.* (2017) 'Biocompatible silver, gold and silver/gold alloy nanoparticles for enhanced cancer therapy: in vitro and in vivo perspectives', *Nanoscale*, 9(43), pp. 16773–16790. doi:10.1039/C7NR04979J.

Sharma, D. *et al.* (2022) 'A highly sensitive immunosensor based on in situ reduced gold-chitosan nanocomposite for detection of monosodium L-glutamate', *Journal of Biosystems Engineering*, 47(1), pp. 28–38. doi:10.1007/s42853-022-00127-z.

Shi, M., Lu, J. and Shoichet, M.S. (2009) 'Organic nanoscale drug carriers coupled with ligands for targeted drug delivery in cancer', *Journal of Materials Chemistry*, 19(31), p. 5485. doi:10.1039/b822319j.

Shin, W. *et al.* (2019) 'Antibacterial nanoparticles: enhanced antibacterial efficiency of coral-like crystalline rhodium nanoplates', *RSC Advances*, 9(11), pp. 6241–6244. doi:10.1039/C9RA00214F.

Sivaram, A.J. *et al.* (2018) 'Recent advances in the generation of antibody–nanomaterial conjugates', *Advanced Healthcare Materials*, 7(1), p. 1700607. doi:10.1002/adhm.201700607.

Slepička, P. *et al.* (2019) 'Methods of gold and silver nanoparticles preparation', *Materials*, 13(1), p. 1. doi:10.3390/ma13010001.

Sletten, E.M. and Bertozzi, C.R. (2009) 'Bioorthogonal chemistry: fishing for selectivity in a sea of functionality', *Angewandte Chemie International Edition*, 48(38), pp. 6974–6998. doi:10.1002/anie.200900942.

Soares, S.F. *et al.* (2019) 'The controlled synthesis of complex hollow nanostructures and prospective applications', *Proceedings of the Royal Society A: Mathematical, Physical and Engineering Sciences*, 475(2224), p. 20180677. doi:10.1098/rspa.2018.0677.

Soetaert, F. *et al.* (2020) 'Cancer therapy with iron oxide nanoparticles: Agents of thermal and immune therapies', *Advanced Drug Delivery Reviews*, 163–164, pp. 65–83. doi:10.1016/j.addr.2020.06.025.

Sokolov, K. *et al.* (2003) 'Real-time vital optical imaging of precancer using anti-epidermal growth factor receptor antibodies conjugated to gold nanoparticles.', *Cancer research*, 63(9), pp. 1999–2004. Available at: http://www.ncbi.nlm.nih.gov/pubmed/12727808.

Sokolov, S. V. *et al.* (2015) 'Reversible or not? distinguishing agglomeration and aggregation at the nanoscale', *Analytical Chemistry*, 87(19), pp. 10033–10039. doi:10.1021/acs.analchem.5b02639.

Song, C. *et al.* (2020) 'High peroxidase-like activity realized by facile synthesis of FeS2 nanoparticles for sensitive colorimetric detection of H2O2 and glutathione', *Biosensors and Bioelectronics*, 151, p. 111983. doi:10.1016/j.bios.2019.111983.

Sorinolu, A.J. *et al.* (2022) 'Influence of silver ion release on the inactivation of antibiotic resistant bacteria using light-activated silver nanoparticles', *Materials Advances*, 3(24), pp. 9090–9102. doi:10.1039/D2MA00711H.

Specht, W. (1937) 'Die Chemiluminescenz des Hämins, ein Hilfsmittel zur Auffindung und Erkennung forensisch wichtiger Blutspuren', *Angewandte Chemie*, 50(8), pp. 155–157. doi:10.1002/ange.19370500803.

Sportelli, M. *et al.* (2018) 'The pros and cons of the use of laser ablation synthesis for the production of silver nano-antimicrobials', *Antibiotics*, 7(3), p. 67. doi:10.3390/antibiotics7030067.

Stasyuk, N. *et al.* (2020) 'Synthesis, catalytic properties and application in biosensorics of nanozymes and electronanocatalysts: A Review', *Sensors*, 20(16), p. 4509.

doi:10.3390/s20164509.

Sun, J. *et al.* (2016) 'Optimizing colorimetric assay based on V_2O_5 nanozymes for sensitive detection of H_2O_2 and glucose', *Sensors*, 16(4), p. 584. doi:10.3390/s16040584.

Tahmasbi, M., Koukabi, N. and Seidi, F. (2022) 'A novel core@double-shell three-layer structure with dendritic fibrous morphology based on Fe_3O_4 @TEA@Ni–organic framework: a highly efficient magnetic catalyst in the microwave-assisted Sonogashira coupling reaction', *Nanoscale*, 14(19), pp. 7189–7202. doi:10.1039/D2NR00303A.

Talham, D.R. (2002) 'Biomineralization: principles and concepts in bioinorganic materials Chemistry Stephen Mann. Oxford University Press, New York, 2001.', *Crystal Growth & Design*, 2(6), pp. 675–675. doi:10.1021/cg020033l.

Thangudu, S. and Su, C.-H. (2021) 'Peroxidase Mimetic Nanozymes in Cancer Phototherapy: Progress and Perspectives', *Biomolecules*, 11(7), p. 1015. doi:10.3390/biom11071015.

Thomas, J.A. *et al.* (2020) 'Immunomagnetic Separation of Microorganisms with Iron Oxide Nanoparticles', *Chemosensors*, 8(1), p. 17. doi:10.3390/chemosensors8010017.

Thorpe, G.H.G. and Kricka, L.J. (1986) '[29] Enhanced chemiluminescent reactions catalyzed by horseradish peroxidase', in, pp. 331–353. doi:10.1016/0076-6879(86)33078-7.

Tiwari, J.N., Tiwari, R.N. and Kim, K.S. (2012) 'Zero-dimensional, one-dimensional, two-dimensional and three-dimensional nanostructured materials for advanced electrochemical energy s', *Progress in Materials Science*, 57(4), pp. 724–803. doi:10.1016/j.pmatsci.2011.08.003.

Tran, N. and Webster, T.J. (2010) 'Magnetic nanoparticles: biomedical applications and challenges', *Journal of Materials Chemistry*, 20(40), p. 8760. doi:10.1039/c0jm00994f.

Trilling, A.K., Beekwilder, J. and Zuilhof, H. (2013) 'Antibody orientation on biosensor surfaces: a minireview', *The Analyst*, 138(6), p. 1619. doi:10.1039/c2an36787d.

Trinder, P. (1969) 'Determination of Glucose in Blood Using Glucose Oxidase with an Alternative Oxygen Acceptor', *Annals of Clinical Biochemistry: International Journal of Laboratory Medicine*, 6(1), pp. 24–27. doi:10.1177/000456326900600108.

Turková, J. (1999) 'Oriented immobilization of biologically active proteins as a tool for revealing protein interactions and function', *Journal of Chromatography B: Biomedical Sciences and Applications*, 722(1–2), pp. 11–31. doi:10.1016/S0378-4347(98)00434-4.

Vangijzegem, T., Stanicki, D. and Laurent, S. (2019) 'Magnetic iron oxide nanoparticles for drug delivery: applications and characteristics', *Expert Opinion on Drug Delivery*, 16(1), pp. 69–78. doi:10.1080/17425247.2019.1554647.

Verma, M. *et al.* (2017) 'Adsorptive removal of Pb (II) ions from aqueous solution using CuO nanoparticles synthesized by sputtering method', *Journal of Molecular Liquids*, 225, pp. 936–944. doi:10.1016/j.molliq.2016.04.045.

Voinov, M.A. *et al.* (2011) 'Surface-Mediated Production of Hydroxyl Radicals as a Mechanism of Iron Oxide Nanoparticle Biotoxicity', *Journal of the American Chemical*

Society, 133(1), pp. 35–41. doi:10.1021/ja104683w.

Wai, J.L. and New, S.Y. (2020) 'Cysteamine-coated gold nanoparticles for bimodal colorimetric detection with inverse sensitivity: a proof-of-concept with lysozyme', *RSC Advances*, 10(2), pp. 1088–1094. doi:10.1039/C9RA07930K.

Wang, N. *et al.* (2010) 'Sono-assisted preparation of highly-efficient peroxidase-like Fe3O4 magnetic nanoparticles for catalytic removal of organic pollutants with H2O2', *Ultrasonics Sonochemistry*, 17(3), pp. 526–533. doi:10.1016/j.ultsonch.2009.11.001.

Wang, Q. *et al.* (2020) 'Dual enzyme-like activity of iridium nanoparticles and their applications for the detection of glucose and glutathione', *RSC Advances*, 10(42), pp. 25209–25213. doi:10.1039/D0RA05342B.

Wang, S. *et al.* (2012) 'Comparison of the Peroxidase-Like Activity of Unmodified, Amino-Modified, and Citrate-Capped Gold Nanoparticles', *ChemPhysChem*, 13(5), pp. 1199–1204. doi:10.1002/cphc.201100906.

Wang, S. *et al.* (2021) 'One Pot Synthesis of Large Gold Nanoparticles with Triple Functional Ferrocene Ligands', *International Journal of Molecular Sciences*, 22(5), p. 2328. doi:10.3390/ijms22052328.

Wang, X. *et al.* (2016) 'Introduction to Nanozymes', in, pp. 1–6. doi:10.1007/978-3-662-53068-9_1.

Wang, X. *et al.* (2022) 'Fast Surface Restructuring within the Gap of Au Nanocube Dimer for the Enhancement of Catalytic Efficiency', *CCS Chemistry*, 4(3), pp. 1074–1086. doi:10.31635/ccschem.021.202100770.

Wang, Z. *et al.* (2019) 'Simultaneous enzyme mimicking and chemical reduction mechanisms for nanoceria as a bio-antioxidant: a catalytic model bridging computations and experiments for nanozymes', *Nanoscale*, 11(28), pp. 13289–13299. doi:10.1039/C9NR03473K.

Wang, Z. *et al.* (2020) 'Structure and activity of nanozymes: Inspirations for de novo design of nanozymes', *Materials Today*, 41, pp. 81–119. doi:10.1016/j.mattod.2020.08.020.

Van Weemen, B.K. and Schuurs, A.H.W.M. (1971) 'Immunoassay using antigen-enzyme conjugates', *FEBS Letters*, 15(3), pp. 232–236. doi:10.1016/0014-5793(71)80319-8.

Weerathunge, P. *et al.* (2019) 'Dynamic interactions between peroxidase-mimic silver NanoZymes and chlorpyrifos-specific aptamers enable highly-specific pesticide sensing in river water', *Analytica Chimica Acta*, 1083, pp. 157–165. doi:10.1016/j.aca.2019.07.066.

Wei, H. and Wang, E. (2013) 'Nanomaterials with enzyme-like characteristics (nanozymes): next-generation artificial enzymes', *Chemical Society Reviews*, 42(14), p. 6060. doi:10.1039/c3cs35486e.

Wei, X. *et al.* (2020) 'Facile ball-milling synthesis of CuO/biochar nanocomposites for efficient removal of reactive red 120', *ACS Omega*, 5(11), pp. 5748–5755. doi:10.1021/acsomega.9b03787.

Welch, N.G. *et al.* (2017) 'Orientation and characterization of immobilized antibodies for

improved immunoassays (Review)', *Biointerphases*, 12(2), p. 02D301. doi:10.1116/1.4978435.

Wilkes, J.S. and Zaworotko, M.J. (1992) 'Air and water stable 1-ethyl-3-methylimidazolium based ionic liquids', *Journal of the Chemical Society, Chemical Communications*, (13), p. 965. doi:10.1039/c39920000965.

Wu, J. *et al.* (2015) 'Growth of Au on Pt icosahedral nanoparticles revealed by low-dose in situ TEM', *Nano Letters*, 15(4), pp. 2711–2715. doi:10.1021/acs.nanolett.5b00414.

Wu, J. *et al.* (2019) 'Nanomaterials with enzyme-like characteristics (nanozymes): next-generation artificial enzymes (II)', *Chemical Society Reviews*, 48(4), pp. 1004–1076. doi:10.1039/C8CS00457A.

Wu, S. *et al.* (2020) 'Colorimetric quantification and discrimination of phenolic pollutants based on peroxidase-like Fe_3O_4 nanoparticles', *Sensors and Actuators B: Chemical*, 303, p. 127225. doi:10.1016/j.snb.2019.127225.

Wu, Y., Gao, Y. and Du, J. (2019) 'Bifunctional gold nanoclusters enable ratiometric fluorescence nanosensing of hydrogen peroxide and glucose', *Talanta*, 197, pp. 599–604. doi:10.1016/j.talanta.2019.01.087.

Xi, Z. *et al.* (2020) 'Strain effect in Palladium nanostructures as nanozymes', *Nano Letters*, 20(1), pp. 272–277. doi:10.1021/acs.nanolett.9b03782.

Xiang, Z. *et al.* (2016) 'Optical determination of hydrogen peroxide by exploiting the peroxidase-like activity of $AgVO_3$ nanobelts', *Microchimica Acta*, 183(1), pp. 457–463. doi:10.1007/s00604-015-1670-x.

Xie, J. *et al.* (2020) 'A sandwich ELISA-like detection of C-reactive protein in blood by citicoline-bovine serum albumin conjugate and aptamer-functionalized gold nanoparticles nanozyme', *Talanta*, 217, p. 121070. doi:10.1016/j.talanta.2020.121070.

Xu, H. *et al.* (2011) 'Antibody conjugated magnetic iron oxide nanoparticles for cancer cell separation in fresh whole blood', *Biomaterials*, 32(36), pp. 9758–9765. doi:10.1016/j.biomaterials.2011.08.076.

Yan, N., Yuan, Y. and Dyson, P.J. (2013) 'Nanometallic chemistry: deciphering nanoparticle catalysis from the perspective of organometallic chemistry and homogeneous catalysis', *Dalton Transactions*, 42(37), p. 13294. doi:10.1039/c3dt51180d.

Yang, D. *et al.* (2018) 'The effect of DNA on the oxidase activity of nanoceria with different morphologies', *Nanotechnology*, 29(38), p. 385101. doi:10.1088/1361-6528/aacf86.

Yang, H. *et al.* (2017) 'A bimetallic (Co/2Fe) metal-organic framework with oxidase and peroxidase mimicking activity for colorimetric detection of hydrogen peroxide', *Microchimica Acta*, 184(12), pp. 4629–4635. doi:10.1007/s00604-017-2509-4.

Yang, S.F. *et al.* (2014) 'Detection of c-reactive protein based on a magnetic immunoassay by using functional magnetic and fluorescent nanoparticles in microplates', *The Analyst*, 139(21), pp. 5576–5581. doi:10.1039/C4AN00921E.

Ye, H. *et al.* (2016) 'Peroxidase-like properties of Ruthenium nanoframes', *Science Bulletin*, 61(22), pp. 1739–1745. doi:10.1007/s11434-016-1193-9.

Yi, G. *et al.* (2018) 'Application of click chemistry in nanoparticle modification and its targeted delivery', *Biomaterials Research*, 22(1), p. 13. doi:10.1186/s40824-018-0123-0.

You, Y., Lim, S. and Gunasekaran, S. (2020) 'Streptavidin-coated Au nanoparticles coupled with biotinylated antibody-based bifunctional linkers as plasmon-enhanced immunobiosensors', *ACS Applied Nano Materials*, 3(2), pp. 1900–1909. doi:10.1021/acsanm.9b02461.

Yu, M.K., Park, J. and Jon, S. (2012) 'Targeting strategies for multifunctional nanoparticles in cancer imaging and therapy', *Theranostics*, 2(1), pp. 3–44. doi:10.7150/thno.3463.

Yu, R.-J. *et al.* (2017) 'Real-time sensing of o-phenylenediamine oxidation on gold nanoparticles', *Sensors*, 17(3), p. 530. doi:10.3390/s17030530.

Zahra, R. *et al.* (2019) 'Effect of secondary phases on the thermoelectric properties of Zn2GeO4 nano-crystals grown by thermal evaporation on Au coated Si substrate', *Physica B: Condensed Matter*, 564, pp. 143–146. doi:10.1016/j.physb.2019.02.061.

Zaitsu, K. and Ohkura, Y. (1980) 'New fluorogenic substrates for horseradish peroxidase: Rapid and sensitive assays for hydrogen peroxide and the peroxidase', *Analytical Biochemistry*, 109(1), pp. 109–113. doi:10.1016/0003-2697(80)90017-2.

Zamboulis, A. *et al.* (2019) 'Polyglycerol hyperbranched polyesters: synthesis, properties and pharmaceutical and biomedical applications', *International Journal of Molecular Sciences*, 20(24), p. 6210. doi:10.3390/ijms20246210.

Zaytsev, V.D. *et al.* (2020) 'Label-free silver triangular nanoplates for spectrophotometric determination of catecholamines and their metabolites', *Microchimica Acta*, 187(11), p. 610. doi:10.1007/s00604-020-04576-1.

Zhang, B. *et al.* (2022) 'Au–Pt nanozyme-based multifunctional hydrogel dressing for diabetic wound healing', *Biomaterials Advances*, 137, p. 212869. doi:10.1016/j.bioadv.2022.212869.

Zhang, K. *et al.* (2019) 'Advances in the Nanocatalyst-Assisted $NaBH_4$ reduction of nitroaromatics in water' , *ACS Omega*, 4(1), pp. 483–495. doi:10.1021/acsomega.8b03051.

Zhang, K., Shaikhutdinov, S. and Freund, H.-J. (2015) 'Does the surface structure of oxide affect the strong metal-support interaction with Platinum? Platinum on Fe_3O_4 (0 0 1) versus Fe_3O_4 (1 1 1)', *ChemCatChem*, 7(22), pp. 3725–3730. doi:10.1002/cctc.201500328.

Zhang, P. *et al.* (2015) 'Rapid and quantitative detection of C-reactive protein based on quantum dots and immunofiltration assay', *International Journal of Nanomedicine*, p. 6161. doi:10.2147/IJN.S89307.

Zhang, Q. *et al.* (2022) 'Gold nanomaterials for oral cancer diagnosis and therapy: Advances, challenges, and prospects', *Materials Today Bio*, 15, p. 100333. doi:10.1016/j.mtbio.2022.100333.

Zhang, X. *et al.* (2013) '$CoFe_2O_4$ nanoparticles as oxidase mimic-mediated chemiluminescence

of aqueous luminol for sulfite in white wines', *Journal of Agricultural and Food Chemistry*, 61(4), pp. 840–847. doi:10.1021/jf3041269.

Zhang, Y. *et al.* (2020) 'Enzyme-like properties of gold clusters for biomedical application', *Frontiers in Chemistry*, 8. doi:10.3389/fchem.2020.00219.

Zhao, C. *et al.* (2016) 'A novel sensor for dopamine based on the turn-on fluorescence of Fe-MIL-88 metal-organic frameworks–hydrogen peroxide–o-phenylenediamine system', *Talanta*, 159, pp. 365–370. doi:10.1016/j.talanta.2016.06.043.

Zheng, C. *et al.* (2016) 'Intrinsic peroxidase-like activity and the catalytic mechanism of gold@carbon dots nanocomposites', *RSC Advances*, 6(42), pp. 35280–35286. doi:10.1039/C6RA01917J.

Zheng, D. *et al.* (2010) 'Preparation and application of a novel vanillin sensor based on biosynthesis of Au–Ag alloy nanoparticles', *Sensors and Actuators B: Chemical*, 148(1), pp. 247–252. doi:10.1016/j.snb.2010.04.031.

Zhou, L. *et al.* (2011) 'General avenue to multifunctional aqueous nanocrystals stabilized by hyperbranched polyglycerol', *Chemistry of Materials*, 23(6), pp. 1461–1470. doi:10.1021/cm1030359.

Zhou, W. *et al.* (2009) 'Biosynthesis and magnetic properties of mesoporous Fe_3O_4 composites', *Journal of Magnetism and Magnetic Materials*, 321(8), pp. 1025–1028. doi:10.1016/j.jmmm.2008.10.007.

Zhu, X. and Gao, T. (2019) 'Spectrometry', *Nano-Inspired Biosensors for Protein Assay with Clinical Applications*. Elsevier, pp. 237–264. doi:10.1016/B978-0-12-815053-5.00010-6.

Zhuge, W. *et al.* (2019) 'Fluorescent and colorimetric immunoassay of nuclear matrix protein 22 enhanced by porous Pd nanoparticles', *Chinese Chemical Letters*, 30(6), pp. 1307–1309. doi:10.1016/j.cclet.2019.02.026.

Żukowski, K., Kosman, J. and Juskowiak, B. (2020) 'Light- of DNAzyme--modified quantum dots', *International Journal of Molecular Sciences*, 21(21), p. 8190. doi:10.3390/ijms21218190.